POLITECNICO DI MILANO

Facoltà di Ingegneria Industriale

Laurea Magistrale in Ingegneria Meccanica

Kite Dynamics and Wind Energy Harvesting

Relatore: Prof. Federico CHELI

Co-relatore: Prof. Paolo MANTEGAZZA

Tesi di Laurea di:

Antonello CHERUBINI Matr. 765379

Anno Accademico 2011 - 2012

Abstract

Conventional wind energy is generated using wind turbines. The global installed power has grown significantly in the last decades and the industry is constantly going towards taller towers and larger rotors to both increase the power output of the generator and capture the more powerful and steady winds available at higher altitudes. By contrast, high altitude wind power refers to newer methods to exploit high altitude winds by using, for example, a tethered airfoil, namely a kite, to pull on a rope and transmit a force to the ground. The force, combined with the velocity of reeling out the cables, eventually produces electrical power. Several industrial players around the world have developed high altitude wind concepts and they are now seeking commercial MW scale power plants. This thesis describes a simulator that uses multibody dynamics, Vortex Lattice Method (VLM) aerodynamics and other models to fully simulate a kite-cables system for high altitude wind power. The VLM simulator was written from scratch and it is a flexible an powerful tool that is capable of investigating the effects of several parameters, such as kite geometry and wind profile. An application of the kite simulator is also developed. The performance improvements due to the optimization of cables aerodynamics are investigated with the kite simulator. The results show that a substantial increase in power output can be achieved by using aerodynamic cables instead of standard cables.

Sommario

L'energia eolica proviene convenzionalmente da turbine ad asse orizzontale composte da una torre e da un rotore. Negli ultimi anni, questo settore ha visto una grande crescita e i nuovi aerogeneratori hanno dimensioni sempre crescenti al duplice scopo di aumentare la potenza prodotta e catturare i venti più forti e stabili che caratterizzano le alte quote. L'eolico d'alta quota si riferisce invece a dei nuovi metodi di sfruttamento dell'energia del vento che fanno uso, ad esempio, di un profilo alare, ovvero un kite, sostenuto da una o più funi. Il kite vola velocemente e trasmette a terra la propria portanza aerodinamica attraverso le funi. Le funi vengono gradualmente srotolate dai tamburi su cui sono avvolte. La velocità di avanzamento delle funi combinata alla forza di trazione su di esse permette la generazione di potenza elettrica. Ad oggi, diverse aziende nel mondo stanno sviluppando questo tipo di tecnologie e alcuni di loro puntano ora a commercializzare macchine sulla scala dei megawatt. Questa tesi descrive un simulatore basato su un modello dinamico multicorpo combinato ad una aerodinamica a reticolo di vortici. Il simulatore è stato scritto per intero appoggiandosi a dei software commerciali ed open-source. Si tratta di uno strumento flessibile e potente che consente di indagare numerose variabili di un sistema eolico di alta quota come ad esempio la geometria del kite e il profilo del vento. In ultimo, la tesi descrive un esempio di analisi effettuata grazie al simulatore, ovvero la stima di incremento di prestazioni dovuta all'utilizzo di cavi dal profilo aerodinamico anziché a sezione circolare. I risultati mostrano un sostanziale incremento della potenza generata.

Contents

CONTENTS

List of Figures

Glossary

AWE Airborne Wind Energy. It is another way of referring to high altitude wind energy.

CF Capacity Factor. For a power plant, it is the ratio of the actual energy output over a period of time and the potential output at full nameplate capacity over the same period.

CS Coordinate System. Reference frame.

DAEs Differential Algebraic Equations. A particular form of equations containing both ODEs and algebraic constraints.

EROEI Energy Returned On Energy Invested. An index measured as the ratio between the energy produced by a particular energy source and the energy used to obtain that production.

HAWE High Altitude Wind Energy. Refers to the energy produced by means of devices that fly or float at a significant distance from the ground.

LEI Leading Edge Inflatable (kite). A type of kite having an inflatable structure to support the canopy. Especially used for kite surfing.

ODEs Ordinary Differential Equations. Equations containing a function of one independent variable and its derivatives.

PDC Partitions Detach Code. A function that helps to obtain proper results while running the kite simulator.

VLM Vortex Lattice Method. It is a computational fluid dynamics method able to compute lift and induced drag.

WPD Wind Power Density. It is the amount of wind kinetic energy flowing through a cross-sectional area of $1\ m^2$ in $1\ sec$.

1

Introduction

1.1   Topic of the thesis

Wind has been an energy source for centuries. Ancient wind mills improved living conditions of the society and helped to automate processes in both agriculture and industry. Nowadays modern wind turbines capture energy from the wind and generate electricity. This industry has grown significantly in the last two decades and is supported by public funds all over the world.

While the conventional wind turbines have been know for centuries, a more recent approach to wind energy is the so called High Altitude Wind Energy (HAWE). This idea is a completely different approach to wind power and it is better explained in the following chapters.

The thesis is the description of a Vortex Lattice Method (VLM) kite simulator created from scratch combining commercial and open source software. The simulator is capable of analysing the dynamics and aerodynamics of the kite-cables system in an high altitude wind power plant. An example of application of the simulator is also provided.

1.2   Structure of the thesis

Chapter 2 describes the potential of the unexploited high altitude winds explaining the reasons why there is so much growing interest from both the scientific and industrial societies.

Chapter 3 illustrates the most interesting kites for power generation, but only in chapter 4 it is made clear how kites and tethered wings can be physically used to generate electricity.

Chapter 5 describes one of the most important parameters in a kite power plant, the aerodynamic efficiency. An insight about the real potential of tethered wings is given thanks to basic models.

Finally, chapter 6 illustrates the VLM kite simulator and in chapter 7 the simulator is used to investigate the performance improvements that could be achieved if aerodynamic cables were used in the the kite system instead of common round cables.

2

Conventional versus high altitude wind energy

Wind at low altitude has been used as a source of energy for hundreds of years. Basically it has been employed in production, agriculture and transport. A modern wind turbine is nothing more than an optimized version of ancient windmills that were used in many industrial applications. Ships were equipped with sails before the modern transport system switched to fossil fuel as a reliable and powerful source of energy.

Wind power comes in the form of a flow of kinetic energy, a noble form of energy which can be easily transformed. It is a massive source of power and, according to the Global Wind Energy Council (1), the global installed wind capacity is 238.3 GW [1] but, nevertheless, only a small fraction of the available wind is exploited. The potential of wind power is relatively low at ground level and increases dramatically with altitude.

Wind properties change significantly with altitude. This can be proven by common experience. At ground level, winds of 10 m/s (36 km/h) are considered strong. But, when flying with a commercial airline, it can happen to see data from the passenger monitor showing wind speeds over 100 km/h. Not only speed increases, but the statistical occurrence of wind is significantly higher when increasing the height. In daily life this can be seen for example when climbing a mountain. Quite often wind is weak at the base and becomes stronger while rising to the summit. These changes in wind

---

[1]238.3 GW is the figure at the end of 2011. 41.2 GW were installed in 2011 alone. It is notable that wind power accounts only for 2 or 3 % of the global power demand.

properties are commonly taken into account when designing important structures such as bridges, skyscrapers, chimneys, towers or electricity power lines.

High altitude winds are stronger, more regular, and with a higher statistical occurrence throughout the year. Some fundamental features of wind that are key to understand the importance of high altitude wind energy are presented in this chapter.

2.1 Wind Power Density

If we consider an area A through which the wind is flowing perpendicularly, being v and ρ its velocity and density, then the total wind power P flowing through that area is

$$P = \frac{1}{2}\rho v^3 A \tag{2.1}$$

where $\frac{1}{2}\rho v^3$ is defined as Wind Power Density (WPD) $[W/m^2]$.

As already said, average wind velocity v increases with altitude and, despite an exponential reduction of density ρ, wind power density increases dramatically with altitude as shown in fig. 2.1, 2.2 and 2.3.

Moreover, as shown in fig. 2.4, high altitude wind power is more evenly distributed all over the planet than ground level wind power. This feature makes it a valuable potential resource for all geographical regions.
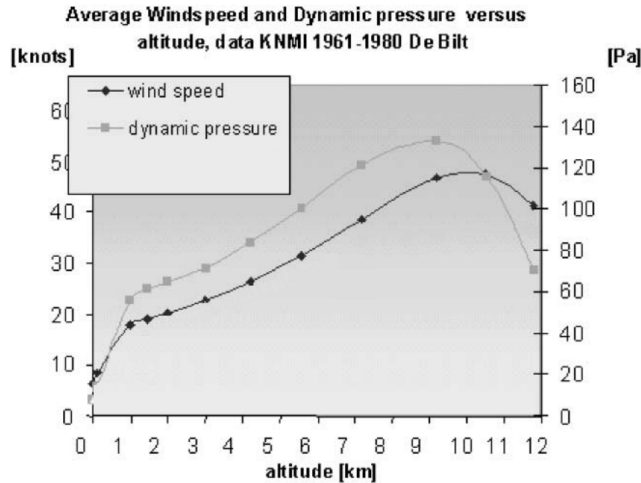
Figure 2.1: Average wind speed and dynamic pressure versus altitude - The figure shows data relative to De Bilt in the Netherlands. Picture from (2).
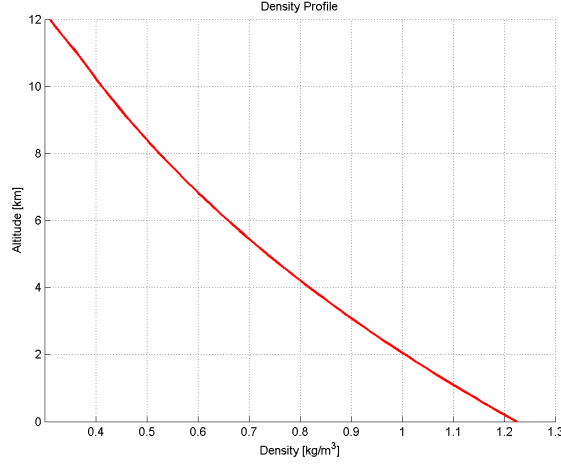
Figure 2.2: Density versus altitude - Data from International Standard Atmosphere (ISA) table.

2.2 The limits of Betz's law

However, not all the kinetic energy of the wind can be converted. Albert Betz (5) in 1919 showed that only 59.3 % [1] of it can be extracted.

With reference to fig. 2.5, it is possible to define a Power Coefficient as follows

$$\frac{P}{\frac{1}{2}\rho v_{in}^3 A} = \frac{1}{2}\left(1 + \frac{v_{out}}{v_{in}} - \frac{v_{out}^2}{v_{in}^2} - \frac{v_{out}^3}{v_{in}^3}\right) \tag{2.2}$$

where V_{in} and V_{out} are the air input and output velocities respectively.

The Betz's limit can be obtained by maximizing the Power Coefficient as shown in fig. 2.6.

The Betz's model is effective in describing the optimum way of converting the kinetic energy of the wind, and it is a fundamental golden rule for wind power applications.

Betz's law is valid under the hypotheses of incompressible, one dimensional and steady state flow as shown in fig 2.5. These hypotheses make it representative of a conventional wind turbine which has a fixed circular area where blades continuously sweep the airflow but these assumptions may no longer be accurate for a high altitude wind plant.

---

[1]This number is called Betz's limit or Betz's coefficient.
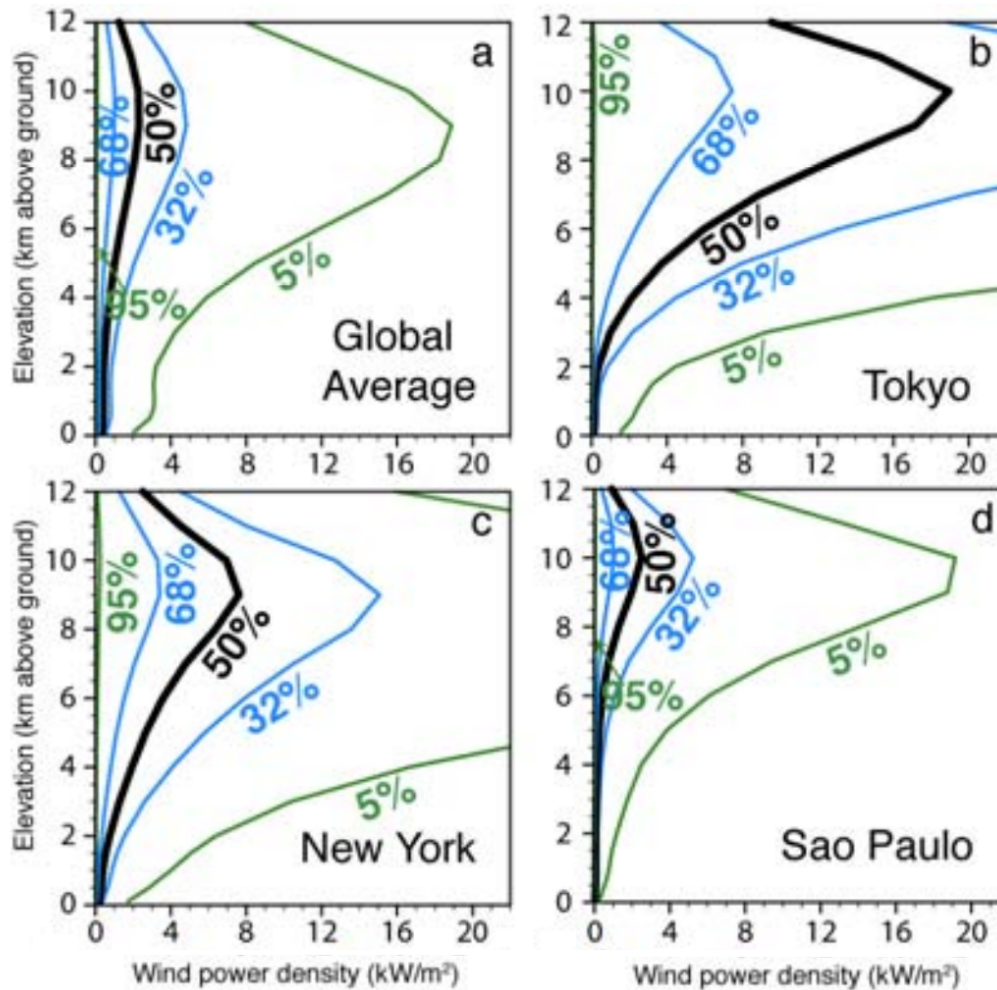
Figure 2.3: Wind power density versus altitude - The figure shows the wind power density that was exceeded 5%, 32%, 50%, 68%, and 95% of the time during 1979-2006 as a function of altitude from the NCEP/DOE re-analyses. Picture from (3, 4).
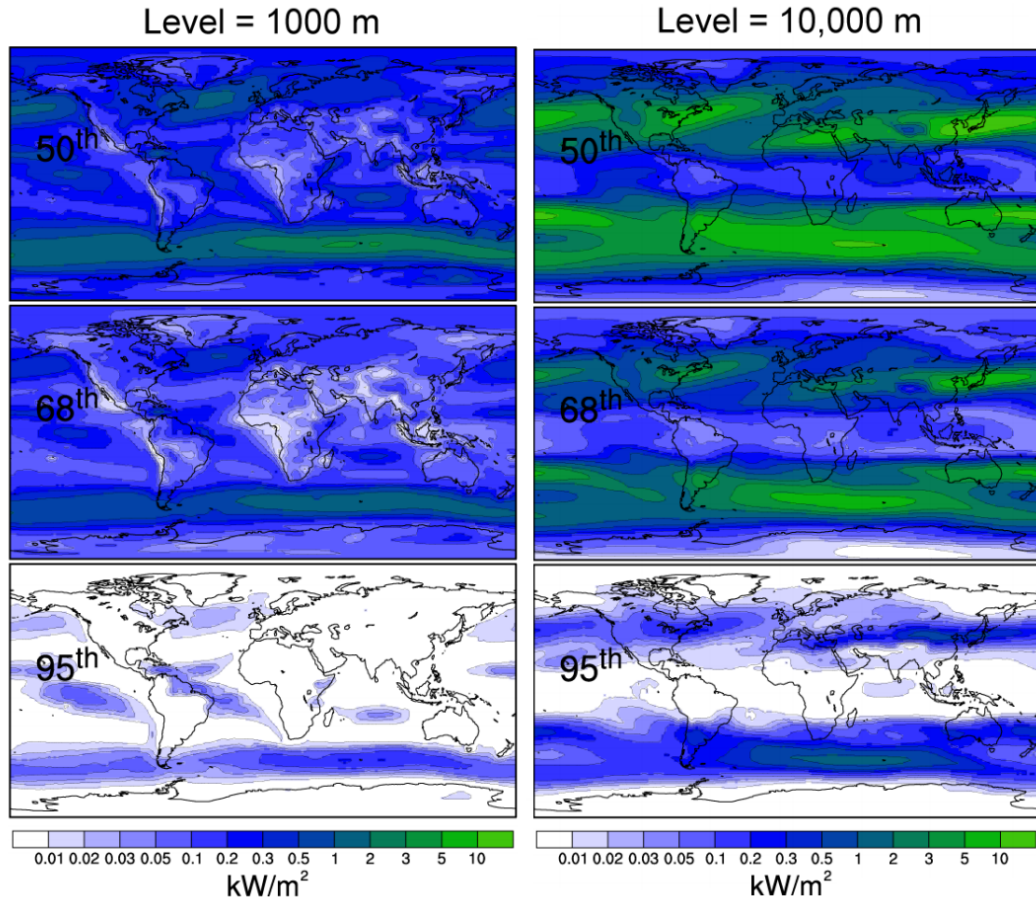
Figure 2.4: Wind power density global map - The maps show the wind power density that was exceeded 50%, 68%, and 95% of the time during 1979-2006 at $1,000$ m (left) and $10,000$ m (right). Picture from (3, 4).
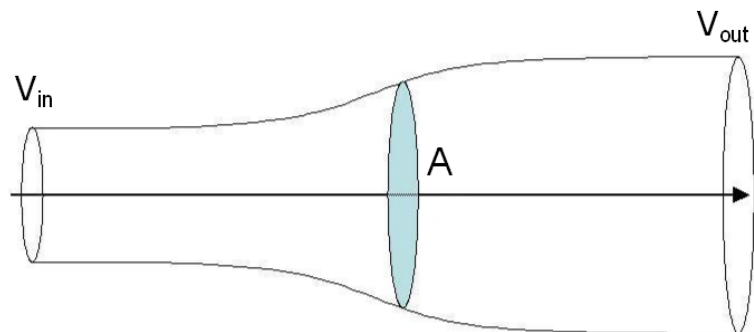
Figure 2.5: Betz's airflow model - Picture in public domain.

7
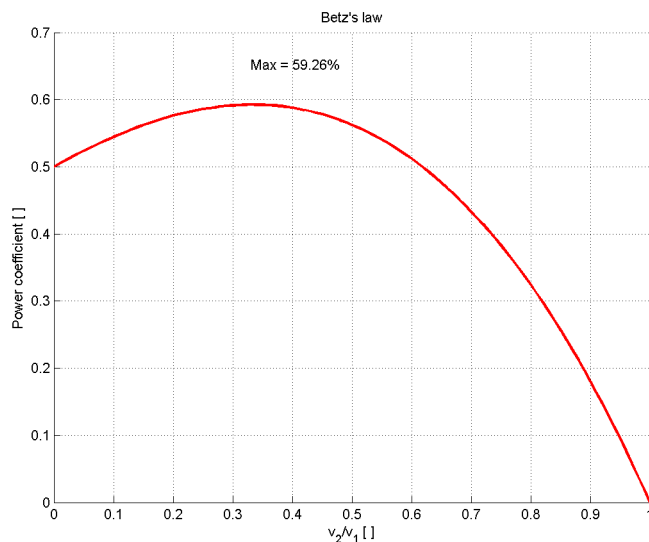
Figure 2.6: **Power coefficient versus** v_{out}/v_{in} **ratio** -

2.2.1 Efficiency

The efficiency of a conventional wind turbine is therefore measured as a ratio with the theoretical limit set by the Betz's law[1].

By contrast, for some high altitude ground-gen concepts[2], this definition of efficiency loses its importance because the interaction between wind particles and the plant would no longer be similar to a one dimensional, steady state flow. Of course it is still not possible to extract all the kinetic energy from an airflow, but the availability of huge areas to be swept asks for new theoretical definitions of efficiency[3].

2.3 Capacity Factor

In spite of being easy to use, clean and free, wind power does not guarantee a constant and reliable operation over time making it hard to compete with conventional fossil fuel.

---

[1]Modern wind turbines, due to aerodynamic, mechanical and electrical losses, can only extract 75 % to 80 % of the original 59.3 %

[2]The features of ground-gen concepts are explained in the following chapters.

[3]Further information about the validity of the Betz's law for high altitude wind systems can be found in (6) and (7).

The ratio of the actual energy output over a period of time and the potential output at full nameplate (nominal) capacity over the same period is called Capacity Factor (CF)[1]. For example for a wind turbine that produces an amount of energy as if it had worked at nameplate power for 2200 hours in a year we can write

$$CF = \frac{Hours\ at\ nameplate\ power}{Hours\ in\ a\ year} = \frac{2200}{24 * 365} = 25\% \tag{2.3}$$

CF is a key design number that strongly affects a wind power plant economic performance as shown in figure 2.7
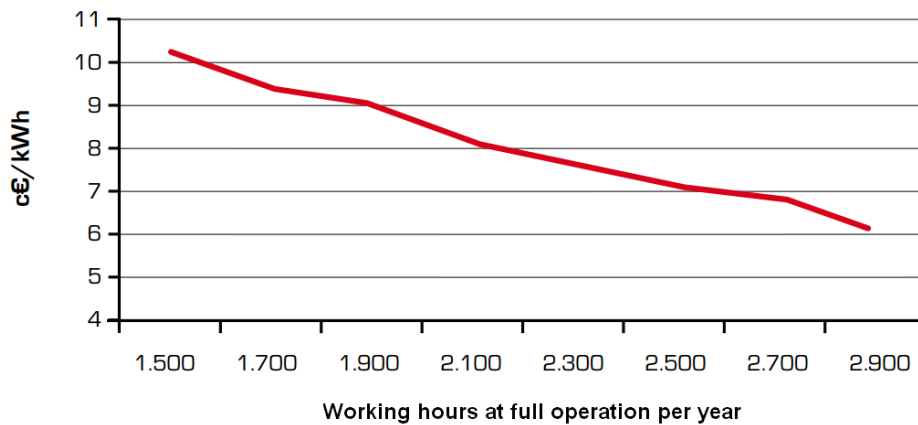
Figure 2.7: Classical wind turbines energy cost - The figure shows the dependence of energy cost on the available wind expressed in hours per year. Building cost is supposed to be 1500 €/kW. Note that with 2200 hours, grid parity can be reached (8c€/kWh according to Italian Power Exchange (IPEX) in 2011). Picture from (9).

Moreover, even though any power plant cannot have $CF = 100\%$, there is another major difference between conventional fossil fuel power plants and wind turbines. Whereas conventional power stations can adjust their power output when required, wind turbines need the wind to be available at the same time and therefore their operation is somewhat randomly chosen by the weather conditions.

Therefore, in order to substantially switch to wind power instead of conventional power, it is fundamental to find windy sites where plants can be operated when needed, reducing the random influence of weather.

---

[1]Any industrial plant for energy production cannot produce the nominal power for 100 % of the time. For example typical numbers for conventional baseload coal plants range from 60 % to 70 % (8).

Moreover, sites that are totally not suitable for conventional wind turbines may be competitive for high altitude wind plants. Figure 2.8 shows data from places that have completely different characteristics at ground level. In Linate wind speed at ground level is below 1 m/s for about 80 % of the time, meanwhile at higher altitude it is higher than 5 m/s for more than 50 % of the time. Fig. 2.9 shows a quick comparison between these two sites in terms of capacity factors.
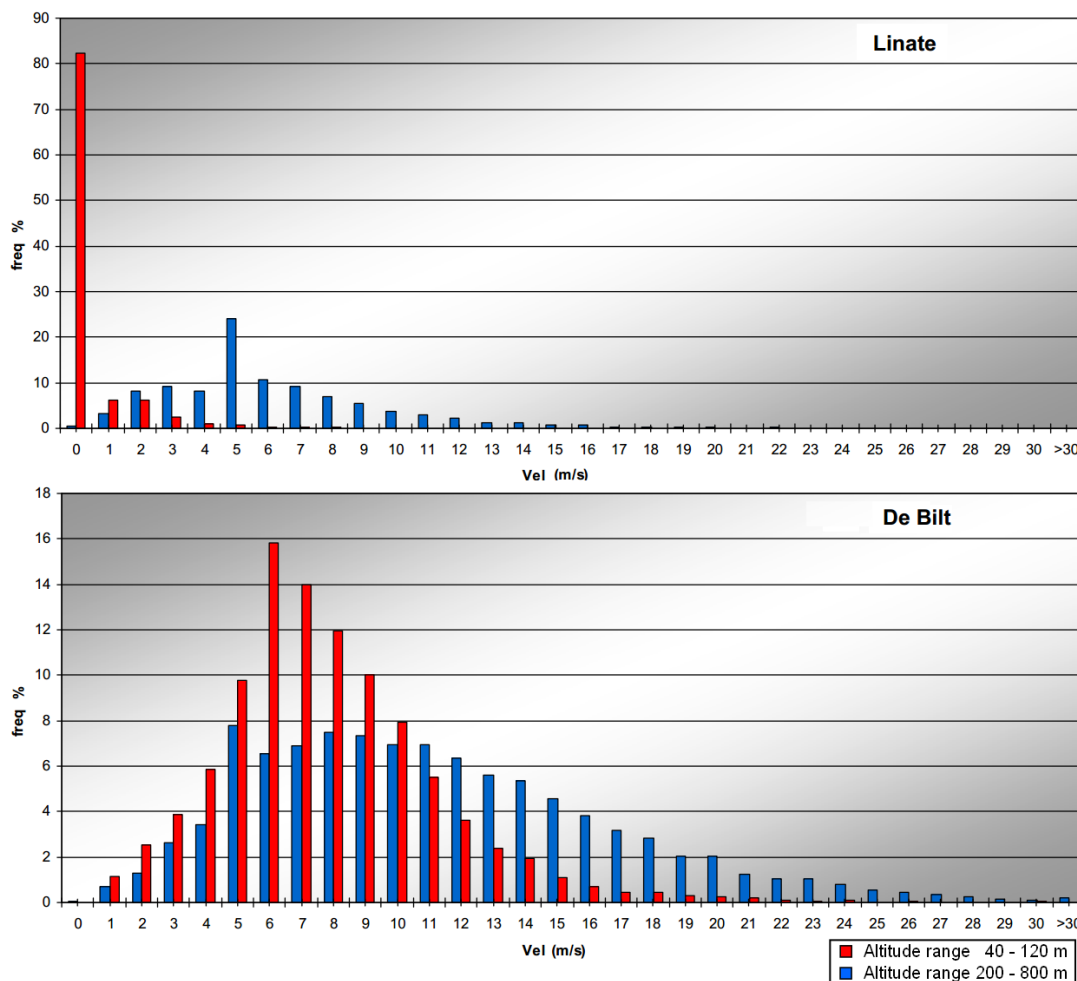
Figure 2.8: Wind speed statistical frequency distribution at different altitudes in Linate, Italy and in De Bilt, Netherlands - This picture shows the different statistical distributions of wind speed at different altitudes. Conventional wind turbines operate in the range of $40 - 120$ m, while airborne wind energy plants work at about $200 - 800$ m. Picture from (10).
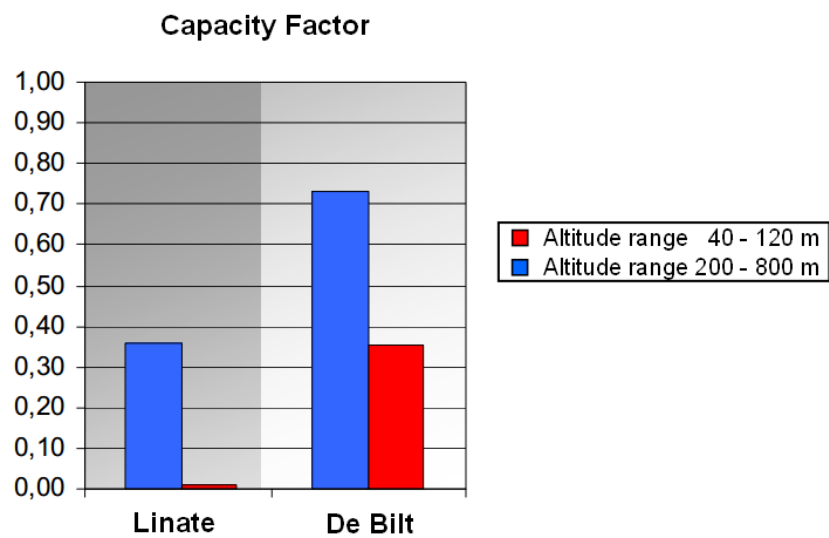
Figure 2.9: CF comparison between sites. - Linate is completely not suitable for conventional wind turbines but an high altitude plant would have a reasonable CF. Conventional wind turbines operate in the range of $40 - 120\ m$, while airborne wind energy plants work at about $200 - 800\ m$. Picture from (10).

2. CONVENTIONAL VERSUS HIGH ALTITUDE WIND ENERGY

3

Kites overview

A kite is a tethered wing, generally made of lightweight materials, that flies or hovers above the ground level. In this chapter a brief overview of the most important types of kites is given.

3.1 History

The use of kites dates back several thousands of years. Though the origin is still not clear, it is a common belief that a major role in the history of kites was played by China and the Asia Pacific region and they were brought to Europe by Marco Polo around 1282 A.D. Throughout the history, kites were used for different purposes: religious, military, scientific and as a source of energy.

A very interesting use of kites for transport came from the idea of George Pocock, an inventor that patented a kite towing system for coaches in 1826. (See fig. 3.1).

The first idea of using kites for power generation dates back about 200 years, but the first theoretical assessment of a MW scale power generation appears only in 1980 in Loyd's paper 'Crosswind Kite Power' (11).

3.2 Types of kites

Kites for entertainment, surf kites, kite planes and rigid wings are all possible configurations for airfoils tethered to the ground. It is here provided a description of the most interesting types for energy production today: ram air kites and Leading Edge Inflatable (LEI) kites.

Figure 3.1: Pocock's 'Charvolant' - A kite-drawn buggy in 1826. Picture in public domain.

3.2.1 Ram air kites

Ram air kites are made of two layers of canopy connected together by chord-wise canopy ribs. A picture representing a ram air kite is shown in fig. 3.2. On the leading edge there are holes (fig. 3.3) through which the wind rams thanks to the dynamic pressure of the relative wind. The resulting pressure difference inflates the kite providing enough stiffness to fly. The overall shape is formed by the bridle system being in equilibrium with the aerodynamic pressure distribution.

3.2.2 Leading Edge Inflatable (LEI) kites

LEI kites have an inflatable pressurized structure[1] made of a main tube running span-wise on the leading edge which is connected to several smaller pressurizes tubes chord-wise. The purpose of the tube is to reinforce the structure and give stiffness to maintain the shape. LEI kites are much easier to de-power than other types of kites and the bridle system may not be present. The stiffness makes them easier to handle during launch and landing procedures. A picture is shown in fig. 3.4.

3.3 World records

3.3.1 Largest traction kite

KiteShip Corporation (USA) used the largest traction kite to propel an 8.5 *tons* yacht near Sydney, Australia, in 2004. It had an area of 420 m^2 and is 'the largest kite ever used to pull a vehicle of any kind' (14).

3.3.2 Largest kite ever flown

'The largest kite ever flown, has a total lifting area of 950 m^2. When laid flat, it has a total area of 1019 m^2. The kite measured 25.475 m long and 40 m wide. The kite was made by Abdulrahman Al Farsi and Faris Al Farsi and flown at the Kuwait Hala Festival in Flag Square, Kuwait City, Kuwait on 15 February 2005' (15).

---

[1]Tubes are usually made of nylon and Dacron, a commercial strong lightweight fabric also used in hang gliders. Tube pressure is usually 0.3 *bar* higher than atmospheric pressure.

Figure 3.2: Skysails ram air kite - A ram air kite towing the ROS-171 'Maartje Theadora'. Picture from (12).

Figure 3.3: Ram air kite details - Two holes in the leading edge keep internal pressure higher when flying. Some cables composing the bridle system are also visible. Picture from (13).

Figure 3.4: Kitesurfers launching a LEI kite - The green inflated structure is clearly visible. Picture in public domain.

3.3.3 Highest kite train

In 1919 a kite train made of 8 kites reached the altitude of 9740 m with about 15 km of cables at the meteorological observatory of Lindenberg, Germany. Today this is still the altitude world record for kite trains (16).

3.4 Kite manoeuvres

A brief introduction on how a kite is practically used is useful for further explanations.

3.4.1 Wind window

Kites cannot fly wherever a user wants. The area in the sky where a kite can fly is called 'Wind window'. When a kitesurfer[1] needs to launch a kite in the air, he starts with the kite positioned at the edge of the wind window where it cannot fly fast and does not create a big force on the tethers. By contrast, if the kitesurfer wants a great pull, then he flies the kite into the middle of the wind window, in the so called 'power zone' where the kite flies fast and generates high lift. A representation of the wind window is shown in fig. 3.5, 3.6 and 3.7. This concept is valid not only for kites, but for all tethered airfoils such as rigid wings or glider planes.

3.4.2 Coordinate system

When referring to the kite position in sky, spherical coordinates are used as shown in fig. 3.8

3.4.3 Kite steering

Kite steering mechanics is a complex subject that involves fluid structure interaction and deformation of the kite itself. The angle of rotation that has to be controlled to steer and perform 8-figures trajectories is the yaw angle.

While tethered rigid wings and glider planes can be manoeuvred by flight control surfaces, canopy kites are controlled by means of structural deformations achieved by applying a differential force in the two main cables[2].

---

[1]This example refers to kitesurfers for an immediate understanding but it is valid also for base stations of high altitude wind power plants.

[2]Left and right cables are those used for steering while other cables can move the leading edge to
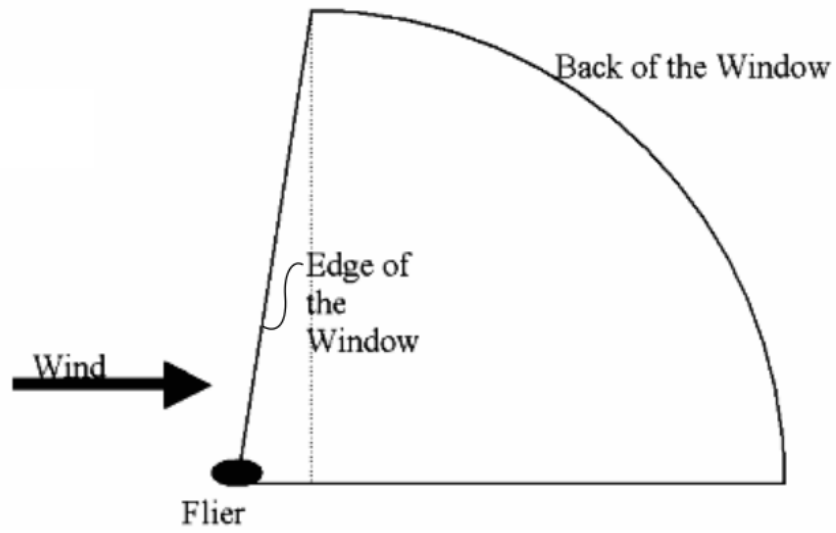
Figure 3.5: Wind window side view - Picture from (17).
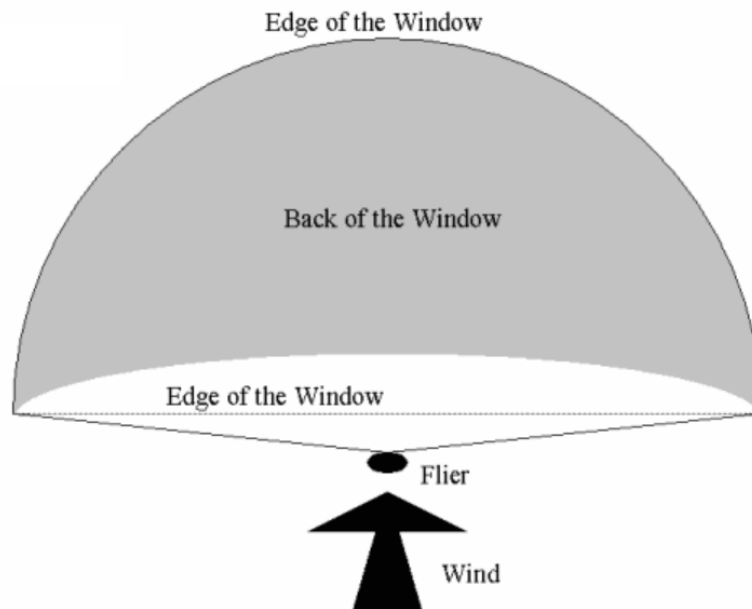
Figure 3.6: Wind window front view - Picture from (17).

Front View – Power Zone
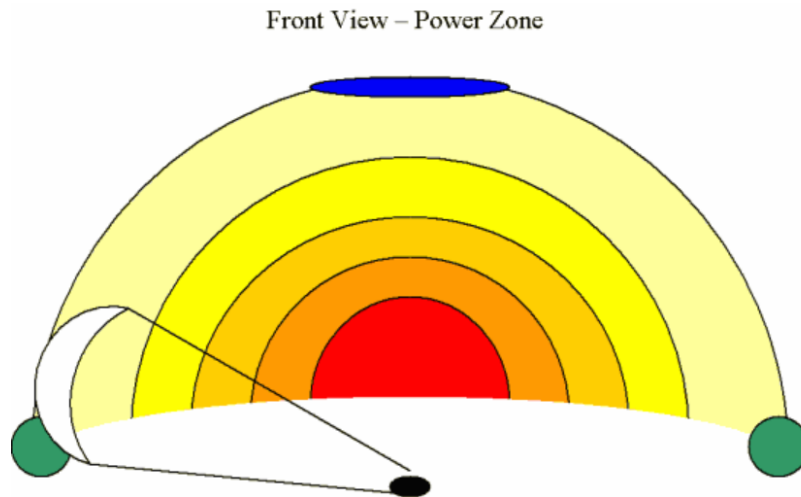
Figure 3.7: Wind window power zone - Front view. In the red central area the kite flies faster generating more lift. Picture from (17).
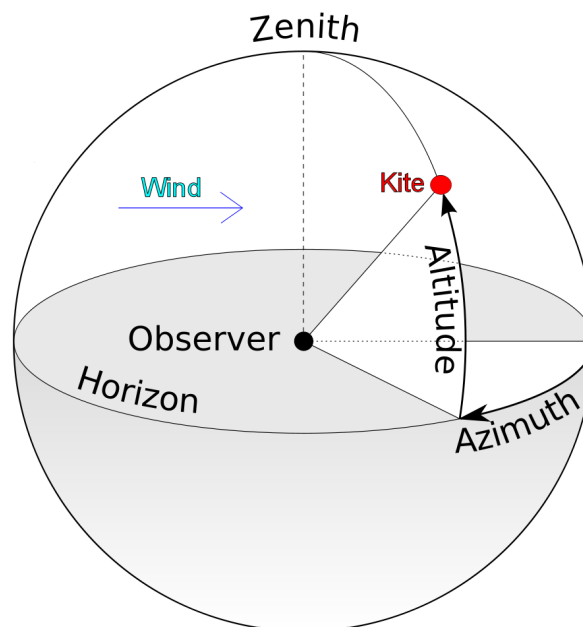
Figure 3.8: Kite coordinate system - The kite is in the power zone when both azimuth and altitude are close to zero. If azimuth angle is close to ± 90 *deg* then the kite is in the edge of the wind window. Picture based on (18).

3.4.4 Kite steering mechanism

Two-lines kites are controlled by applying a differential force in the cables. Common experience tells us that pulling the right or left line results in clockwise or counter-clockwise motion respectively[1]. Exactly what mechanism is responsible for this behaviour is the subject of a strong debate among kite designers and kite surfers around the world. Several different hypotheses have been made.

In (19) a LEI kite[2] is analysed with a detailed multibody model showing that the yawing of the kite is mainly due to a deformation shown in fig. 3.9. The relative displacement of the wing tips creates an offset so that the aerodynamic forces in spanwise direction generate a yaw moment.
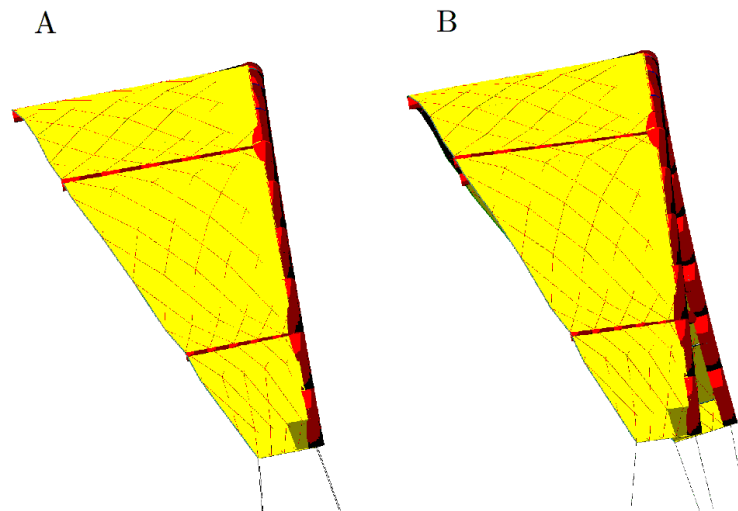
Figure 3.9: Kite steering mechanism - The kite before the right steering input (A) and after (B). Relative wind goes from right to left. Picture from (19).

In (20) a static model of a kite represented by flat disks showed that 'when the kite is held with a roll angle applied, the disks angles of attack become unequal. This causes a change in the magnitude, direction, and point of action of the aerodynamic forces on each disk, which can lead to a yaw moment'.

---

reduce the angle of attack and de-power the kite.

[1]As seen from the base station or kite surfer.

[2]Commercial surf kite, Naish Aero 6.

While in the VLM kite simulator shown in the following chapters, the yaw moment is due to the local twist of the wing tips which changes the aerodynamic forces. This last steering mechanism is much more similar to that of a paraglider.

4

High altitude wind plants

This chapter aims to provide a general introduction of the research state of the art. Until now, there have been several attempts for extracting power from high altitude winds[1]. High altitude wind energy is a relatively new field of study and the most important steps towards industrial maturity have been made in the last decade.

There are several companies involved in this field and some of them promise to be ready for large scale contracts in a short time, but still none of them already made it to massive energy production and sales.

4.1 Common features

Before introducing the main industrial configurations to extract power from high altitude winds, it is important to say that all these concepts share a few common components that are:

- one or more electrical generators,

- one or more tethers (cables),

- an aerodynamic flying device, being a kite, a rigid wing, a kite plane, a gyrocopter, a balloon, etc..

Examples can better clarify how those components are functionally linked together.

---

[1] High altitude winds contain higher power than ground level winds as shown in chapter 2.

4.2 Ground-gen and fly-gen

A major feature that can help to classify the different concepts is whether the electrical generators are placed on board the flying device or at the ground station. If the electricity is produced at the ground station it is referred to as ground-gen, whereas if the generation is in the air then it is called fly-gen[1]. Schematic representations of both these concepts are shown in fig. 4.1.
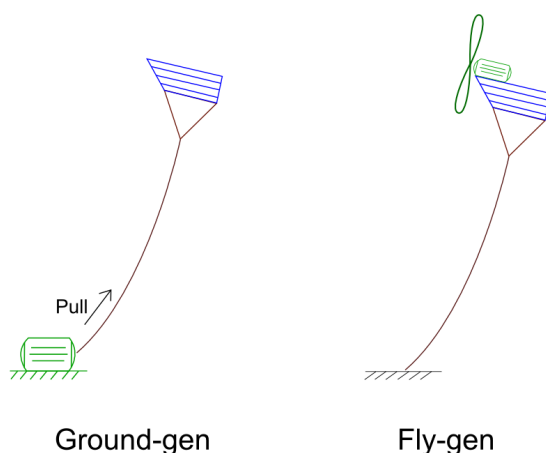
Ground-gen   Fly-gen

Figure 4.1: Ground-gen and fly-gen concepts - Ground-gen has the generator at the ground station, fly-gen has a flying generator (usually, but not always, a wind turbine).

4.3 Ground-gen state of the art

Among the major organizations involved in ground-gen technologies, a comprehensive view is provided here with four examples[2]: Kitegen, Skysails, TU Delft, Ampyx Power.

4.3.1 Basic mechanism

It is important to know that almost all ground-gen systems share the same working principle. Power is not generated continuously but is generated in power cycles made of two phases as shown in fig. 4.2. During the reel-out phase[3] the flying device is driven

---

[1]Energy produced by fly-gen concepts is often referred to as Airborne Wind Energy (AWE), though often AWE is used with the same more general meaning of high altitude wind energy.

[2]Other ground-gen companies and concepts are active around the world, but are not described.

[3]Also called power phase.

in loops with horizontal-8-figure shape at high speed, while the cable is slowly reeled out. The generators produce then a large amount of power P_{out} thanks to the traction force F_{out} combined to the reel-out speed v_{out} of the cables.

$$P = F_{out}v_{out} \tag{4.1}$$

During the reel-in phase the flying device is controlled in such a way that its traction force becomes negligible, for example is kept at the side of the wind window. Electricity generators reverse their function and work as motors to quickly retract the cables. Reel-in phase needs energy.

The energy generated during reel-out phase substantially exceeds the energy needed during the reel-in phase, thus making it possible for the system to globally generate power. An example of the resulting time history is shown in fig. 4.3.

Reel-out phase (energy generation)

Reel-in phase (energy consumption)
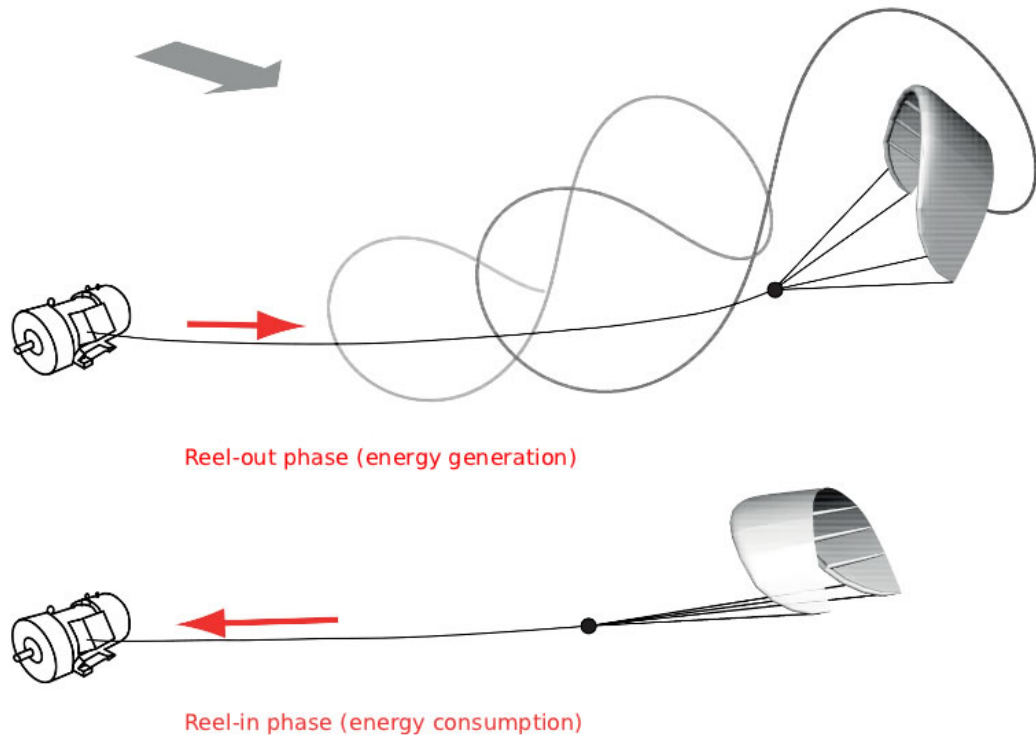
Figure 4.2: Pumping cycle phases - Reel-out phase (top) with kite pulling the cables by flying 8-figures. Reel-in phase (bottom) with motors drawing back the cables while kite is not generating high lift force. Picture from (21).
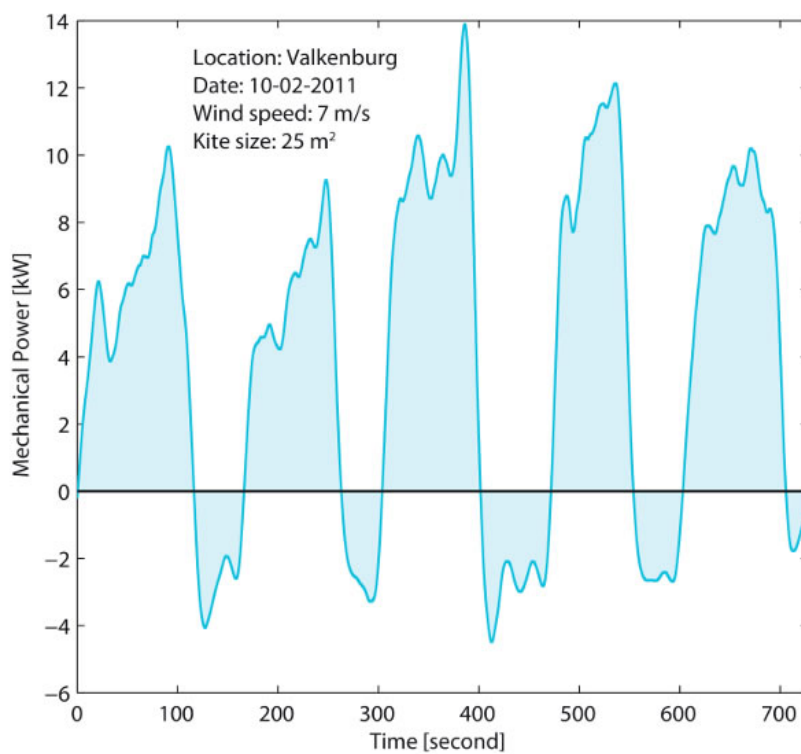
Figure 4.3: Power generation time history - Reel-out phases generate power (output), while reel-in phases require power to draw the cables back. Almost five complete cycles are shown. Picture from (21).

4.3.2   Kitegen

The Kitegen project involves several organizations in Piedmont, Italy and has built a 3 MW power plant which is currently in test phase. Kitegen project proposes two main configurations: Kitegen Stem and Kitegen Carousel. The company is now planning to build a wind farm composed of 50 Kitegen Stem machines.

The 3 MW power plant is a Stem system and is shown in fig. 4.4. It uses the general pumping cycle[1] already described. It uses a kite with 2 independent cables, one cable for each wing tip. Several generators/motors are used to control each single tether so that the kite can steer and perform 8-figures manoeuvres.

Figure 4.4: Kitegen Stem - 3 MW power plant, located in Sommariva Perno (CN), Italy. Picture from (22).

The Carousel is a larger scale system (figs. 4.5 and 4.6). According to (23), this configuration would allow GW scale power production: 1 GW would be possible with a diameter of 1500 m, using 8 km^2 of land and it would bring energy cost[2] down to about 10-15 €/MWh.

---

[1]Also referred to as yo-yo cycle.

[2]Currently the cost of energy from fossil fuels ranges between 60 and 70 €/MWh.
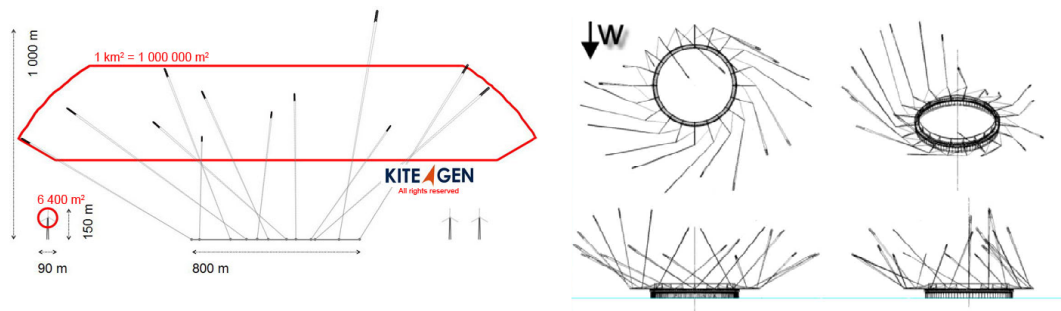
Figure 4.5: Kitegen Carousel configuration - Large scale power plant, concept. Picture from (24).
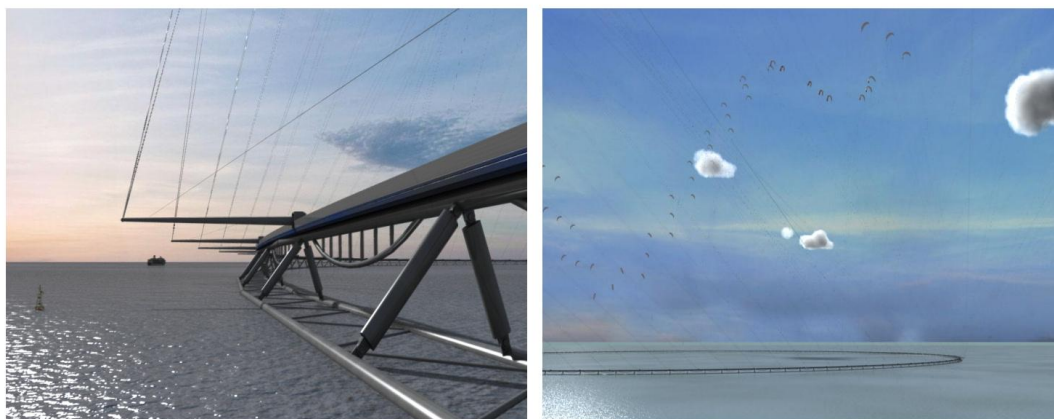
Figure 4.6: Kitegen Carousel offshore - Offshore *GW* scale power plant, concept. Picture from (24).

Currently, the company is mainly using leading edge inflatable kites, but research is being done to use a semi-rigid wing which would be light-weight, with an high aerodynamic efficiency and capable of bearing high loads (25). The concept of the wing is shown in fig. 4.7.

Figure 4.7: Semi-rigid wing - High efficiency wing, concept. Picture from (25).

4.3.3 Skysails

Skysails GmbH is a German company active in the field of kite power. In addiction to electricity generation, they also offer wind propulsion systems for ships as shown in fig. 4.8. The kite towing system reduces fuel consumption (fig. 4.9). At the moment, SkySails is finalising the development of a 320 m^2 kite capable of generating tractive forces of up to 16 *tons*. During operations, Skysails towing kites can reach speeds of up to 200 km/h.

4.3.4 TU-Delft

Delft University of Technology is an important institution that carries out research in airborne wind energy. They fly a 25 m^2 LEI kite as shown in fig 4.10 and recently

Figure 4.8: Skysails kite towing system - Kite towing the ship with only one cable. Picture from (12).
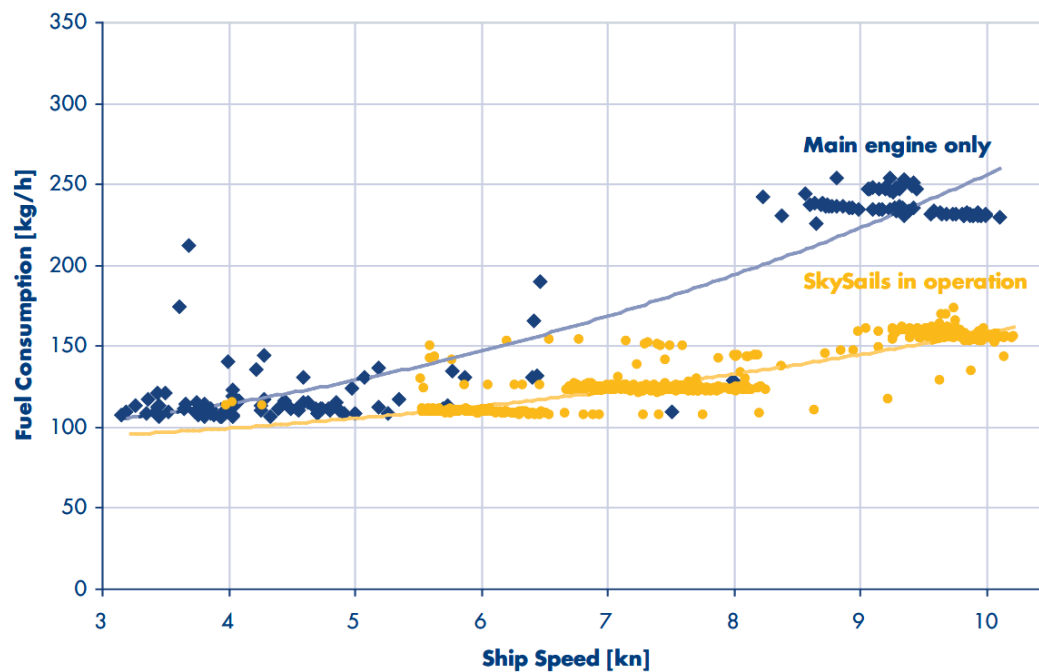
Figure 4.9: Skysails fuel consumption - Comparison of fuel consumption aboard MV 'Theseus'. Picture from (26).

achieved automatic flight. The link to the base station is achieved with only one cable and the flight control is done remotely with a suspended control unit which, beside steering manoeuvres, allows to control the angle of attack for de-powering the kite when needed[1]. Their prototype can generate 6.5 kW average power with a wind speed of 7 m/s as shown in fig4.3.

Figure 4.10: TU Delft kite - 25 m^2 leading edge inflatable kite with suspended, tele-operated control unit. It can reach 70 - 90 km/h generating a force of about 4000 N. Picture from (27)

4.3.5 Ampyx Power

Ampyx power is a Dutch company developing a ground-gen concept. Their system uses a glider plane tethered with one cable to perform the pumping cycle as shown in fig. 4.11. They are currently working on a prototype with a wingspan of 5.5 m, though their final aim to achieve 1 MW scale plants. Such plants would have wingspans of $35 - 40 \ m$, aircraft load of 400 kN, cable diameter of 30 mm and weight around 3000 kg.

---

[1]Note that to have de-powering capability, kites need at least an additional tether. For example, kites with two power cables such as those used by kite surfers have a third line to de-power the kite.
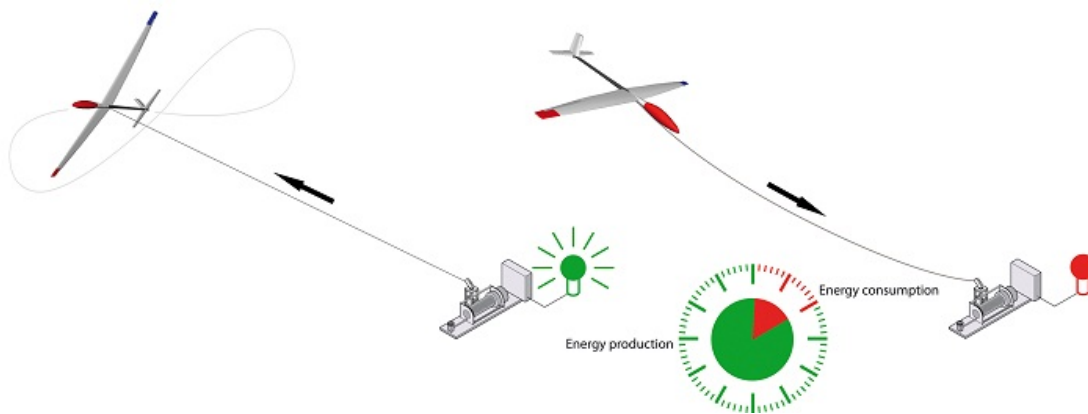
Figure 4.11: Ampyx Power concept - Glider plane reel-out (left) and reel-in (right) phases. Picture from (28).

4.4 Fly-gen state of the art

Among the major organizations involved in fly-gen technologies, one example is provided here: Makani Power.

4.4.1 Makani Power

Makani Power is a company based in California, they fly a rigid wing with turbines on board as shown in fig. 4.12. Makani achieved autonomous power generation in July 2011 and is currently developing a 600 kW airborne wind turbine.

Their system uses a rigid wing flying a circular pattern (fig. 4.13) while the turbines on board capture the wind power which is then transmitted to the ground through the tether. Note that there is no pumping cycle and the cable therefore does not need to reel in and out during normal operation.

4.4.2 Others

Other companies are building or have built prototypes that, instead of quickly sweeping trough the air, capture wind energy by hovering in one position high above the ground. Such concepts are not described here.
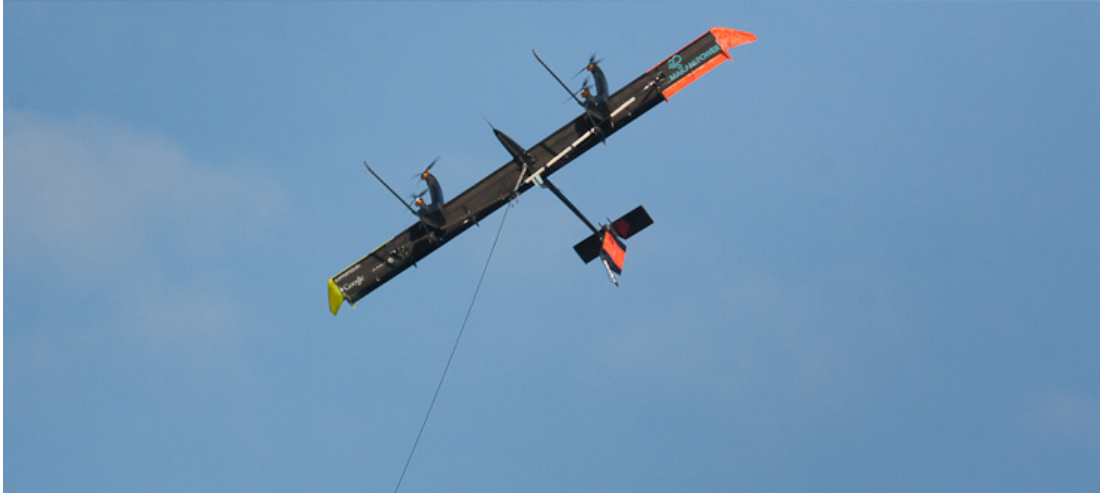
Figure 4.12: Makani Power wing - The wing with turbines on board is held by the power cable. Picture from (29).

4.5 Technologies discussion

A brief discussion related to the most important topics of ground-gen and fly-gen technologies is provided.

4.5.1 Energy Returned On Energy Invested (EROEI)

An important index to measure the performance of an energy source is the EROEI. It measures the ratio between the energy produced by a particular energy source and the energy used to obtain that production.

$$EROEI = \frac{E_{out}}{E_{in}} \tag{4.2}$$

It is clear from its definition that, for example, large scale power plants for primary energy production need to use technologies with $EROEI > 1$, while energy vectors[1] have $EROEI < 1$. EROEI, being based on physical quantities does not depend on economical variables such as inflation and cost of fuel. It is therefore a more robust index, especially when dealing with long term analyses. EROEI has its drawbacks and

---

[1]Technologies to deliver the energy from the source to the place where it is consumed, such as hydrogen or batteries.
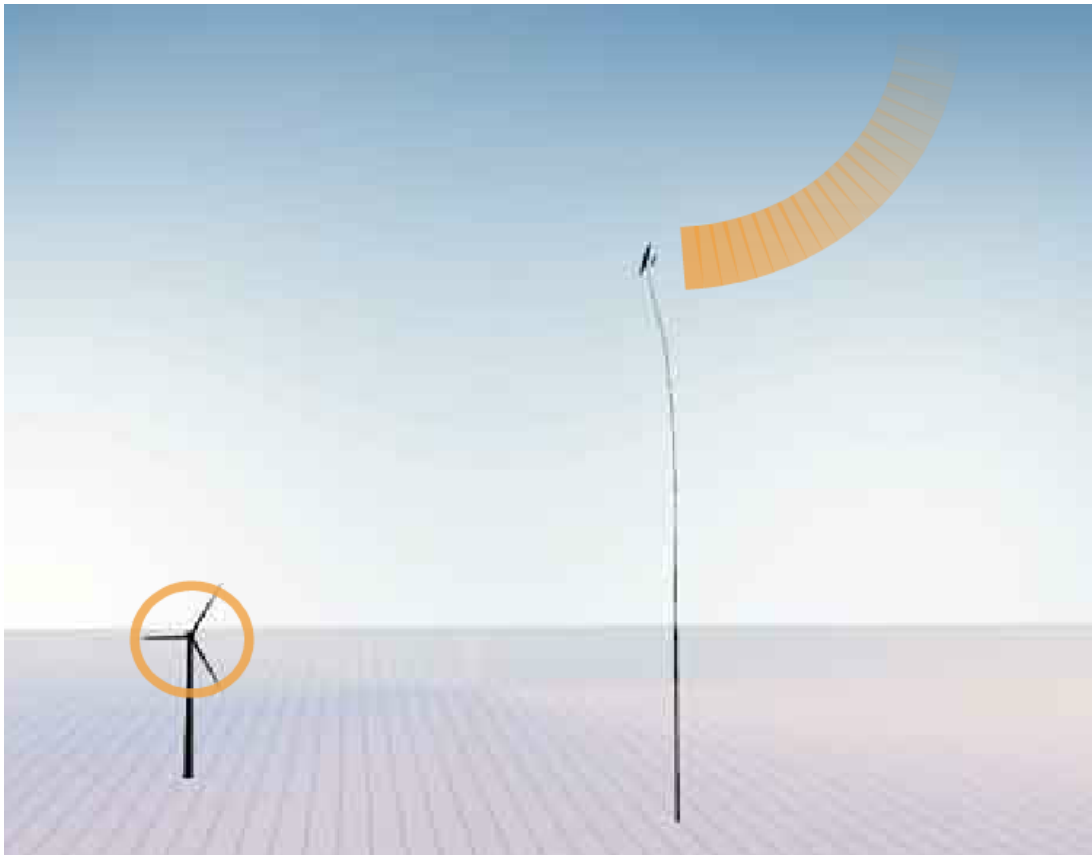
Figure 4.13: Makani system - In a conventional wind turbine (left), about 80 % of the generated power comes from the outermost 20 % of the blades. In an high altitude wind plant (right) the kite trajectories have greater potential to better exploit the airflow swept by the wing. Picture from (30).
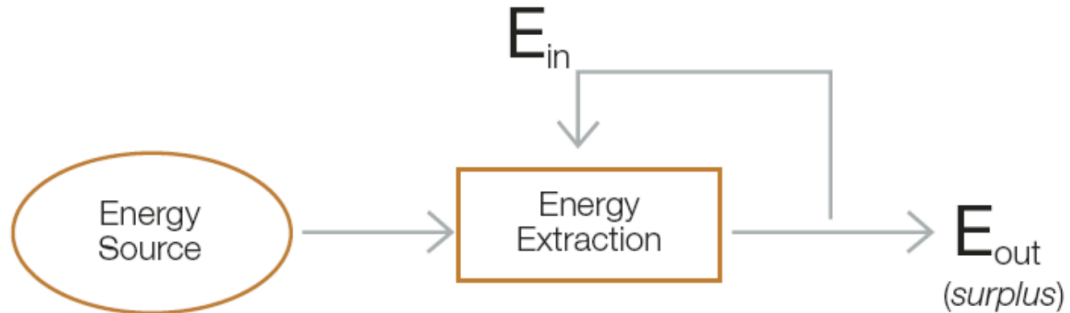
Figure 4.14: EROEI index meaning - It is important to be aware that EROEI is not an energy balance. The energy coming from the original energy source is not included in the denominator. For wind power for example, the kinetic energy of the wind (energy source) is neglected. Picture from (31).

in some cases it should not be considered the only relevant index[1]. It also might be hard to compute and taking account different cost factors may lead to very different results. It is anyway a useful index that helps us to quantify the effort needed to generate energy and is therefore related to the economical performance of a plant.

High altitude wind plants have a great potential in this sense. According to conservative estimates the EROEI of a Kitegen Stem system greatly exceeds that of conventional wind power (32) and assumes values comparable to that of oil[2]. Estimates of Kitegen Carousel are even more optimistic (33). Fig. 4.15 shows examples of EROEI for conventional sources.

4.5.2 Power output

On order to match the electricity demand, a power plant has to supply energy continuously. Configurations such as those of Kitegen Stem or TU Delft need to store the energy generated during reel-out phases and release that energy during reel-in phases while concepts such as those of Kitegen Carousel or Makani Power have the advantage of naturally generate a more constant power output[3].

---

[1]For example, an energy source may be very convenient in terms of EROEI without being enough to satisfy the demand, or without being present in a certain geographical area.

[2]Referred to oil easy to extract, as it generally was several decades ago.

[3]Wind power may not be present all the time but, when wind is available, also periodical movements (8-figures or circular patterns) and natural wind turbulence make the power output not constant.
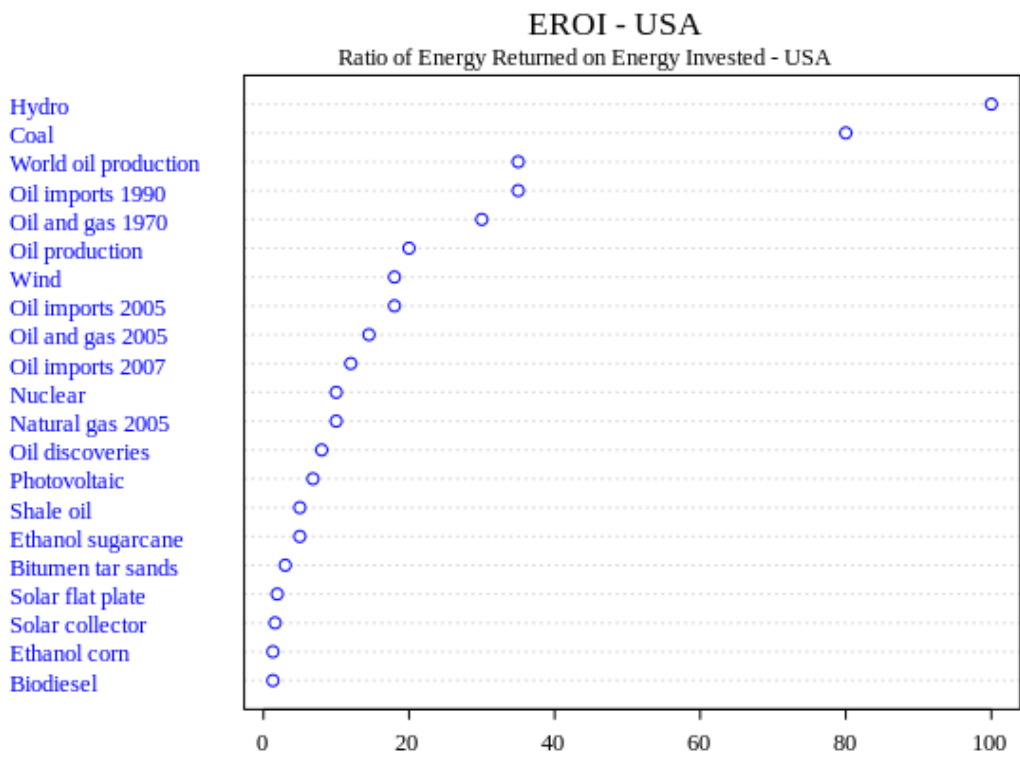
Figure 4.15: Approximate EROEI of various energy resources for the United States - Energy sources are listed with decreasing EROEI index. EROEI values are on the horizontal axis. Picture from (34), data from (35).

36

4.5.3 Launching

It may happen to have a strong wind at high altitude meanwhile having a very low wind at ground level. In such scenario, Makani Power has a built-in ability to automatically take off and reach a reasonable altitude. By contrast, for a ground-gen concept, launching phase needs other methods to be implemented.

4.5.4 Weight restrictions

Lifting up in the air a kite is very different then lifting a wind-turbine. Ground-gen technologies, having their generators at the ground station, are less limited in weight and dimensions. Moreover, generators for ground-gen do not have to be lightweight and are therefore cheaper, requiring less design accuracy.

4.5.5 Long cables controllability

Thinking of a small kite with very long cables may raise some concerns about the feasibility of the flight itself. However several tests[1] showed that the controllability of the kite when flying with very long cables is not a problem as the manoeuvres become slower and the high altitude wind steadier. Furthermore if the cables twist, meaning for instance that the kite has made at least one complete turn in a circular pattern, common kitesurfing experience tells us that this is not a problem and Kitegen claims than the kite is still controllable even after 10 twists (36).

4.5.6 Durability

Kites, such as those used by TU Delft and Kitegen are inherently less reliable then a rigid wing. The lower cost of materials comes together with a lower durability and the need to safely predict the life limits of such materials.

Tethers are made of lightweight strong Dyneema[2] fibers. Expensive as they are, assessments of cables fatigue life in ground-gen concepts is vital for the profitability of the systems (fig. 4.16).

---

[1] By TU Delft and Kitegen. Note that in TU delft configuration the steering mechanism always controls short cables.

[2] Used, among others, by Kitegen and Skysails, this fiber has a density of 970 kg/m^3 and is therefore slightly lighter than water.
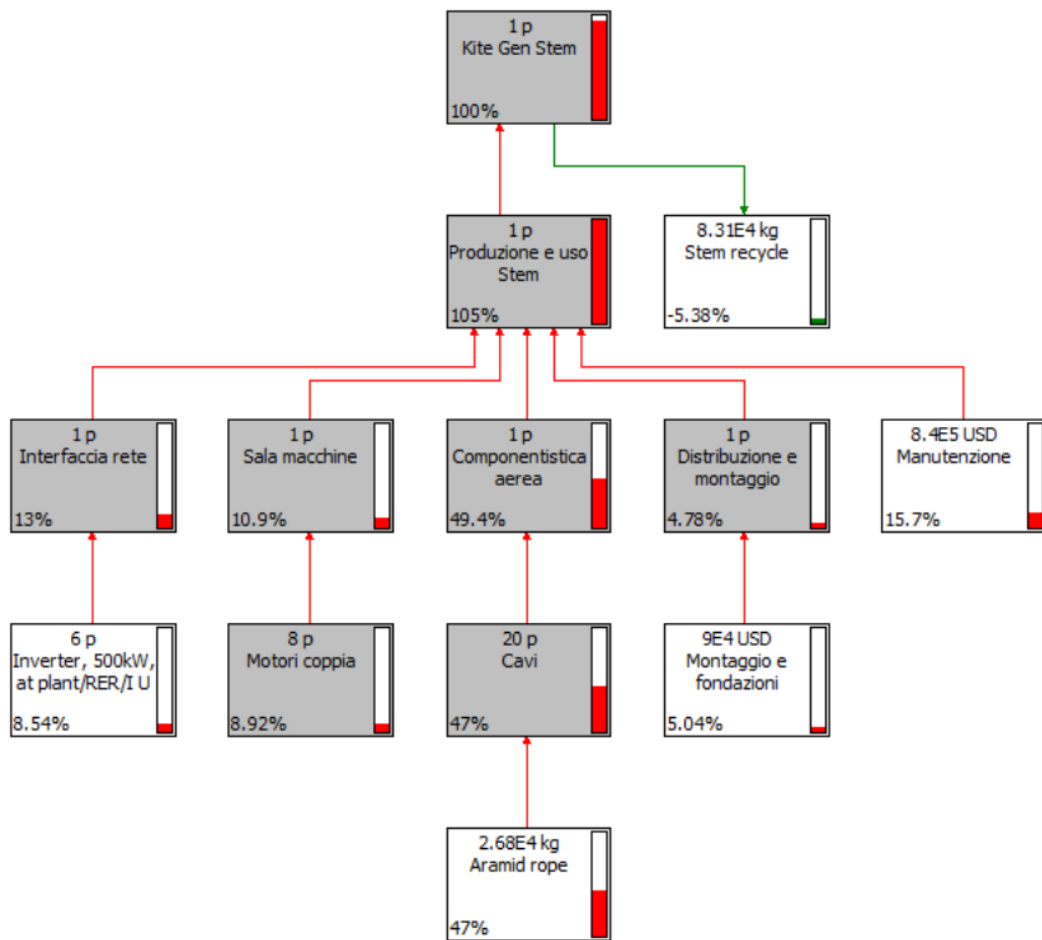
Figure 4.16: Kitegen Stem life cycle assessment - In the computation of the total energy needed to produce a Kitegen Stem plant, cables account for almost 50 % of the total energy. Picture from (32).

4.5.7 Safety concerns

High altitude wind power plants have several problems to be tackled. First of all, the flying device may crash into the ground, or even against an aircraft (37, 38).

Figure 4.17: Safety risks - Picture from (37).

Possible solutions could be to install high altitude wind farms offshore or in areas with low population density, or to set up no-fly zones similar to those already in use for nuclear power plants or oil refineries.

High altitude wind power plants have to deal with large amounts of power and energy and this creates electrical related issues. While ground-gen technologies only need to supply energy to the grid, fly-gen technologies have to first transmit their electrical energy from the flying device to the ground station. In this last case the tethers would necessarily be electrified[1].

---

[1]Further design details are then required. For example fly-gen company Makani Power makes use of redundancy such as duplicate control surface and avionics.

4. HIGH ALTITUDE WIND PLANTS

5

The importance of aerodynamic efficiency

Aerodynamic efficiency is defined as the ratio between lift and drag and is a fundamental design variable for high altitude wind energy systems. In this chapter the reasons why this is perhaps the most important aerodynamic parameter for kite design are explained.

$$E = \frac{L}{D} = \frac{C_L}{C_D} \tag{5.1}$$

5.1 Crosswind model

In systems such as those of Kitegen or Skysails, the kite is in the power zone during the pumping cycle (see fig. 3.7). Flying in the power zone allows an higher kite velocity, which leads to higher lift and higher generated power. To keep the kite flying in the power zone the kite is therefore controlled into figure-of-8 or circular patterns. In this case the kite is said to be in crosswind flight.

5.1.1 Simple model

Analysing the velocity triangle of crosswind flight is a fundamental step to understand the strength of high altitude wind power. A very simple mathematical model describing the crosswind horizontal flight at 0 *deg* elevation angle (altitude) and 0 *deg* azimuth[1] is shown in fig. 5.1. It is a simplified version of Loyd's model (11). Inertia forces are

---

[1]This means that the tether is aligned in the direction of the wind.

neglected, as the kite is assumed to be in steady state flight conditions. Reel out speed is assumed to be zero and cables aerodynamic drag is not taken into account.
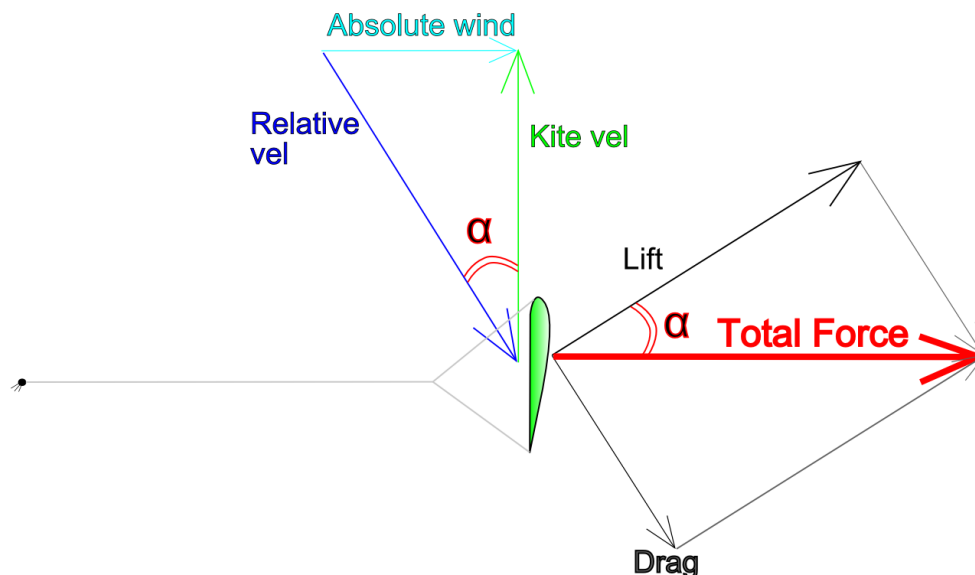
Figure 5.1: Crosswind steady state flight - View from the top. Given a certain absolute wind speed, an high lift to drag ratio means an high kite velocity. Notice that α is not necessarily equal to the angle of attack.

In fig. 5.1 there are two vector sums, one is the wind velocity triangle and one is the aerodynamic force composition. From the similitude of these two triangles it is possible to write

$$\frac{V_{kite}}{V_{wind}} = \frac{L_{ift}}{D_{rag}} = E \tag{5.2}$$

where V_{kite} is the kite velocity, V_{wind} is the absolute wind velocity. The tether force T is in equilibrium with the aerodynamic forces[1] and is

$$T = \sqrt{L^2 + D^2} = L\sqrt{1 + \frac{1}{E^2}} \tag{5.3}$$

---

[1]Notice that, because of the equilibrium, the aerodynamic force must lie in the direction of the cables as there are no other inertia forces.

Lift force is

$$L = \frac{1}{2}\rho(V_{kite}^2 + V_{wind}^2)C_L A = \frac{1}{2}\rho V_{wind}^2(E^2 + 1)C_L A \qquad (5.4)$$

If the aerodynamic efficiency is high, then the tether force is

$$T \approx \frac{1}{2}\rho V_{wind}^2 E^2 C_L A \qquad (5.5)$$

This simple model highlights the importance of aerodynamic efficiency. For example, using conservative numbers, having $E = 10$ and $V_{wind} = 6$ m/s means that the kite can achieve velocities up to 60 m/s which for a 16 m^2 kite can generate a tether force of about 15000 N depending on the lift coefficient.

5.1.2 Loyd's model

In his paper (11), Loyd included the reel out speed and calculated that the optimum power output P_{opt} for crosswind flight occurs at reel out speed equal to 1/3 of the wind absolute velocity and is equal to

$$P_{opt} = \frac{1}{2}\rho V_{wind}^3 \frac{4}{27}E^2 C_L A \qquad (5.6)$$

where $\frac{1}{2}\rho V_{wind}^3$ is the wind power density. In his paper, Loyd also showed that keeping the kite fixed in the wind window[1] results in a much lower power output.

From this model it is clear that, for high altitude wind plants that fly crosswind neglecting the cables drag, the aerodynamic efficiency, more exactly the factor $E^2 C_L$, plays a fundamental role. A graph showing this factor for the wing described in section 7.4.1 is plotted in fig. 5.2.

---

[1]The kite is kept at the highest possible altitude, much like a child playing with a single line kite would do.
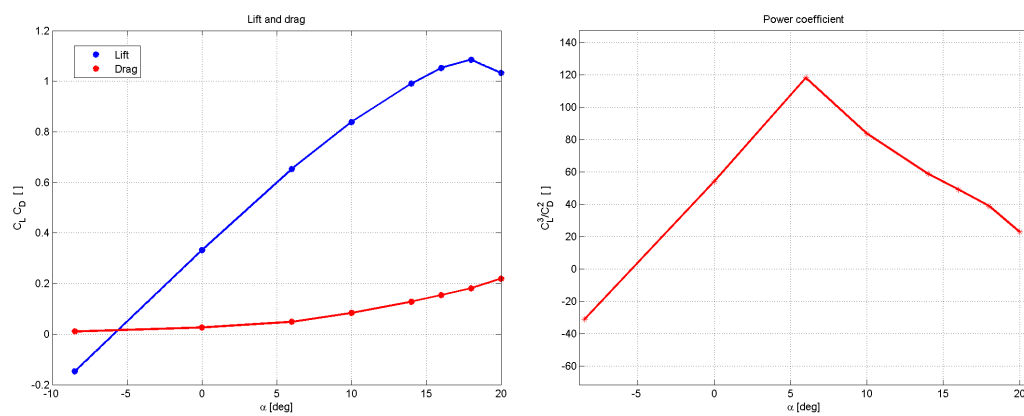
Figure 5.2: Power coefficient according to Loyd's model - E^2C_L as function of the angle of attack.

6

VLM Kite simulator

In this chapter, a description of the multiplate VLM kite simulator developed in this thesis is provided. It is implemented in the Matlab-SimMechanics environment together with a modified version of the aerodynamic open-source software Tornado. The first integrates the dynamics of the kite-cables system, represented with a multibody model and the second computes the aerodynamic forces to be used during the integration. In addition to these, a model for taking account of the aerodynamic drag on the cables is illustrated. An introductory graphical representation of the VLM kite simulator is in fig.6.1.

6.1 Kite dynamics and previous work overview

6.1.1 Kite models

Several models have been proposed for analysing the dynamics of kites. In (39) a few of them and their validation are discussed: a point model, a rigid-body arc shaped model and a flexible multi-plate model. Other models have also been developed in the literature.

The point model is very simple and considers the kite as a point with mass. This kind of analysis is used to roughly investigate trajectories and performance of the kite. It cannot be used to study the kite's flexible structure and is not suitable for control design either.

Another approach considers the kite as one rigid body in a 3D space. An example of such model for a kiteplane can be found in (40) where the number of degrees of
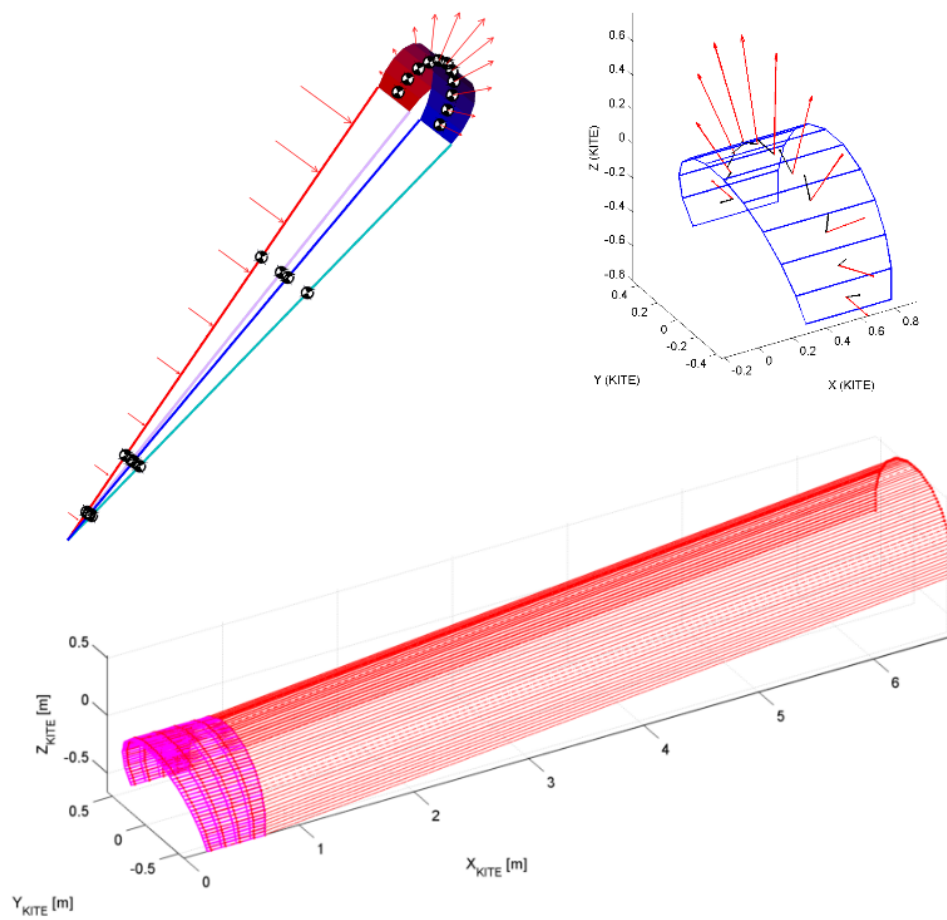
Figure 6.1: Kite VLM simulator - Multibody layout (top left). Kite geometry (top right). Vortex lattice (bottom).

freedom is reduced from 6 to 5 by coupling together the roll and yaw motion.

A further increase in complexity leads to flexible body models where deformation occurs through predetermined modes. And, finally, more complex models are the multiplate flexible models. Fig. 6.2 shows a kite composed of multiples flat partitions that can pitch and roll independently from each other allowing the kite to twist and flap[1].
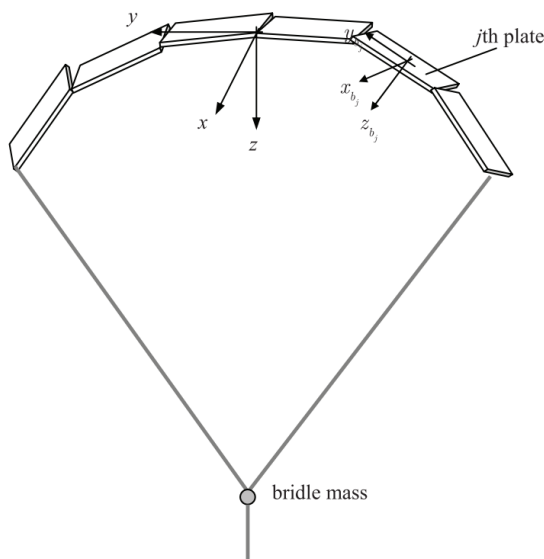
Figure 6.2: Multiple flat plate kite - Multiplate flexible model. Picture from (39)

To analyse the behaviour of the the kite canopy and the important fluid structure interactions that occur during flight, a multibody model is developed in (19). A picture illustrating the detailed modelling reached in this work is in fig. 6.3.

In this thesis a multiplate model with vortex lattice method aerodynamics is described.

6.1.2 Cable models

In a high altitude wind plant the kite-cable interaction cannot be neglected. Cables mass may represent almost the total mass of the system. They are also used to control the kite by generating the needed deformation to eventually modify the aerodynamic

---

[1]Also called jellyfish motion, flapping is an arc shape bending that makes the C-shape curvature increase and decrease.
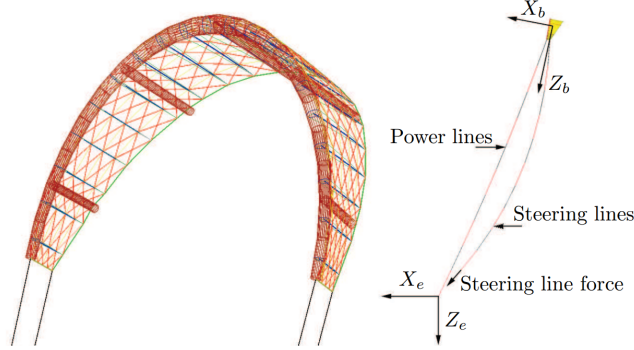
Figure 6.3: Multibody kite - Detailed multibody analysis. Picture from (19).

forces distribution. The cables model therefore plays a fundamental role in determining the performance of a tethered kite.

Several publications are available in the field of cables in general. Energy balances and forces distribution are common methods to deal with the physics of the problem. Also for airborne wind energy purposes, many structural cable models have been proposed. For example the length can be modelled by varying the stiffness and damping factor of a spring and damper system in such a way that a long cable has high damping and low stiffness while a short cable has low damping and high stiffness[1] or the cable might be modelled as a rigid rod either with or without mass. In (19) and (41), a more complex approach considers the cable as a set of hinged rigid bodies, similar to a nth pendulum. Such models are shown in fig. 6.4.

In this thesis each tether is modelled as a rigid rod with a spring-damper system for elongation and control.

6.2 SimMechanics

SimMechanics is a commercial simulation environment integrated in Matlab for 3D multibody systems. Such systems are modelled with block diagrams representing bodies, constraints and force elements. The software automatically builds and solves the equations of motion of the entire system.

---

[1]The spring and damper also models the 2 % maximum strain of a Dyneema cable.
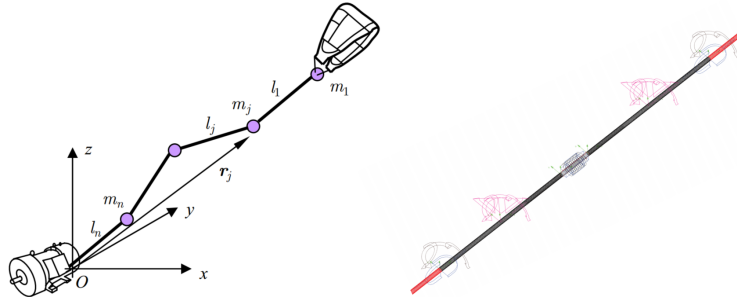
Figure 6.4: Multibody cable models - Cable sections are hinged together. Pictures from (41) and (19).

6.2.1 Solving the equations of motion

The process involves several steps as shown in fig. 6.5.

First, the data entries of the block diagram are checked. Then the physical network[1] is built and the system of equations can be constructed[2]. These equations are finally solved by numerical integration[3].

6.2.2 DAE and ODE

'A physical system can be modelled with Ordinary Differential Equations (ODEs), algebraic equations or both. ODEs govern the rates of change of system variables and contain some or all of the time derivatives of the system variables. Algebraic equations specify functional constraints among system variables, but contain no time derivatives of system variables. Without algebraic constraints, the system is differential (ODEs). Without ODEs, the system is algebraic. With ODEs and algebraic constraints, the system is mixed Differential-Algebraic (DAEs).'[4] (44).

---

[1]Further details about physical networks can be found in (43).

[2]There are two types of system variables: dynamic and algebraic. The difference between the two is whether the time derivative of the variable appears or not in the equation of motion.

[3]During the simulation, in case of an event such as, for example, a discontinuity resulting from a valve opening or a hard stop, the solver performs a transient initialization. More information can be found on (42).

[4]It is important to note that Matlab solvers can only handle ODEs or index-1 DAEs. So, if needed, 'the index of the system of equations is reduced by identifying the higher index constraint equations and then differentiating these equations in time. By doing this, it is possible to reduce many common
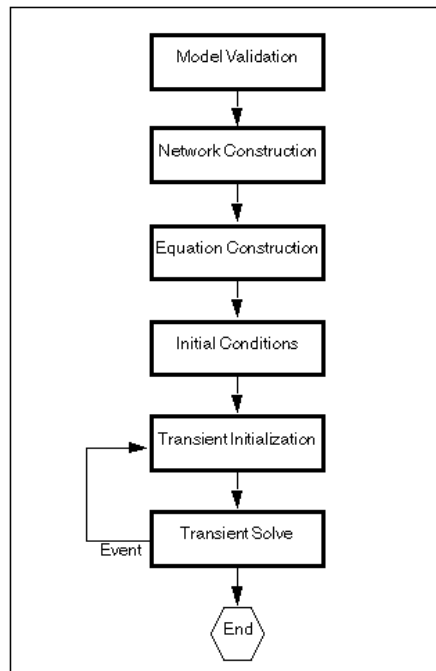
Figure 6.5: Solver run flow chart - The main steps for solving a physical model are shown. Picture from (42).

6.3 Vortex Lattice Method with Tornado

Tornado is an open source software[1] based on Vortex Lattice Method (VLM). It computes the aerodynamic forces distribution for custom aircraft geometries and custom flight conditions.

6.3.1 Vortices and induced drag

Vortices are spinning flow patterns that are generated by lifting surfaces. An example in shown in fig 6.6. In an aircraft, they are generated by the pressure difference between top and bottom sides of a wing and are responsible for decreasing the lift[2] thus resulting in the lift-induced drag. This effect is taken into account by the VLM in that it models the flow field induced by the vortices.

---

index-2 problems to index-1 and index-0. Once the index has been reduced, the resulting system is presented to the integrator as a DAE or ODE depending on the type of integrator. The integrator integrates the system to generate the simulation results.'(43).

[1]The software was written originally by Tomas Melin (45). It is possible to download it from (46).

[2]If compared with the lift that would be generated by a wing of infinite span.

50

Figure 6.6: Vortex pattern generated by the passage of an aircraft - Picture from NASA in public domain.

6.3.2 How steady VLM works

The Vortex Lattice Method used in this simulator represents the wings as planar surfaces on which a system of horseshoe vortices is placed as shown in fig. 6.7. Each horseshoe, also called vortex sling, is composed of seven vortex segments[1]. Each of them induces a flow field in the potential flow domain. The strength of each vortex sling is computed by imposing the boundary conditions[2]. Once that this is done, the forces acting on the panels can be computed using the Kutta-Joukowski theorem.

It is important to note that Tornado only performs steady state simulations. This also means that the program cannot compute important time dependent factors such as $C_{L\dot{\alpha}}$.

6.3.3 VLM range of operation

The vortex lattice method is only valid with small angles of attack, where the potential flow is a reasonable approximation of reality. Fig. 6.8 shows an example of results

---

[1]Standard VLM uses three vortex segments and each panel has a wake (coming off that specific panel) which is in a different position than all other panels' wakes. Tornado uses seven vortex segments and the wake coming off the trailing edge of each panel realigns with the wake of the last panel behind it which contains the trailing edge of the wing. Further details can be found in (45).

[2]The flow field has to be tangent at each panel (at the panel's collocation point).
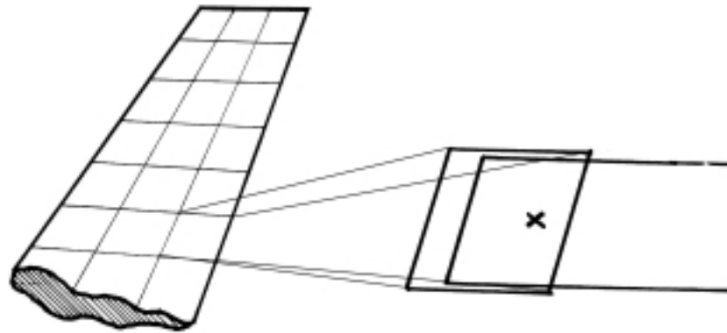
Figure 6.7: Horseshoe vortex system on a single panel - In this example the wing has 21 panels each panel has its own vortex sling but only one is shown. The enlarged panel shows how the vortex horseshoe is positioned with respect to the collocation point where the boundary conditions will be met. Picture from (45).

obtained with a known geometry in Tornado.

6.4   Kite cables layout

The simulator uses a flexible multibody kite held by four cables. Front cables are used to control the angle of attack while rear cables allow the kite to yaw. An example of this layout is show in fig. 6.9.

6.5   Kite model

6.5.1   Geometry

The kite geometry is built following the Tornado preprocessor format which has a great flexibility[1]. This means that the geometry can either be constructed following the Tornado instructions or can be manually edited. An example of a kite geometry is shown in fig. 6.10. The kite is modelled as a wing made of several rigid 'partitions'. Each partition is then divided into several 'panels'as illustrated in fig. 6.11. For each

---

[1]The only requirement is that the kite has to be symmetrical about the XZ plane (kite coordinate system) and without twist at the wing tips. A tool to check if the dihedral, sweep, and twist make a symmetrical geometry has been implemented.
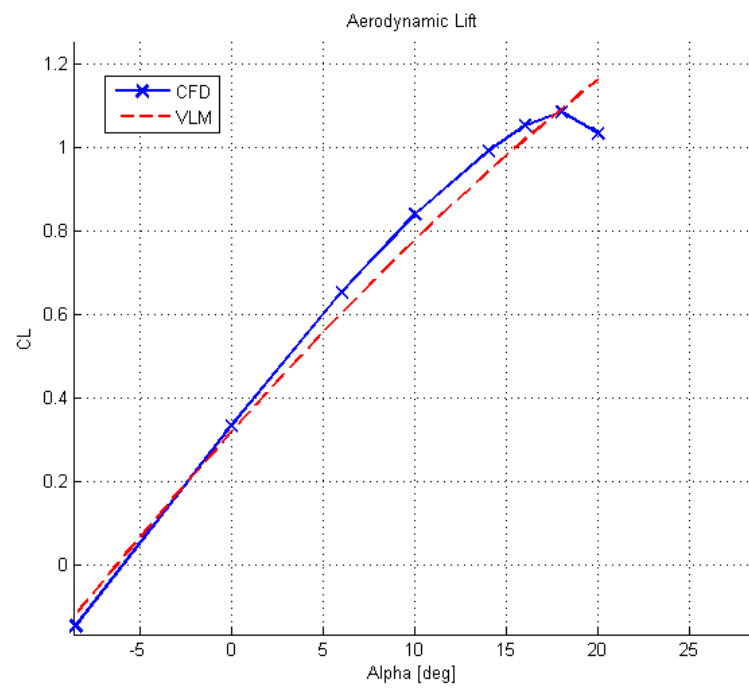
Figure 6.8: VLM and linear aerodynamics - In this example, VLM produces good lift coefficients with angles of attack smaller than 18 *deg*.
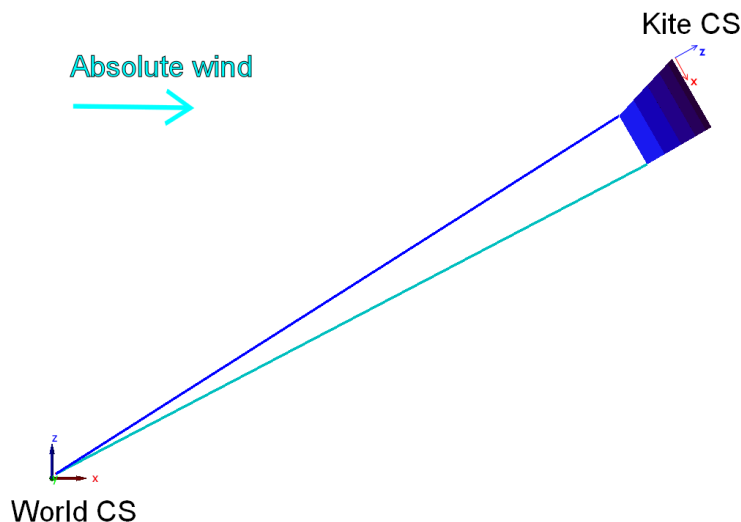
Figure 6.9: Kite global layout - Side view. The kite simulator uses four cables to control the kite. The right cables are shown here. Blue: front cable. Light blue: rear cable. The two main Coordinate Systems (CS) of the simulator are also highlighted.

partition the user can change dihedral, twist, sweep, taper, dimensions and number of panels.

6.5.2 Structural model

Each partition is modelled as a rigid body and is linked together with the next one by means of rotational springs and dampers. The result is an overall flexible kite with its own structural stiffness[1]. During the simulation each partition can assume its own orientation and the overall shape of the kite can therefore change. Two examples are shown in fig. 6.12 where the kite flaps and twists.

6.5.3 Inertial properties

For each rigid partition also the inertial properties have to be chosen.

---

[1]This model can be adapted to both a LEI kite and a ram air kite (described in section 3.2). A LEI kite is held at the wing tips and the shape is given by the stiffness of the inflatable tubes and can therefore flap easily by locally changing its dihedral. A ram air kite does not have any structural stiffness and the shape is usually given by the bridle system and therefore could be better represented with a stiff dihedral behaviour.
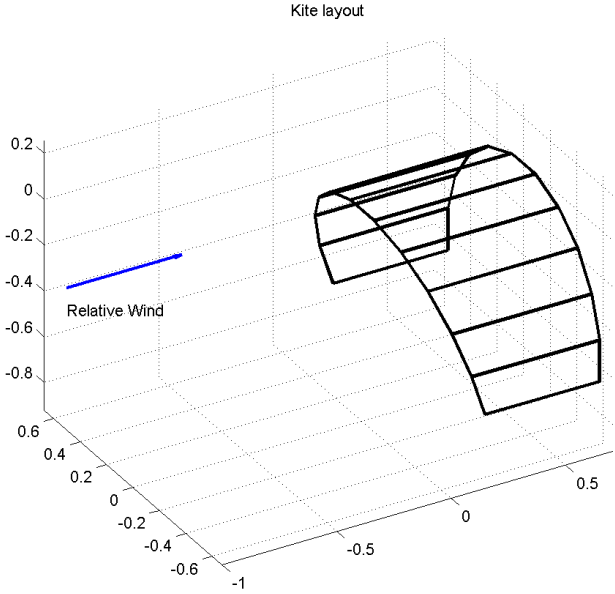
Figure 6.10: Example of kite geometry - The kite is composed of 11 partitions.
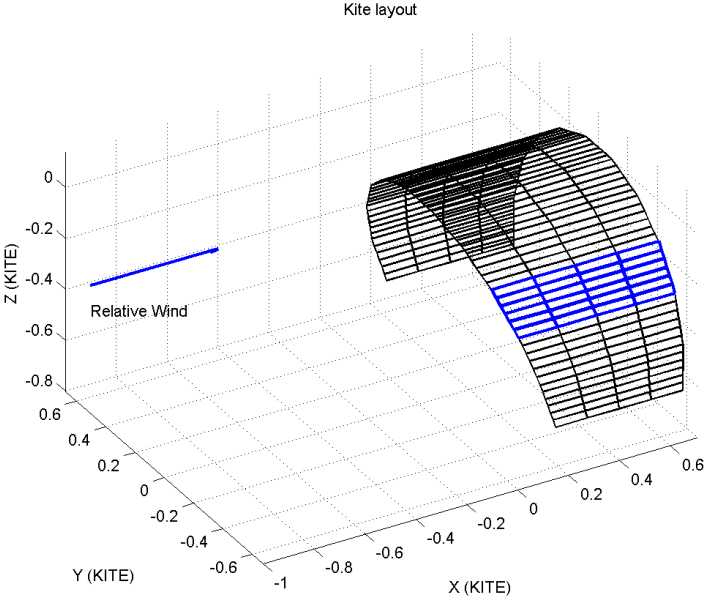
Figure 6.11: Example of kite geometry - Each of the 11 partitions has 24 panels: 4 chordwise by 6 spanwise.
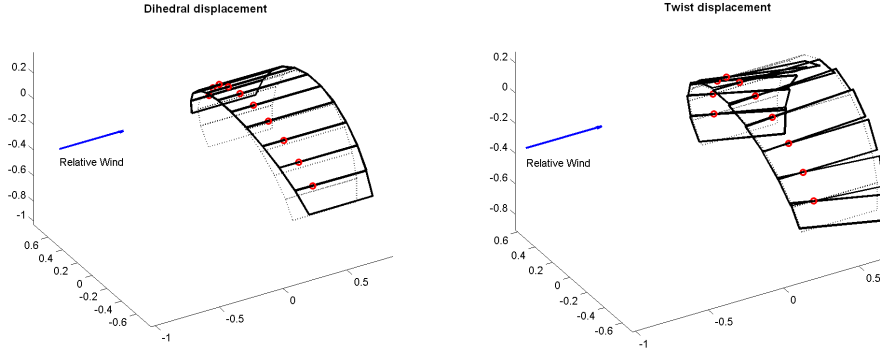
Figure 6.12: Structural model - Each partition is linked to the next by means of springs and dampers. Hinges are placed at one quarter of the chord.

The mass is computed as the product of the canopy mass per square meter and the area of the partition. The actual density varies depending on the dimensions of the overall kite and ranges from about 0.5 kg/m^2 in small kites to 2.5 kg/m^2 in larger ones. The area and centre of gravity are computed numerically depending on the input geometry.

As for the inertia tensor, the partition is assumed to be a thin homogeneous rectangular parallelepiped as shown in fig. 6.13. The inertia tensor $\mathbf{I}_{part}$ is therefore defined as

$$\mathbf{I}_{part} = \begin{bmatrix} Ixx_{CG} & 0 & 0 \\ 0 & Iyy_{CG} & 0 \\ 0 & 0 & Izz_{CG} \end{bmatrix}$$

$$Ixx_{CG} = \frac{m(y^2 + b^2)}{12} \tag{6.1}$$

$$Iyy_{CG} = \frac{m(x^2 + b^2)}{12}$$

$$Izz_{CG} = \frac{m(x^2 + y^2)}{12}$$

where m is the mass, x is equal to $(L_1 + L_3)/2$, b is the spanwise length of the partition and y is the thickness. Dimensions are in $[kg \ m^2]$.
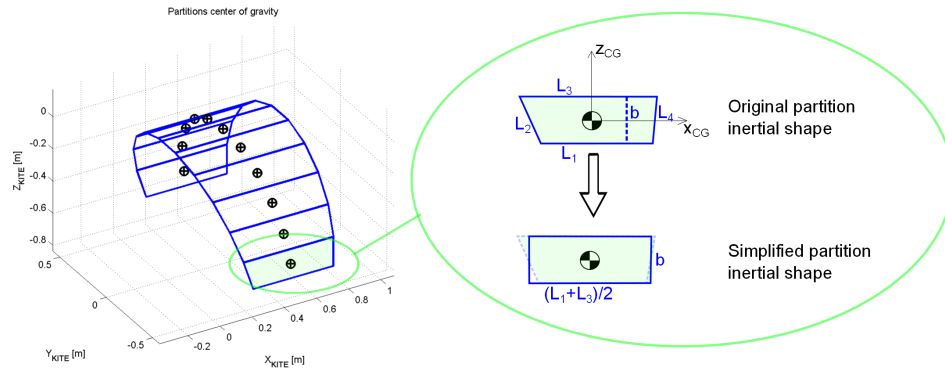
Figure 6.13: Partition inertial model - Each partition is assumed to be a thin homogeneous rectangular parallelepiped.

6.6 Cables model

6.6.1 Cables structural model

Each cable is modelled as an homogeneous rigid rod. Bending of the cable is not permitted and no modes of vibrations are taken into account. Such model makes sagging impossible even for long cables. Sagging creates a small delay in the transmission of the control forces between the ground station and the kite. Though some authors in the industry do not consider the cable delay a big problem, however for others this approximation is not always reliable and is more close to reality when the cables are short because the great tension makes them straight without any curvature. But, as the cables become longer, this model cannot take account of cables' slight bending which in reality delays the control input and puts a limit on the maximum length of the tethers (19). Fig. 6.14 illustrates the rigid bodies layout composing each cable.

Each rod is composed of three aligned rigid sections. The first is hinged to the ground. The second is connected to the first by means of a spring and damper in the direction of the cable. The third is rigidly welded to the second. The cable is finally hinged to the kite.

This model is not used to reel in and reel out the kite[1]. The spring and damper

---

[1]Simulate the pumping yo-yo cycle would be easy to do by changing the inertial properties during the simulation and actuate a force on the second section of the cable accordingly.
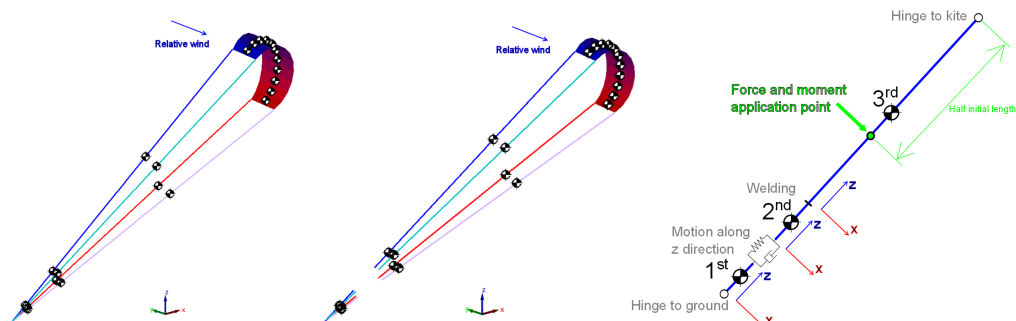
Figure 6.14: Cables inertial model - Cables at their initial length (left). Cables after an exaggerated extension (middle). Cable model (right). Notice that the blue (red) cable is the one that a kitesurfer would hold in his right (left) side. 3D parallel view might be tricking.

emulate a simple PD control on cable length with constant reference to avoid unwanted reel in and reel out during manoeuvres but, at the same time, allow the cable to extend and shrink by means of a sliding motion of the second section.

The reason why the ability to slide is necessary is because the ground station controls the kite by means of forces applied to the tethers. Without the sliding degree of freedom any force applied would be immediately transferred to the ground without controlling the kite. Rear cables are used to steer and front cables are used to control the angle of attack.

The rigid connection between the second and the third sections has no physical meaning, but allows the SimMechanics user to easily retrieve the cable's internal forces and moments during the simulation to check if they are consistent with other data.

This layout is only one of the many possible multibody layouts that can be implemented.

6.6.2 Inertial properties

For each cable, or better for each cable's rigid section, mass and inertia tensor have to be computed.

The mass is computed as a product between the volume in m^3 and the density in kg/m^3. The material is Dyneema, already mentioned in 4.5.6. Cables mass accounts for most of the total mass of the system: for example a 16 m^2 kite would have a mass

of about 8 kg, while two cables properly dimensioned, each 1000 m long, would weight together approximately 200 kg. The resulting cables-to-kite mass ratio is then 25.

The inertia tensor $\mathbf{I}_{cable}$ for each section is computed considering the cable as an homogeneous cylinder.

$$\mathbf{I}_{cable} = \begin{bmatrix} Irr_{Cable} & 0 & 0 \\ 0 & Irr_{Cable} & 0 \\ 0 & 0 & Izz_{Cable} \end{bmatrix}$$

$$Irr_{Cable} = \frac{ml^2}{12} \tag{6.2}$$

$$Izz_{Cable} = \frac{mr^2}{2}$$

where m is the mass of the cable, r is the radius, and l is the length. Dimensions are in $[kg \ m^2]$.

6.6.3 Cables aerodynamic model

As previously explained, the cable structural model is an extensible straight cylinder. A mesh is built on the actual length of the cylinder so that the tether is divided into n elements[1]. Each element has its own properties. The force computation on each element is based on a simple decomposition of normal and tangential drag[2]. Fig. 6.15 illustrates the process.

On each element i the velocity triangle is built considering that every element has its own velocity $\mathbf{V}^i_{element}$ and is immersed in a different absolute wind $\mathbf{V}^i_{world}$. A generic 3D wind profile can be used. The relative wind component $\mathbf{V}^i_{rel}$ is therefore computed.

$$\mathbf{V}^i_{rel} = \mathbf{V}^i_{world} - \mathbf{V}^i_{element} \tag{6.3}$$

Note that the relative wind has a different orientation on each cable element as show in fig. 6.16.

The aerodynamic force is computed by separating the radial V^i_{radial} and tangential V^i_{tang} relative wind components.

---

[1]Note that these n aerodynamic elements are different from the three rigid sections described in 6.6.1.

[2]Further details about normal and tangential forces on inclined cylinders can be found in (47).
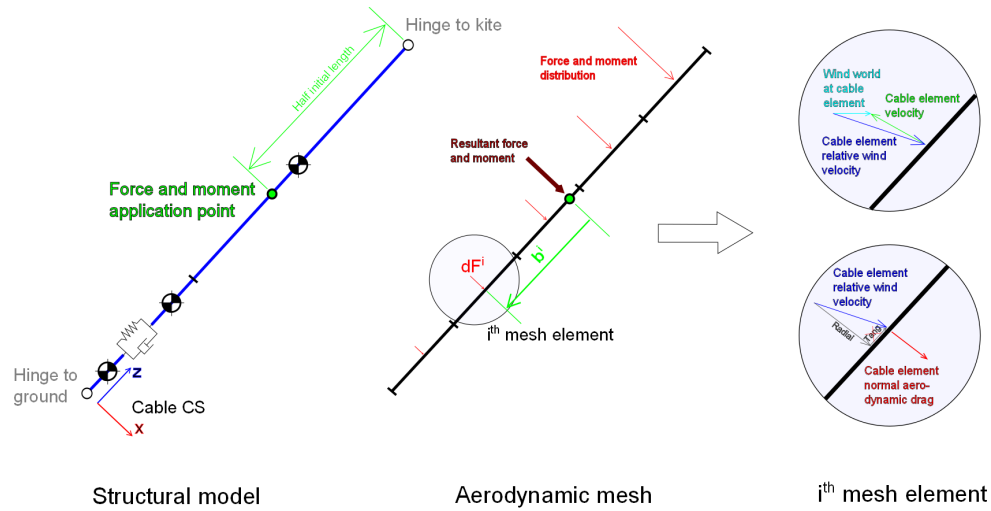
Figure 6.15: Cables aerodynamic model - An example of mesh with five elements. Each element has its own aerodynamics.
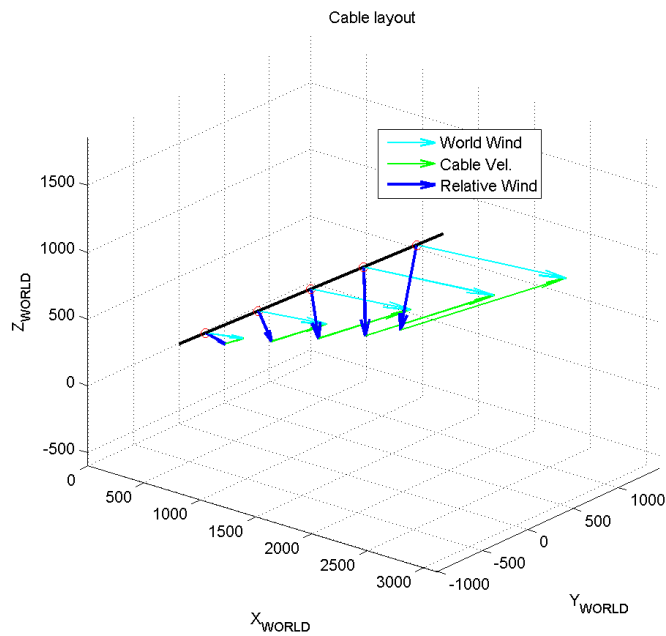
Figure 6.16: Element velocity triangles - An example of mesh with five elements. Relative velocity distribution is twisted along the cable. Values are exaggerated in this example. Ground is at the origin of the axes.

$$\mathbf{V}^i_{rel} = \begin{Bmatrix} V^i_x \\ V^i_y \\ V^i_z \end{Bmatrix}$$

where x, y, z refer to the cable coordinate system.

$$V^i_{radial} = \sqrt{V^{i2}_x + V^{i2}_y} \tag{6.4}$$

$$V^i_{tang} = V^i_z \tag{6.5}$$

Each relative wind component eventually results in an element force considering the element aerodynamic coefficient.

$$dF^i_{radial} = \frac{1}{2}\rho^i {V^i_{radial}}^2 dz D^i C^i_x \tag{6.6}$$

$$dF^i_{tang} = \frac{1}{2}\rho^i {V^i_{tang}}^2 dz D^i C^i_f \tag{6.7}$$

where ρ^i is the air density at the element (as function of the altitude), dz is the element length, D^i is the element characteristic length (diameter or chord), C^i_x and C^i_f are the radial and tangential drag coefficients.

The aerodynamic drag component parallel to the cable dF^i_{tang} is neglected and only the perpendicular force dF^i_{radial} is taken into account[1].

$$dF^i_{tang} = 0 \tag{6.8}$$

Once that the aerodynamic forces are computed they are expressed in a common reference system (cable CS) to obtain the aerodynamic force distribution $\mathbf{dF}^i$.

$$\theta^i = \arctan \frac{V^i_y}{V^i_x} \tag{6.9}$$

$$dF^i_x = dF^i_{radial} \cos(\theta^i) \tag{6.10}$$

---

[1]In other words the friction coefficient C^i_f, which is about 0.02 and would slightly contribute to generate more power, is assumed to be zero. This approximation is not so relevant in that the normal drag coefficient C^i_x is normally about 1.0.

$$dF_y^i = dF_{radial}^i \sin(\theta^i) \tag{6.11}$$

$$dF_z^i = dF_{tang}^i = 0 \tag{6.12}$$

$$\mathbf{dF}^i = \begin{Bmatrix} dF_x^i \\ dF_y^i \\ dF_z^i \end{Bmatrix}$$

The force distribution has to be eventually integrated to generate one equivalent force for the overall rigid cable and, likewise, the equivalent transport moment. The transport moment distribution $\mathbf{dM}^i$ is computed as cross product between the element force $\mathbf{dF}^i$ and its distance $\mathbf{b}^i$ from the application point as shown in fig. 6.15.

$$\mathbf{dM}^i = \mathbf{b}^i \times \mathbf{dF}^i \tag{6.13}$$

$$\mathbf{F}_{tot} = \begin{Bmatrix} F_x \\ F_y \\ F_z \end{Bmatrix} \qquad \mathbf{M}_{tot} = \begin{Bmatrix} M_x \\ M_y \\ M_z \end{Bmatrix}$$

$$F_x = \sum_{i=1}^{n} dF_x^i \qquad M_x = \sum_{i=1}^{n} dM_x^i$$

$$F_y = \sum_{i=1}^{n} dF_y^i \qquad M_y = \sum_{i=1}^{n} dM_y^i$$

$$F_z = \sum_{i=1}^{n} dF_z^i \qquad M_z = \sum_{i=1}^{n} dM_z^i$$

The multibody environment eventually applies the resultant force and moment to the cable's application point.

6.6.4 Cables aerodynamic model summary

The described numerical model has significant advantages if compared to an analytical model. For example it can easily take account of a generic wind profile (in altitude),

difference in air density and difference in the cable's section[1]. Off course the disadvantages are a higher computational time and the need of running a full kite-cable simulation to compare cables performances.

An example of three dimensional application in a cable with different aerodynamic properties is shown in figs. 6.17, 6.18, 6.19,
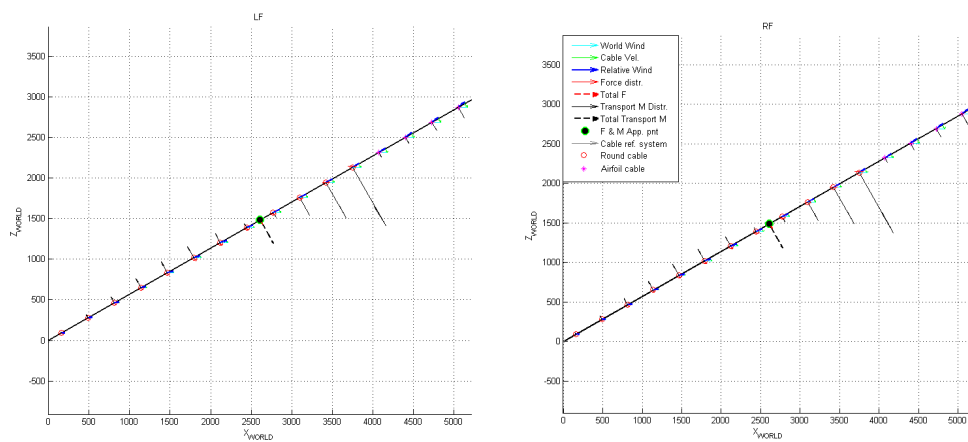
Figure 6.17: Cables drag example - Side view. Upper 20% of length is aerodynamically shaped, and lower 80% is round. Kite altitude $= 30deg$, azimuth close to zero. Kite is going horizontally towards negative azimuth (negative y coordinate). Ground is at the origin of the axes. Absolute wind goes in the x direction.

6.7 Simulator overview

A basic run flow chart of the simulator is shown in fig. 6.20.

6.7.1 Tornado initial setup

Together with the geometry, other important variables are chosen by the user. The most important are absolute wind speed, kite initial position and orientation in the

---

[1]The cable section is round in case of common cables, but could also be aerodynamically shaped to reduce the drag and improve the global aerodynamic efficiency.
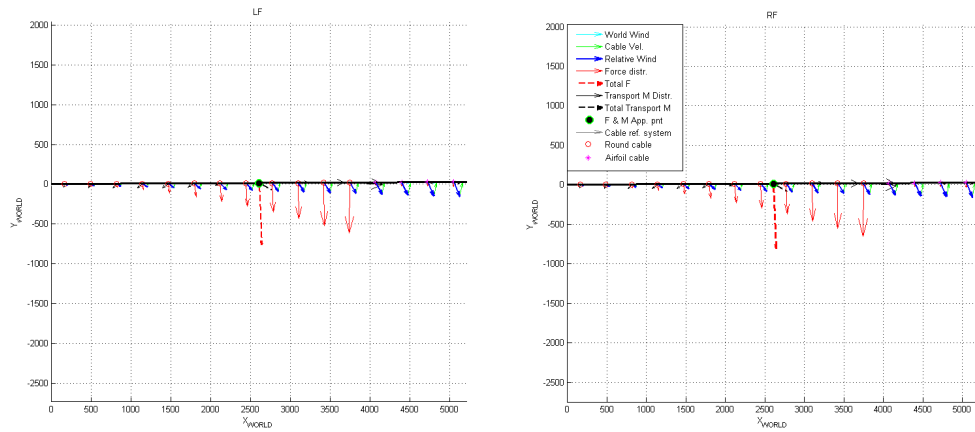
Figure 6.18: Cables drag example - Top view. Upper 20% of length is aerodynamically shaped, and lower 80% is round. Kite altitude about 30 *deg*, azimuth close to zero. Kite is going horizontally towards negative azimuth (negative y coordinate). Ground is at the origin of the axes. Absolute wind goes in the x direction.
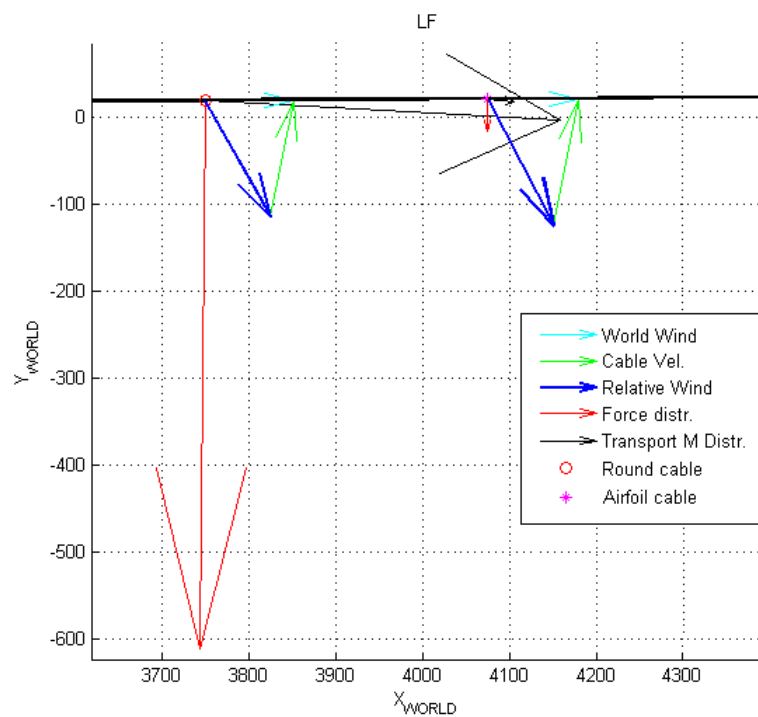
Figure 6.19: Cables drag example - Top view. Detail of the velocity triangles and the resulting forces and moments. Kite altitude about 30 *deg*, azimuth close to zero. Kite is going horizontally towards negative azimuth (negative y coordinate). Ground is at the origin of the axes. Absolute wind goes in the x direction.
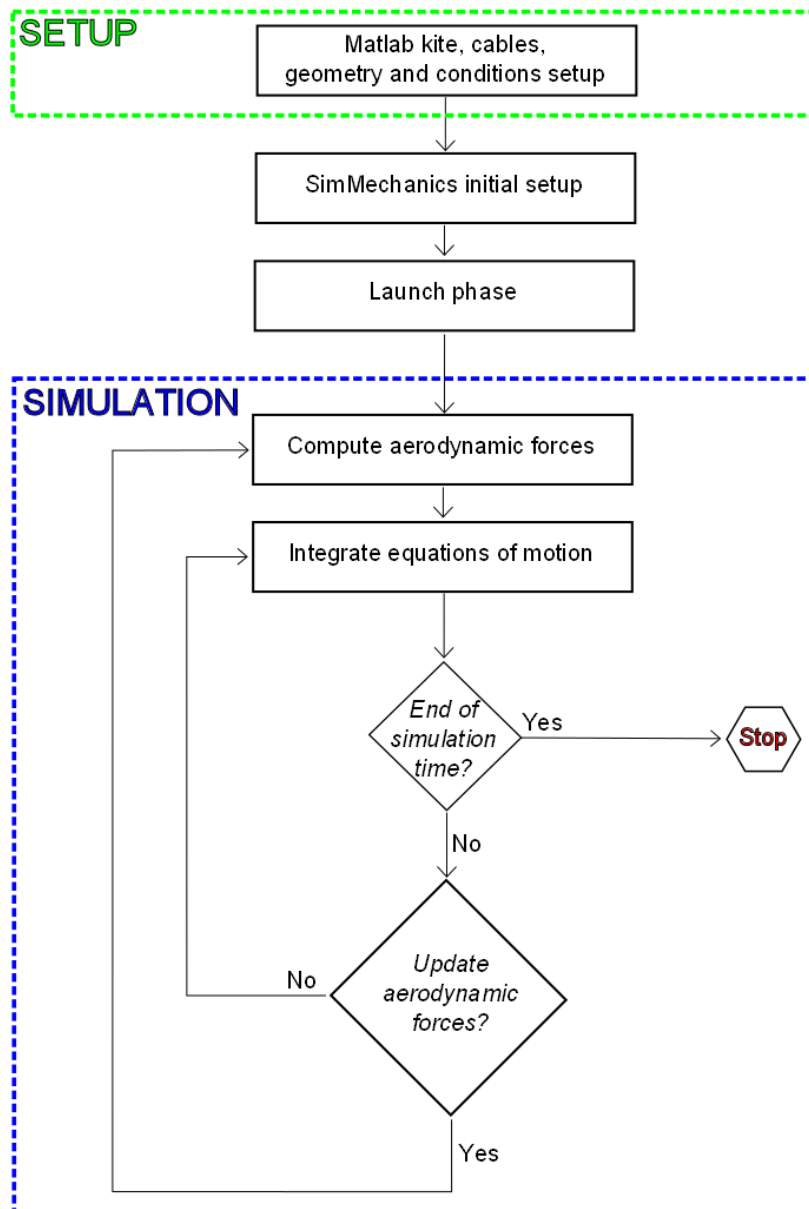
Figure 6.20: Kite simulator run flow chart -

sky, kite mass, structural spring and dampers constants, integration parameters and also length, mass and aerodynamic properties of the cables.

6.7.2   SimMechanics initial setup

The kite simulator does the necessary computations to import the geometry. A tool to automatically perform this task was written. Understanding and computing all the variables is a very time consuming process in that 3D geometry and angles have to be carefully analysed. All the needed inertial properties and configuration parameters are then passed to the SimMechanics environment which eventually builds the physical model and the equations of motion.

6.7.3   Launch phase

The launch phase is needed to start the simulation in any position in the wind window. This is because at the beginning of the simulation the kite has null velocity and not all the possible orientations would result in a proper launch. To start moving in a correct manner the kite should accelerate toward minus x (kite CS). For example if the kite is positioned as shown in fig. 6.21 (A), the first aerodynamic VLM computation would yield an acceleration in the proper direction[1]. But if the kite is initially positioned as in (B) then the kite can not launch properly.

So, to avoid this problem, at the beginning of the simulation, for a limited time, the simulator does not compute the aerodynamic forces and moments but, instead, applies fixed forces[2] as shown in fig. 6.22.

6.7.4   Simulation

After the launch phase, the simulation includes also the aerodynamic forces computations. The VLM Tornado-based functions allow to find the force distribution on the panels at each time step. Figs. 6.23 and 6.24 illustrate an example of results.

The SimMechanics environment then integrates the equations of motion modifying the position, velocity and geometry of each partition. The simulation time is constantly

---

[1]It should be said that if the kite has no velocity then the angle of attack is much above the linear aerodynamic range in which VLM simulations are reliable as explained in section 6.3.3. In that case simulation is valid only after the kite achieves a reasonable velocity, with a lower angle of attack.

[2]Fixed in the kite coordinate system.
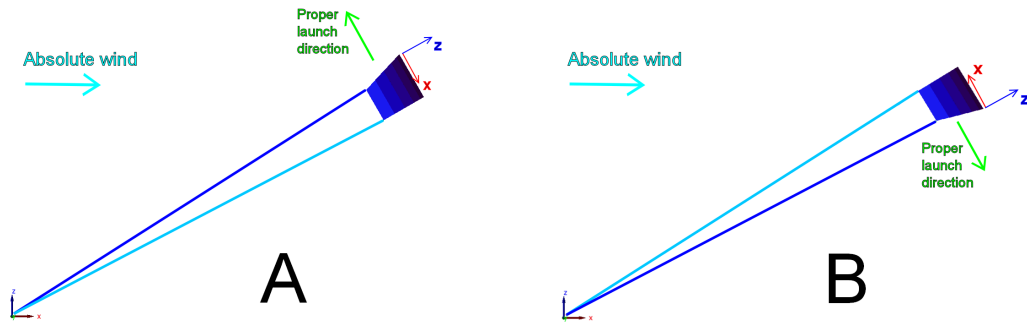
Figure 6.21: Launch phase allows any initial position - At the beginning of the simulation the kite has null velocity. A: an initial VLM would result in proper acceleration. B: an initial VLM would not result in proper acceleration.
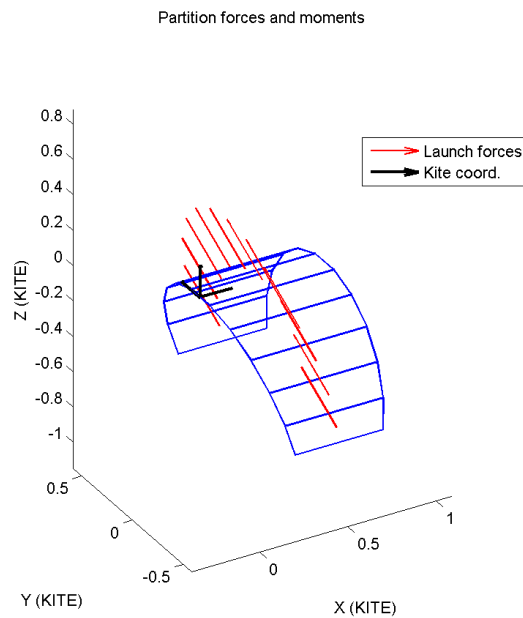
Figure 6.22: Launch phase - A small constant force is applied on each of the 11 partitions.
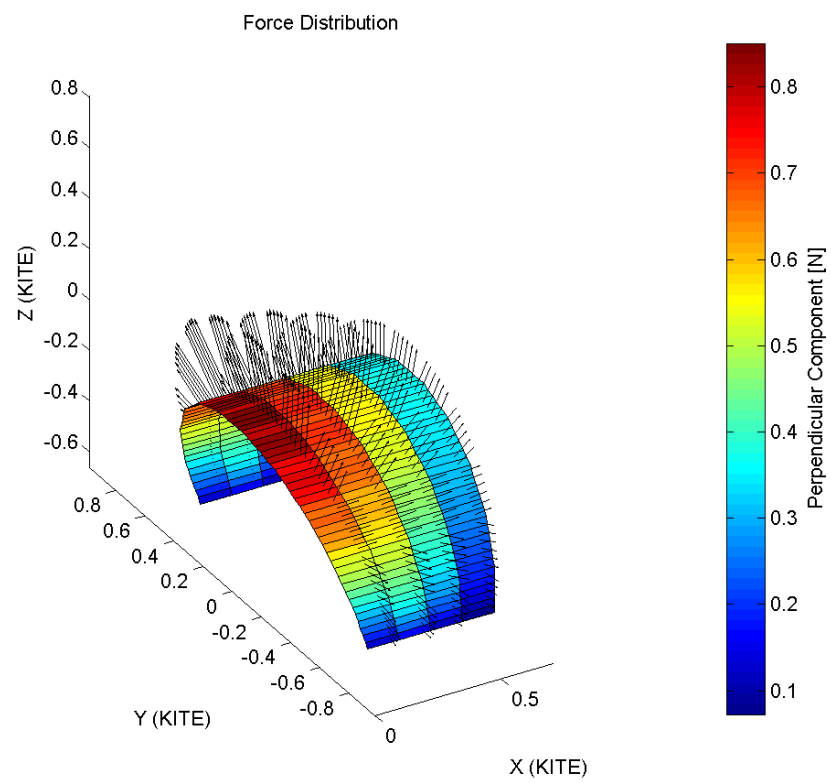
Figure 6.23: VLM results - The VLM functions continuously compute the aerodynamic forces during the simulation.

Partition forces and moments
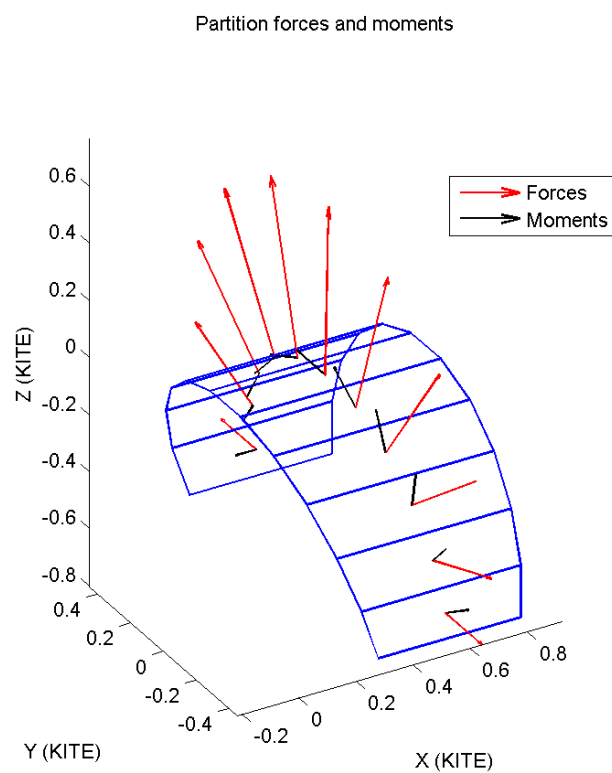
Figure 6.24: VLM results sum - The force distribution is integrated in order to have one force and one moment on each partition so that they can be easily handled in the multibody model.

monitored and, at regular time intervals, the aerodynamic functions are activated to update the force and moments outputs.

The cycle goes on until the simulation ends.

6.8   SimMechanics block diagram

The SimMechanics multibody model is illustrated in this section. The main block diagram is shown in fig. 6.25. Four main parts compose the block diagram: kite physical model, kite aerodynamics, cables physical and aerodynamic model, control panel.

6.8.1   Kite physical model

The blocks in this section build the model already described in section 6.5 importing most of the data needed for the simulation initial setup (sections 6.7.1 and 6.7.2). A zoom of the block diagram is in fig. 6.26

6.8.2   Kite aerodynamics

During the simulation, the kite geometry[1] is constantly monitored and it is converted in a format compatible with Tornado. The same is also valid for the relative wind conditions on the kite coordinate system. These data are passed to the Tornado-based functions which perform the aerodynamic computations. The SimMechanics block diagram is in fig. 6.27.

6.8.3   Cables physical and aerodynamic model

This block diagram builds the model already described in section 6.6. There are four blocks, one for each cable, and each of them is structured as shown in fig. 6.28.

6.8.4   Control panel

The kite needs to be controlled by traction forces on cables. The front cables control the angle of attack and the rear cables make the kite steer.

---

[1]Meaning dihedral and twist angles.
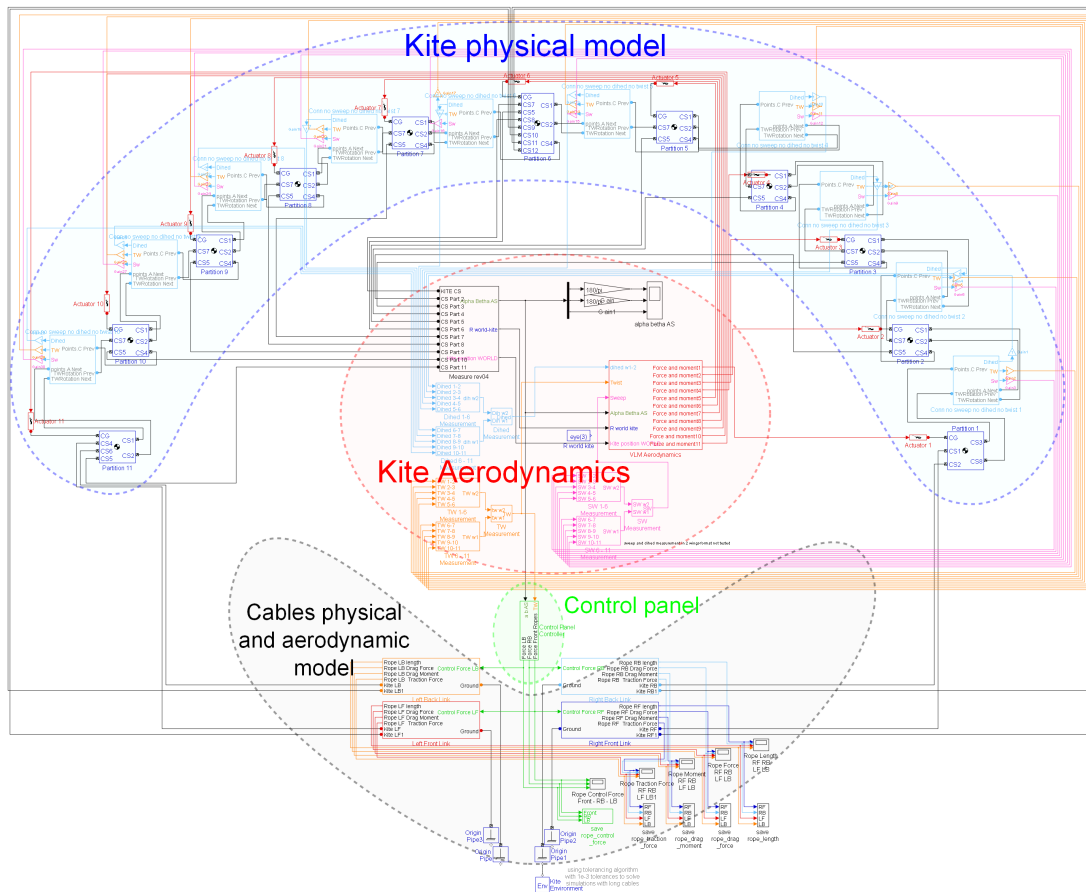
Figure 6.25: Kite simulator SimMechanics model - The block diagram with its subsystems is shown in this picture. The kite physical model is composed of 11 rigid bodies (partitions) joined together with 10 spring-damper systems. Cables are modelled as rigid rods with their inertial and aerodynamic properties. The kite aerodynamics subsystems analyse the current geometry and relative wind and compute the forces and moments with the Vortex Lattice Method by means of an S-function based on Tornado routines. A control panel allows the user to perform manoeuvres and change the angle of attack.
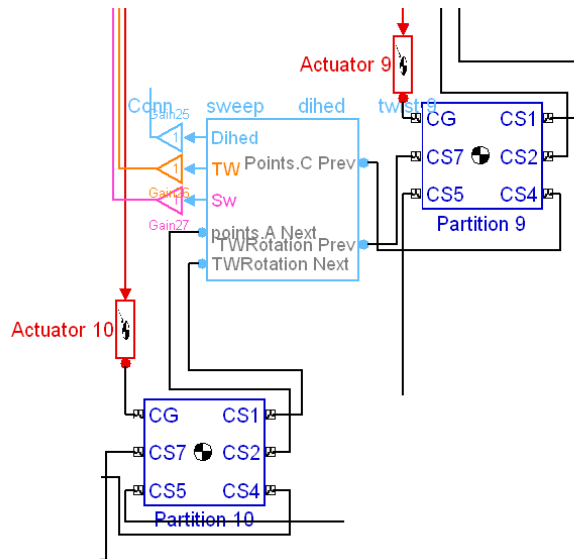
Figure 6.26: Rigid partitions and their link - Example of the block diagram of two partitions linked together.

To control the angle of attack a simple proportional controller is used[1], while the steering manoeuvres are manually chosen. The user can control the kite by using the control panel shown in fig. 6.29. Several switches allow to apply steering forces on the rear cables at any time during the simulation and change the angle of attack controller set point.

6.9   Tornado-based VLM functions

To simulate the aerodynamics of the kite, VLM method is implemented. The operation flow chart describing the process is in fig. 6.30.

During the simulation the necessary geometry data and wind conditions are taken as input from the SimMechanics environment.

The VLM core is activated only if enough simulation time has elapsed since the last VLM computation[2].

---

[1]Such simple controller does not follow precisely the set point, but is enough to keep the kite stable during flight.

[2]A typical value for the time step might be 0.01 *sec*, meaning that the next VLM would be performed after at least 0.01 *sec*. The VLM time step cannot be exactly fixed when the a variable time step integrator is chosen in the SimMechanics environment, but if the user sets a maximum step size
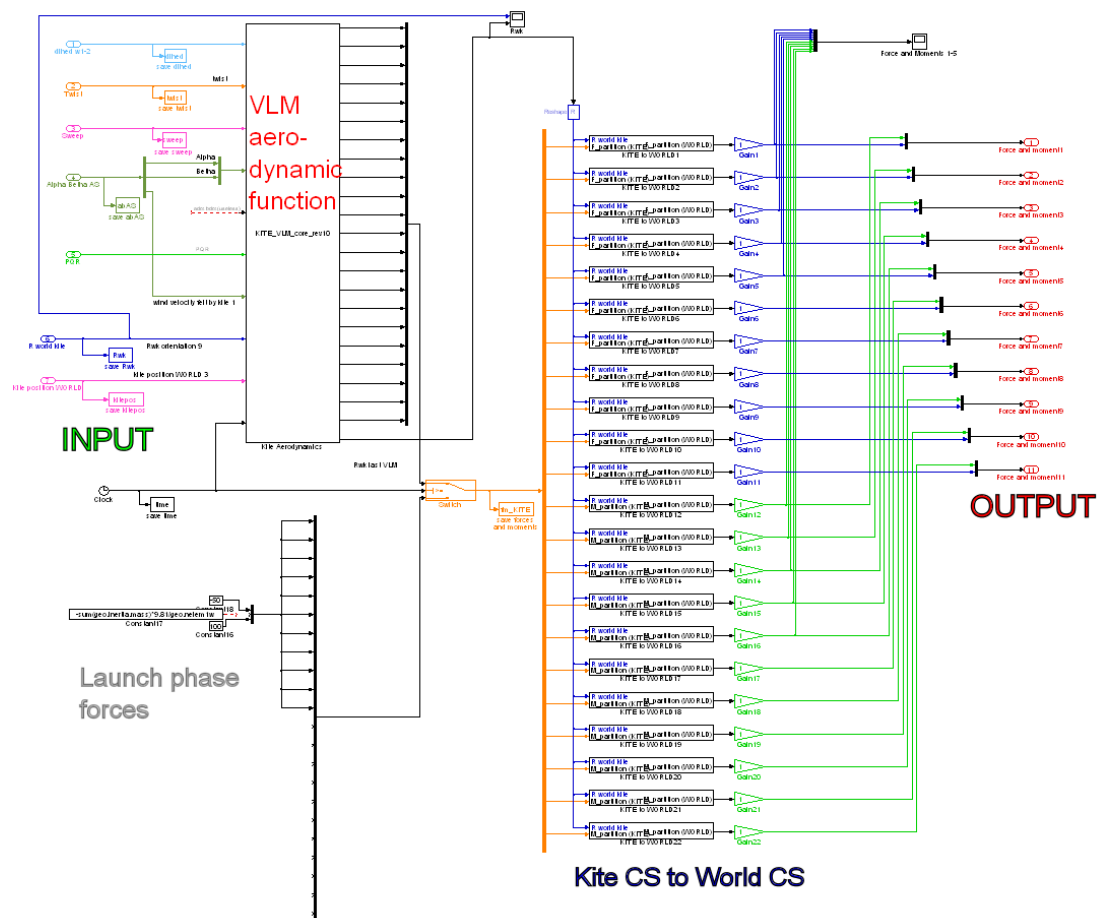
Figure 6.27: Kite aerodynamics SimMechanics model - This is the block diagram that takes in input the geometry and wind conditions (already in Tornado-compatible format) and outputs the aerodynamic forces and moments to be applied on the kite.

Figure 6.28: Cables physical and aerodynamic model - The cable inertial model takes as input the control forces and provides to the aerodynamic block the necessary information to compute the cable's drag.

Figure 6.29: Control panel - The manual switches can be toggled while the kite flies.
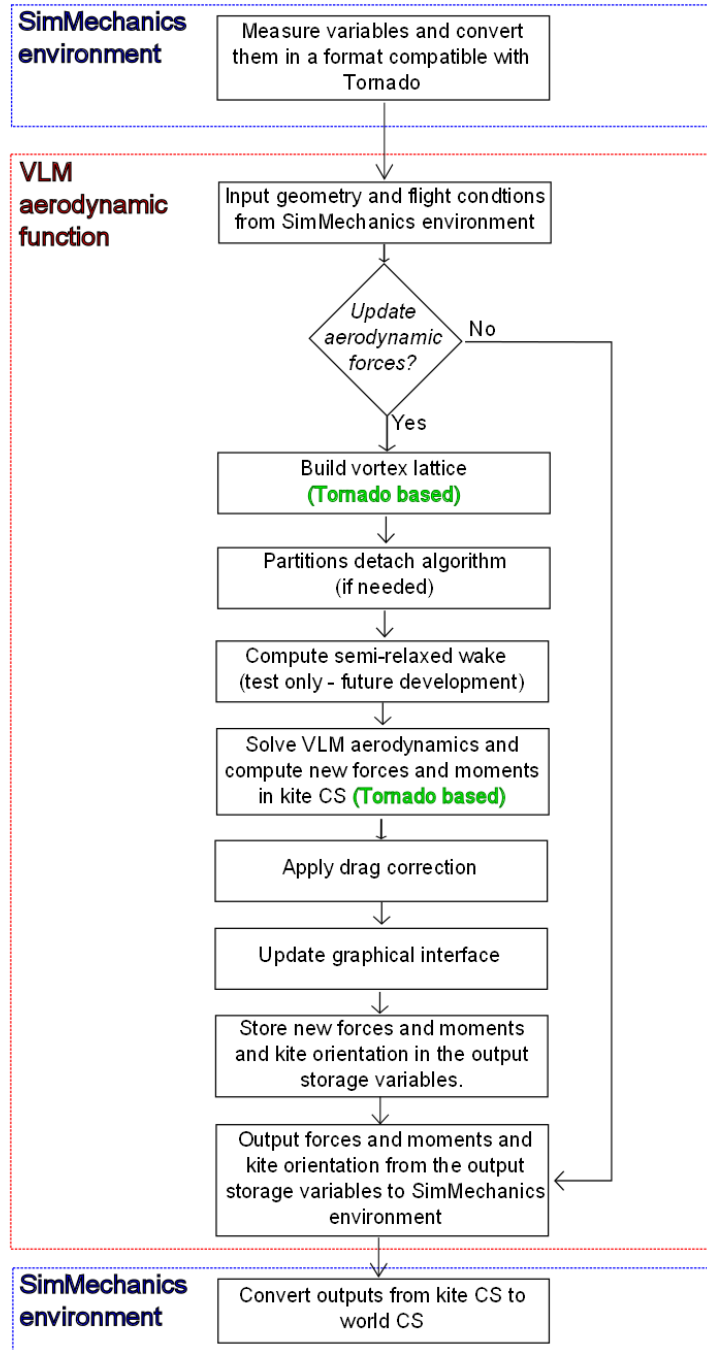
Figure 6.30: Kite aerodynamics run flow chart - Several functions were written to perform the operations inside the red box 'VLM aerodynamic functions'. The Tornado-based operations implement the method described in section 6.3.

A When the VLM core is activated several operations are performed. A detailed view each of them is given in this section.

6.9.1 Vortex lattice

First the vortex lattice is built following using the Tornado method described in section 6.3.2.

6.9.2 Partitions Detach Code

With the kite modelled as rigid partitions joined together, the VLM method may suffer of bad conditioned solving matrix, thus making the results unreliable. This problem is typically caused by geometric overlaps in that some collocation points may be too close to vortex segments thus having a very important coefficient in the solving matrix.

Small angles do not cause sensible overlapping and the Partitions Detach Code (PDC) is normally not needed, but becomes necessary in case of extreme geometry configurations as shown in fig. 6.31.

In the kite model two partitions are linked together by springs and dampers and relative angular displacements are allowed between them as shown in fig. 6.12. Two adjacent partitions have zero relative angles when they form a flat geometry, whereas they have relative dihedral ψ_{dih} and twist ψ_{tw} when they form geometrical discontinuities. Typically, when two partitions are joined with large dihedral and twist angles, then the PDC becomes necessary. If only one of these two angles is relevant then the geometry does not create a badly conditioned matrix.
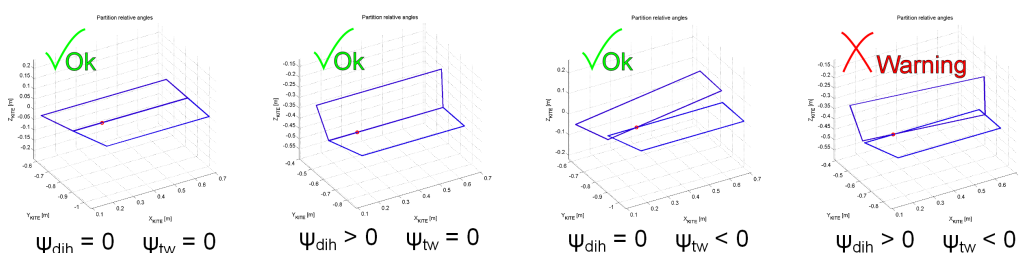
Figure 6.31: Geometry overlaps - Relative dihedral and twist angles may cause two partitions to overlap. When both angles are large the solving matrix becomes badly conditioned. Deformations in this picture are exaggerated.

in the integration then the VLM actual time steps are very close to the desired value of 0.01 *sec.*

The PDC solves the problem of overlapping by detaching the partitions. Considering C as the chord length where the two partitions are joined, the distance d between two adjacent partitions is chosen by means of empirical relations as follows:

$$d = C * |\psi_{dih1} - \psi_{dih2}||\psi_{tw1} + \psi_{tw2}|k_1 k_2/2.7; \qquad (6.14)$$

$$k_2 = 1 - |\psi_{tw1} - \psi_{tw2}| * 180/4\pi \qquad (6.15)$$

if k_2 has a negative value then it is reset to zero.

k_1 is chosen depending of he needs of the user. For most manoeuvres a coefficient $k_1 = 1/6$ is enough and this is called PDC mode 1. While in some case, called PDC mode 2, the coefficient can be chosen as $k_1 = 1/3$ if $\psi_{tw1} < 0$ and $\psi_{tw2} < 0$ or $k_1 = 1$ in the others ψ_{tw} configurations.

An example of result is shown in fig. 6.32
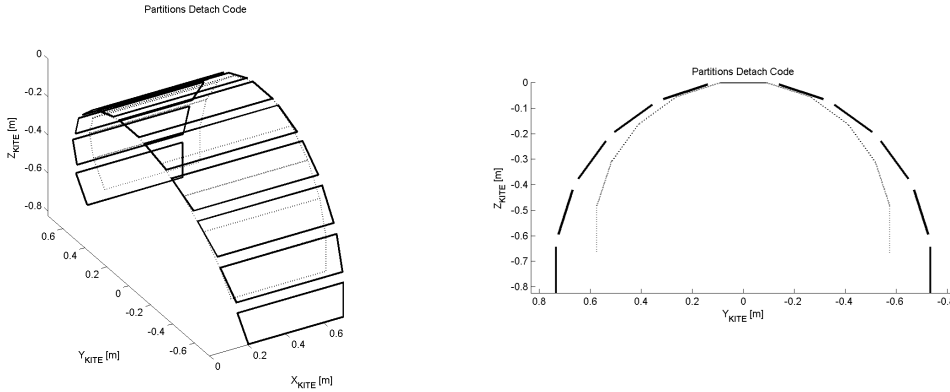
Figure 6.32: Partitions detach example - The PDC detaches the geometry and the vortex lattice. Displacements are exaggerated.

Note that the partition detach code acts only in the aerodynamic model, it does not affect the inertial SimMechanics model.

Considering that, without using the PDC, VLM results are meaningless due to the high condition number of the solving matrix, then it is not easy to analyse the effects of the detach code itself. However it can be tested in cases where the PDC is not needed. The code in mode 1 has proven to yield relatively small difference in the lift coefficient[1],

---

[1]Example: a lift coefficient of 0.319 (without PDC) becomes 0.308 (with PDC).

while more significant difference are obtained in with PDC in mode 2.

Again, the PDC can be completely deactivated during most kite flights in that small geometry deformations do not create high condition numbers in the VLM solving matrix.

6.9.3 Semi relaxed wake

VLM simulations performed by Tornado are stationary. The wake layout is therefore computed as if the kite has flown for a long time with the given flight conditions[1]. Unsteady VLM cannot be performed by Tornado and its implementation would require radical changes in the program itself.

However it is possible and is relatively easy to build a code that modifies the vortex lattice layout so that the wake follows the movements of both the kite and the absolute flow field. To achieve this, a function was written. It tracks the position of the trailing edge of the kite and adds the absolute wind to create generic vortex slings made of n segments instead of seven. Each time the wake is updated, the oldest wake segments are removed and new segments are added to the trailing edge of the kite so that the number of segments is kept constant during the simulation[2].

The code is completely compatible with Tornado[3] and can be therefore activated seamlessly. An example of result is shown in fig. 6.33.

6.9.4 Solve aerodynamics

The vortex lattice is solved following the Tornado method described in section 6.3.2.

6.9.5 Drag correction

In chapter 5 it is explained why the aerodynamic efficiency is a fundamental parameter in some airborne wind energy concepts. Then it is clear that, more than any other wing coefficient, aerodynamic efficiency has to be accurately reproduced by the kite simulator in order to obtain reliable and robust results. Unfortunately, VLM simulations are know

---

[1]Relative wind speed, angle of attack, angle of sideslip, roll pitch yaw angular velocities. All these variables change at each time step during the simulation.

[2]It is important to notice that, unlike other free wake computations, in this semi relaxed approach the vortex segments are displaced only by the absolute wind and their path is not affected by the vorticity of the segments themselves.

[3]See ref. (45) at 7.2.2, Time Dependent Factors.
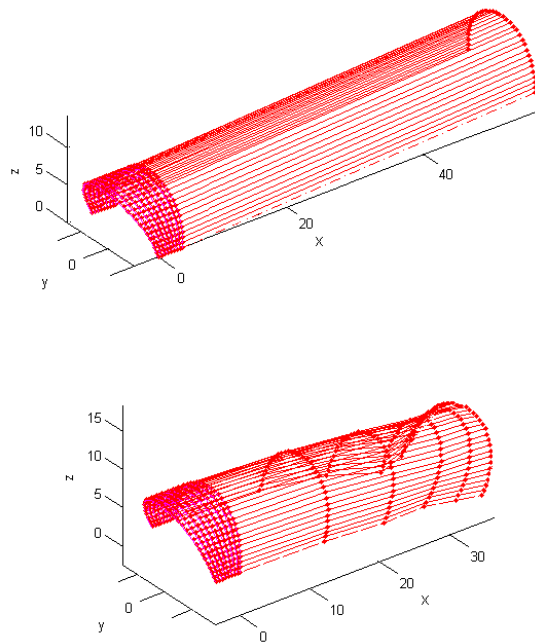
Figure 6.33: Semi relaxed wake example - Steady state vortex lattice (top). Semi relaxed vortex lattice (bottom). The length of the wake is shortened for a better graphical representation.

to be quite good in generating the lift coefficient, but the same cannot be said for the drag coefficient because VLM does not take account of the viscous drag.

For this reason, a correction for the drag coefficient has to be done. The model used in the kite simulator is:

$$C_D^* = \beta C_D^{vlm} + \gamma \tag{6.16}$$

where C_D^{vlm} is the overall kite drag coefficient found by the VLM simulation, C_D^* is the new coefficient and β and γ are correction factors that can be determined with known data before running the kite simulator. After C_D^* is determined, the force distribution is modified accordingly.

An example of drag correction based on CFD and experimental data is shown in fig. 7.6.

6.9.6 Update graphical interface

The kite simulator constantly shows the kite layout, the aerodynamic forces and other relevant data to the user. Fig. 6.34 shows a comprehensive view of the main graphical interface.

6.9.7 Aerodynamic forces and moments output

The simulation environment can use smaller time steps than the aerodynamic functions. This means that the output of the VLM core has to be coherent in time. To obtain a proper simulation, forces, moments and their orientation in space are kept constant (in the world coordinate system) between each VLM aerodynamic computation. So forces and moments are temporarily stored together with the rotation matrix between kite and world CS. For example, if instead of storing the kite orientation, the simulator used the orientation signal coming from the simulation, then in between two VLM computations the forces would slightly rotate from their initial orientation in the world CS. Storing temporarily all these values therefore allows a proper simulation.

Forces and moments in the storage variables are finally output to the SimMechanics environment.
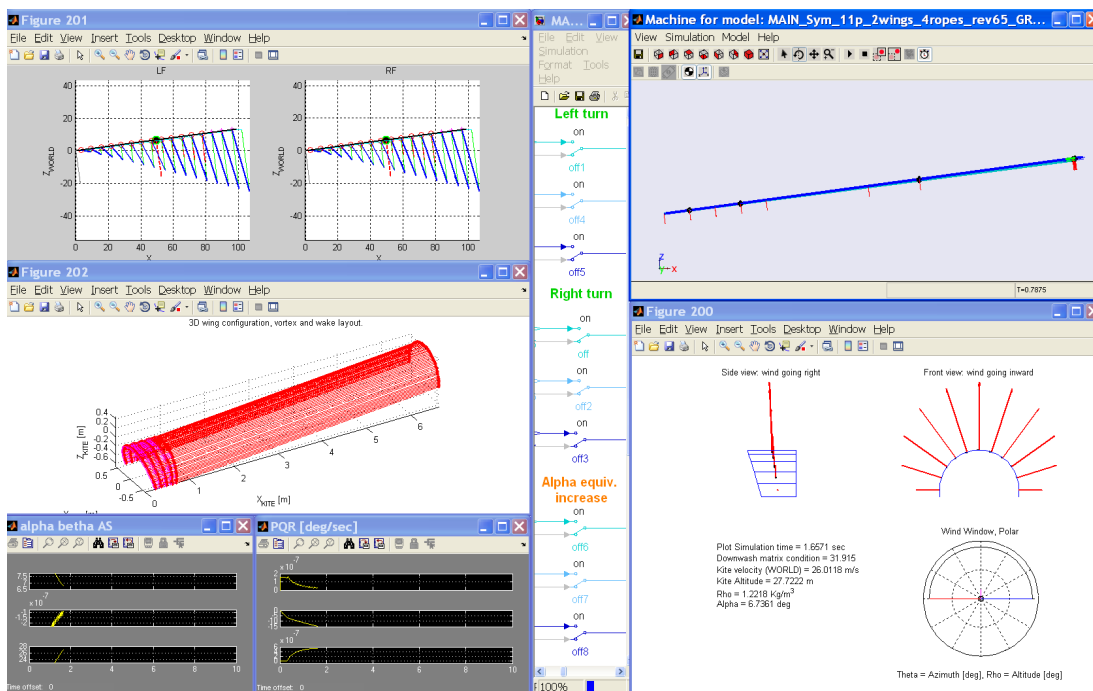
Figure 6.34: VLM kite simulator graphical interface - 3D kite-cables system (top right). Aerodynamic forces and moments on partitions and polar trajectory (bottom right). Control panel (middle). Velocity triangles and forces on cables aerodynamic mesh (top left). Steady VLM wake layout (middle left). Angle of attack, sideslip, relative wind velocity, roll, pitch and yaw (bottom left).

6.10 VLM kite simulator and kite simulation toolbox

This section aims to provide a general view about the simulator strengths, limits and approximations.

If compared to other kite models, the VLM kite simulator is very detailed and flexible. Of course the kite problem is mathematically extremely difficult to handle and every model requires important assumptions regarding the structure and the aerodynamics. If compared to a classical aircraft, the kite dynamics is more complex in that it deeply relies on deformations of the structure. Simulators are very powerful tools that enable us to analyse and study complex non-linear phenomena. At present there are several kite simulations available from literature. Many of them were developed for real time control purposes and others are used to simulate the kite behaviour. Simple models are based on stronger assumptions and give basic results but, at the same time, are easier to solve, require less computational effort and can be used for real time control. By contrast, the more a model becomes complex, the more details it can analyse but, of course, it requires more efforts to be built and solved.

This thesis develops a quite complex simulator. As pointed out in section 6.1, there are many simpler models in literature. It would not be wise to compare them with the VLM simulator and therefore it is presented here a comparison with the so called 'kite simulation toolbox' developed by Jeroen Breukels in (19).

Like the VLM simulator, the kite simulation toolbox is a detailed multibody model that completely simulates a kite-cable system. The Breukels toolbox is much more detailed in both the kite and the cables dynamics but uses a different method to compute the aerodynamic forces. The physical model is composed by three parts: the cables, the inflatable kite structure and the canopy as shown in fig. 6.3. By contrast, the VLM simulator has a simple structural model composed only by 33 rigid bodies. It does not require much computational effort and therefore is easier to handle and allows faster but at the same time flexible analyses.

6.10.1 Cable dynamics

Cable modes of motion can be divided into two main categories, fast motions and slow motions (48). The fast motions are generally small in amplitude and occur along the line

direction. The waves travel fast[1] and are usually not relevant in the global kite-cable dynamics. By contrast, the slow motions are responsible for large displacements in the direction perpendicular to the line and therefore can generate considerable delays in the control inputs and may have a significant impact on stability. Cable sagging strongly depends on the tension of the line. Increasing the tension makes a tether straight, while a low tension allows cables to bend more. In configurations where the power lines are also the control lines, such that of Kitegen, the amount of bending is roughly the same on each cable, whereas if there are both power lines and control lines the cable sagging may be different on each cable depending on the tension. Also gravity and length of the lines of course influence the displacement in the direction perpendicular to the line.

In Breukels' toolbox the cables are composed of an arbitrary number of rigid segments hinged together with springs and dampers as shown in fig. 6.4 (right). By contrast the VLM simulator models each cable as a rigid rod composed by three rigid bodies with a spring-damper system to allow extension and control as shown in fig. 6.14.

Both the simulation toolbox and the VLM simulator neglect the dynamics of the fast motions. The effects of the high modulus of elasticity of the cables material is not considered since the cables are infinitely stiff and cannot deform. The dynamics of slower motions is definitely better represented by the Breukels toolbox in that it allows the cables to sag under the effects of both aerodynamic drag and tension. The VLM simulator can only model the global inertia of the cables and is capable of changing the length during a simulation to represent the reel in and reel out phases.

6.10.2 Cable aerodynamics

As for the cable aerodynamics, both the simulation tools use a similar model. The only difference is in the decomposition of the drag force. The simulation toolbox computes the x, y, z drag components each with the respective velocity, while the VLM simulator combines the perpendicular velocities to form a radial velocity and from this value computes the radial drag force which in turn is decomposed back to the two perpendicular axes as described in section 6.6.3. Under the hypotheses of low sagging and relative wind velocity aligned with one axis, the simulation toolbox and the VLM simulator yield the same aerodynamic forces.

---

[1]An investigation of the speed of propagation from (49) suggests a value greater than 5000 m/s.

6.10.3   Kite dynamics

The dynamics of the kite itself is mathematically difficult to handle and the deformation, i.e. the structural model, plays a fundamental role in the steering manoeuvres. Section 3.4.4 describes different steering mechanisms available in literature. As explained in section 3.2, the structural behaviours of a LEI kite and of a ram air kite are very different. The inflatable structure, the bridle system and the aerodynamic forces all together give the kite its final shape.

An inflatable structure that is subjected to increasing bending has first a 'unwrinkled' phase with mostly linear behaviour, then come the 'wrinkled' and 'collapsed' phases where the tube exhibits strongly non linear behaviour. The tube bears an increasing load until eventually the structure collapses reducing the load bearing capacity to almost zero as shown in fig. 6.35.
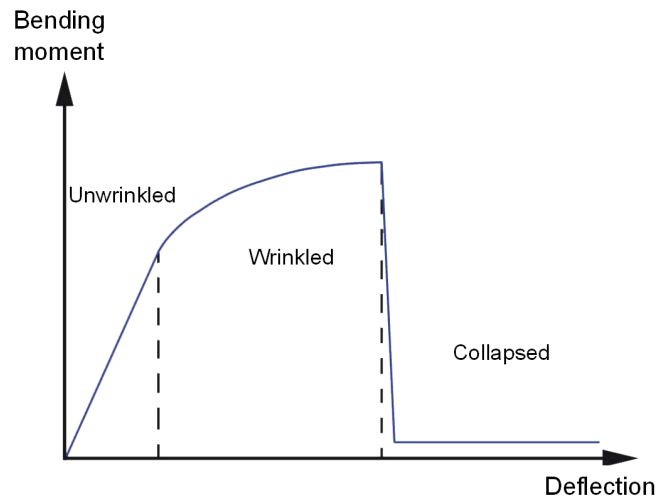
Figure 6.35: The three states of an inflatable beam - Linear behaviour, non-linear behaviour, collapse. Picture from (50).

In the Breukels toolbox every inflated tube of a LEI kite is modelled as well as the canopy. The inflatable structure is composed by a set of rigid bodies connected together with springs and dampers whose behaviour matches the real one. The canopy is modelled as a web of springs and dampers. By contrast, the VLM kite simulator models both the canopy and the structural tubes as a simple multiplate geometry composed by 11 plates joined together with springs and dampers.

The Breukels approach is definitely more accurate for a LEI kite or a kite plane, but it would require substantial changes to adapt to a ram air kite structure. On the other hand, the VLM simulator, once a proper identification is done, could be easily adapted to both a LEI kite or a ram air kite or even to an optimized airfoil wing as in fig. 4.7.

6.10.4   Kite aerodynamics

The kite aerodynamics in the simulation toolbox is computed as follows. First, 2-dimensional profiles of a LEI kite single-membrane airfoil are investigated by means of many CFD analyses as shown in fig. 6.36, then the obtained data are processed to build a function that inputs the angle of attack, the camber and the airfoil thickness and outputs lift, drag and moment. Afterwards these aerodynamic actions regarding 2D airfoils are processed to be valid also for a 3D arc-shaped wing using a model based on vortex lattice method. By contrast the VLM simulator has a much more straightforward aerodynamics that takes in input the global geometry and the global wind conditions and outputs the lift, drag and moment on each of the 11 partitions as described in section 6.9 and in fig. 6.24.

The method implemented in the simulation toolbox is much more complex and takes a big effort especially in the setup phase with the advantage of being computationally lighter during the simulations than the VLM simulator which performs a CPU intensive VLM computation at each time step[1]. Both the simulation toolbox and the VLM simulator have limits in the range of operation. The simulation toolbox algorithms are limited by the CFD preliminary analysis, whereas, as described in section 6.3.3, the VLM is limited in the range of linear aerodynamics in a way that there are no constraints on the simulation itself but only on the validity of the results, meaning that the VLM simulator can run under conditions outside the linear aerodynamics and still produce realistic behaviours that indeed are not reliable and cannot be trusted.

It is important to underline that the VLM simulator in his current state makes an approximation in the way the kite is twisted. As already pointed out in section 6.5.2, the flexibility of the kite is given by springs and dampers that link together rigid partitions. This means that, when the kite twists, there are geometrical discontinuities

---

[1]In the simulation toolbox, the fast aerodynamic algorithms do not result in a very fast global simulation due to a high complexity in the multibody dynamics.

in the structure and also in the aerodynamic model which in reality are not present in any kite. In the aerodynamic point of view, this approximation makes the results less reliable and the model could be improved in the future by allowing a flexible behaviour without necessarily creating geometrical discontinuities in the vortex lattice.
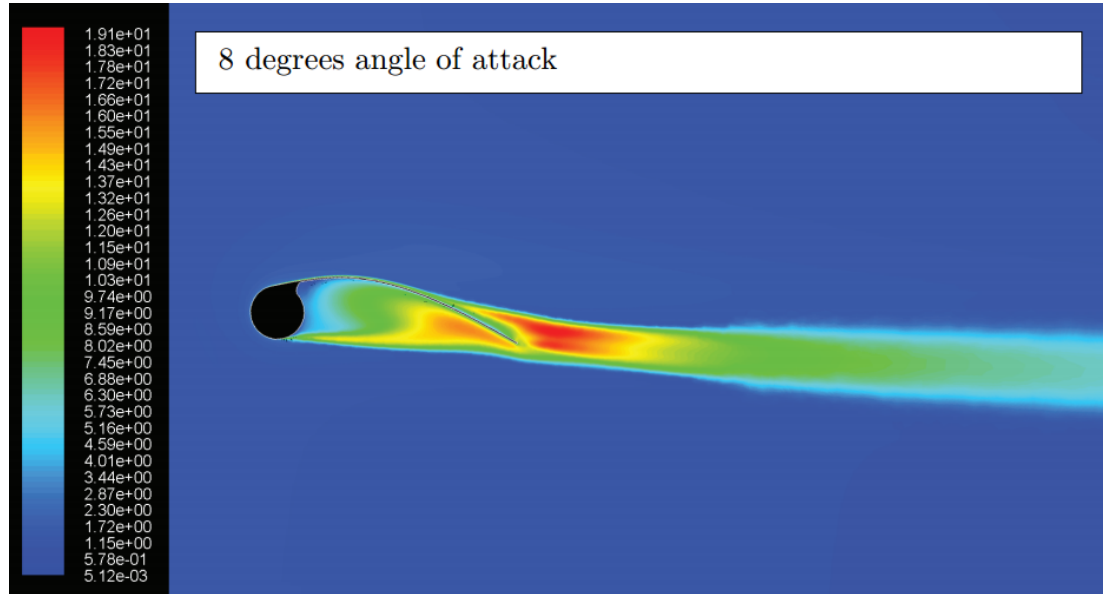
Figure 6.36: Example of CFD analysis - CFD of a single-membrane LEI kite profile. Plot of turbulence intensity at 8 degrees angle of attack. Picture from (19).

6.10.5 VLM simulator summary

With the code developed in this thesis, it is possible to:

- Investigate the kite geometry effects.

The kite geometry is very flexible and easy to change. The VLM simulator uses the open-source Tornado format which allows to investigate the effects of custom dimensions, taper, dihedral, twist and sweep. The geometry setup is easy and composed by few parameters. Any geometry is possible, from a small surf kite to for example a 300 m^2 ship towing kite as well as optimized future geometries.

- Investigate the cable properties effects.

The user can change dimensions and aerodynamic properties. The flexibility of the algorithm can model at the same time both aerodynamic and round segments. Cable sagging however is not allowed during the simulation.

- Steer the kite and perform manoeuvres.

The kite can yaw in the wind window and follow figures-of-8 trajectories.

- Use a custom wind profile.

Wind average speed changes with altitude as a custom function.

7

Aerodynamic cables analysis with the VLM kite simulator

The VLM kite simulator described in chapter 6 is a comprehensive flexible tool for analysing the behaviour of a kite. A generic kite geometry can be chosen and a multibody simulation with VLM aerodynamics is performed.

The simulator could be used for very different purposes. For example, to investigate some geometric features such as dimensions, aspect ratio, taper, twist and sweep or to study the effects of different wind profiles with altitude. All these different parameters may have an impact on several variables of interest, such as the electricity power output or the controllability of the kite itself and so on. The kite simulator is therefore a very powerful and flexible tool to consider when studying kite aerodynamics.

Model validation is the main problem to be solved. Structural and aerodynamic properties require further research in order to be proven fully reliable. However in this chapter just an example of application is shown. The simulator is used in such a way to minimize the impact of the non validated features on the results and to find rigorous data. The field of interest is the cables aerodynamics impact on a kite power plant.

7.1   Objective of the analysis

This analysis is an example of application of the VLM kite simulator. The aim is to simulate the performance improvements of an high altitude wind power plant that uses aerodynamically profiled cables instead of conventional round cables.

7.1.1 Aerodynamic cables

High altitude kite systems have been tested during the last decade, the technology is
at an early stage of development and there are still wide ranges of improvements before
those systems may reach industrial maturity. As described in chapter 5 the aerody-
namic efficiency is a key parameter that might make these technologies so attractive
economically and environmentally. Nowadays optimized gliders reach aerodynamic ef-
ficiencies above 60 with rigid wings and high wingspans. An optimized kite should have
quite high efficiencies and the industry aims to produce mass scale cheap wings with
aerodynamic efficiency of 20.

In this scenario, standard round cables reduce the performance of the system and
increase the aerodynamic drag. Then it is clear that tethers put an additional limit
both onto performance and altitude. The effects of a long cable are in contrast with
the effect of the wind profile in altitude. While the wind power density increases with
altitude, the aerodynamic efficiency of the kite-cables system decreases due to higher
drag on the longer cables. An optimal altitude for crosswind flight therefore depends
on the wind profile, the kite aerodynamic efficiency and the cables drag.

7.2 Methodology of the analysis

Three simulation variables are studied:

- cables length,

- aerodynamic length percentage,

- initial elevation angle (altitude).

Their effects on the the system performance at different altitudes are analysed with the
VLM kite simulator.

The global analysis is made of several batches of simulations.

In each batch the percentage of aerodynamic cable length and the elevation angle
are both constant. Only the cable length is changed in each simulation. Each batch is
composed of about 10 simulations.

So, for example, to investigate the behaviour of the kite-cable system at 30 *deg*
elevation angle, 50 % aerodynamic cable and cable total length between 100 *m* and

500 m, then a batch of 5 simulations with [100 200 300 400 500] meters of cables lengths is performed.

7.2.1 Horizontal flight

The aim of the analysis is to investigate the effects of cable aerodynamics alone. Therefore the chosen trajectory is the simplest. During each simulation the kite flies straight with a constant elevation angle and crossing the zero azimuth. The flight lasts for a few seconds and the kite has enough time to reach its maximum velocity and traction force. An example of trajectory is shown in fig. 7.1.
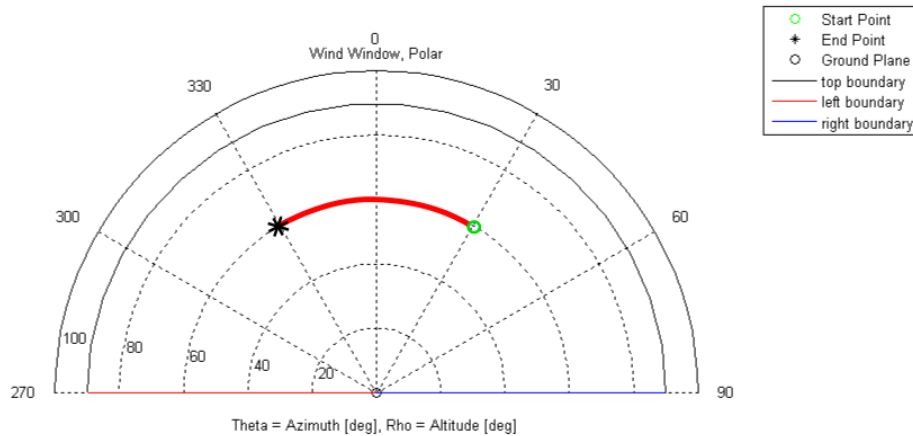
Figure 7.1: Trajectory at 60 *deg* **elevation angle** - An example of trajectory followed by the kite in one single simulation. Notice that in this representation all ground is in one point and the side borders of the wind window are the red and blue line at the bottom. Constant altitude is represented as a circumference.

7.3 Cables model

In order to reduce the aerodynamic resistance of cables and increase the electricity production the industry is moving towards optimized cables that would increase the aerodynamic efficiency of the system.

With reference to patent (51), a cable composed by both a round section and an aerodynamic section as been simulated with the VLM kite simulator using the model

explained in section 6.6. A picture showing the cables aerodynamic model is in fig. 7.2.
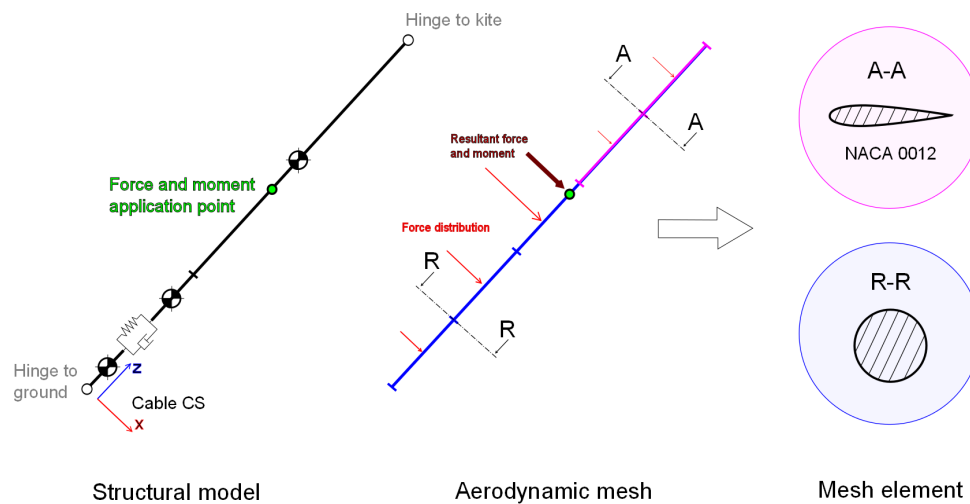
Figure 7.2: 40 % **aerodynamic cable** - An example of aerodynamic mesh of 5 elements
and 40 % aerodynamic cable. Actually the mesh is composed by 16 elements and different
aerodynamic percentages are simulated.

7.3.1   Cables drag coefficient

As for the round section, the cables drag coefficient were chosen based on the available
data on smooth cylinders as illustrated in fig. 7.3. During flight, cables Reynolds
number is in the order of magnitude of 10^4 and therefore a constant drag coefficient
equal to 1 has been chosen. By contrast, the aerodynamic section has a much lower
drag. According to (51), an optimistic value of 0.05 has been used.

Round cables have a diameter of 8 mm. A single cable with this dimension could
withstand a force of 55000 N and operate in this condition with a safety coefficient
of about 3.8. The aerodynamic cable chord is 16 mm, the traction resistance of the
cable is more difficult to estimate, but simple calculations based on the section area
suggest that this would operate with a safety coefficient of about 1.29. These values
are optimistic[1].

---

[1]Maximum usable wind speed is assumed to be 12 m/s. Cables technical data from (52). Safety
coefficients as estimated in (51).
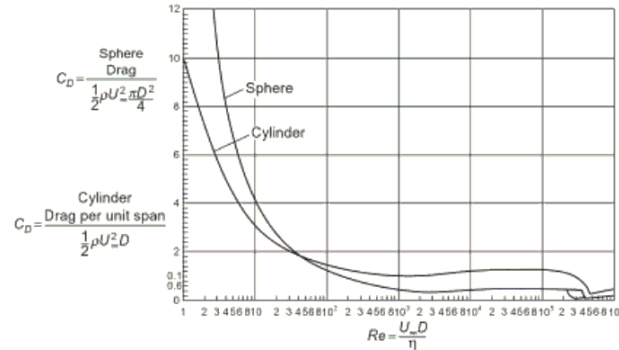
Figure 7.3: Cables drag coefficient - Aerodynamic drag as function of Reynolds number in smooth cylinders. Picture from (53).

7.4 Kite model

7.4.1 Geometry

Since, as explained in section 6.9.5, the VLM aerodynamics needs a validated drag to correctly estimate the aerodynamic efficiency, then a geometry for which aerodynamic data are available has to be chosen.

In ref. (54) aerodynamic lift and drag curves are available for the wing showed in fig. 7.4.

That geometry was reproduced in the VLM kite simulator as shown in fig. 7.5.

7.4.2 Structural rigid model

The model described in section 6.5.2 is simplified, the kite is kept completely rigid. With this assumption the structural and aerodynamic models do not have geometric discontinuities and therefore represent reality with much more confidence[1].

In any case these details of the kite model are not relevant for our analysis since we are investigating the performance increase by using aerodynamic cables. Therefore, the main requirement for the kite model is to be realistic in the simulations.

Each partition inertial model (fig. 6.13) assumes a constant thickness of 0.1 m^2.

---

[1]Though the kites described in section 3.2 are extremely flexible, the assumption of rigid kite is not completely far from reality in that, during flight, a bridle system combined with a proper kite shape may perform a straight flight with a wing that does not deform.

[2]Notice that the maximum thickness of the Clark Y profile with 2.18 m wingspan would be 0.255 m.
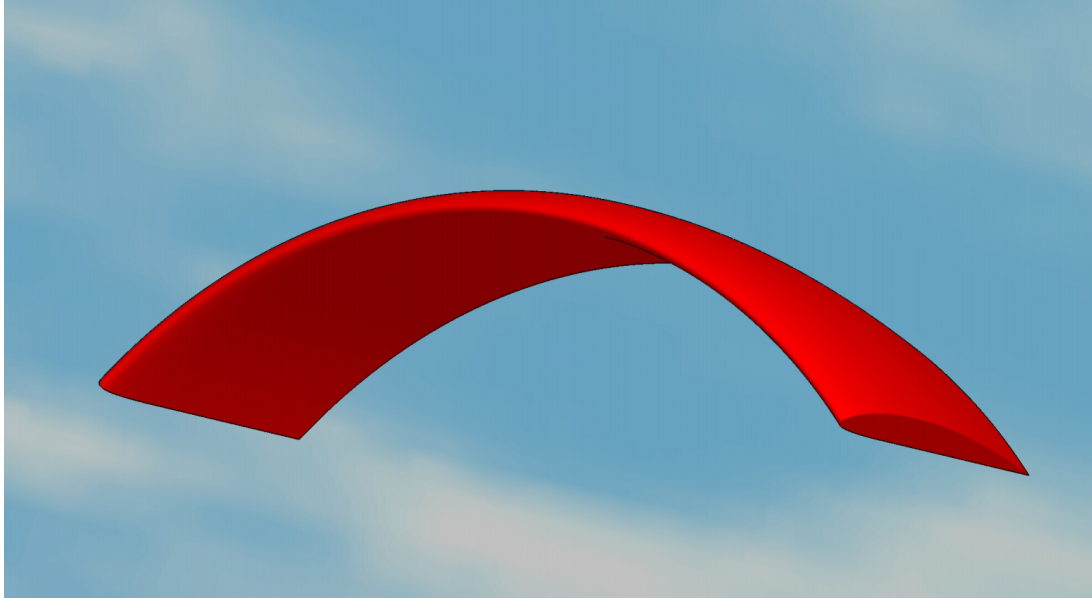
Figure 7.4: Kite geometry 3D - The chosen kite geometry. Picture from (54). Rigid
wing, Clark Y profile.

7.4.3 Drag correction

To best match the real aerodynamic efficiency the drag correction model explained in
section 6.9.5 has β and γ equal to 1.0 and 0.012 respectively:

$$C_D^* = C_D^{VLM} 1.0 + 0.012 \qquad (7.1)$$

The aerodynamic properties of this geometry are shown in fig. 7.6. Two different
models to find β and γ coefficients are shown. Referring to the figure legend, in 'VLM
correction least square', β and γ are chosen to minimise the error in the aerodynamic
efficiency, whereas in 'VLM correction', β and γ are chosen using $\beta = 1.0$ and adding
γ as a viscous drag. This second model was chosen because the aerodynamic efficiency
values are more accurate in the range of angles of attacks used during the simulation.

7.5 Multibody simulation parameters

7.5.1 Solver for the kite model

Several different solvers are suitable for the kite model.

Airfoil	Clark Y	
Chord	2,18	m
Span	7,34	m
Planform area	16,00	m^2
Aspect ratio	3,36	
Mass	7,84	kg
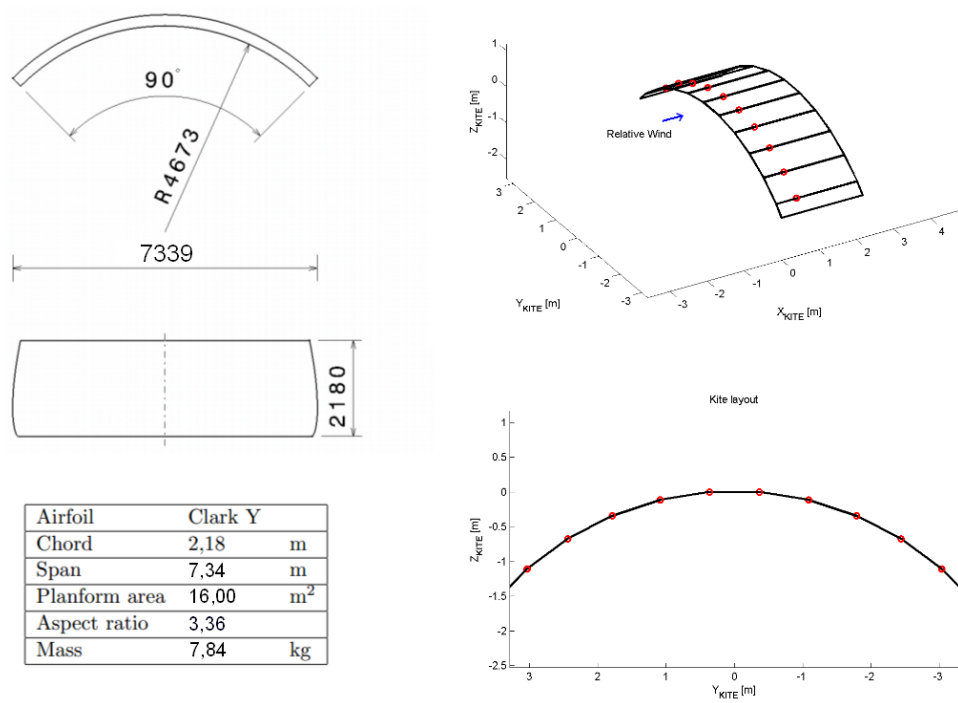
Figure 7.5: Kite geometry in kite simulator - Top left of the picture from (54).

95

Figure 7.6: Drag correction - Aerodynamic efficiency (right). Lift (top left). Drag (bottom left).

The first choice to be done is between a fixed-step and a variable-step solver. For fixed-step solvers the duration and the accuracy of the simulation depend directly on the chosen s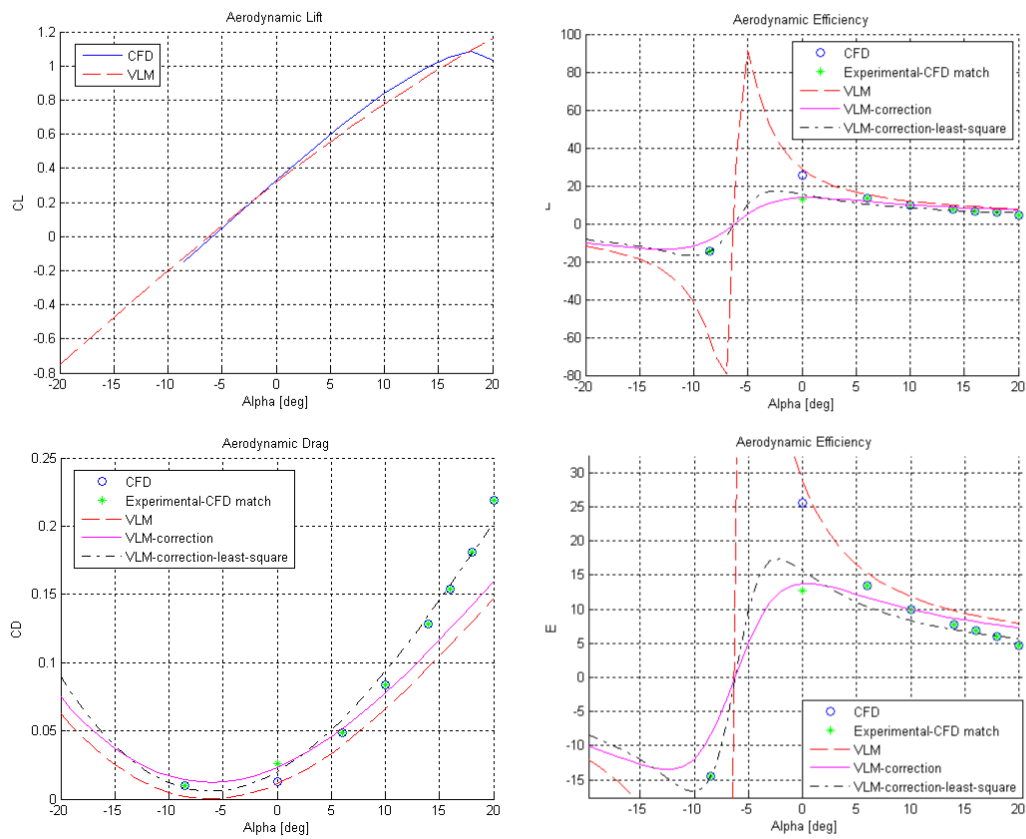tep size, while for variable-step solvers the step size is continuously adjusted during the simulation to satisfy the error tolerances requested by the user depending on the system dynamics (55). It is important to consider that the simulation time is relatively long for the kite model. Using a standard laptop[1], flying the kite for 1 second may require up to 1700 seconds (28 minutes) of computations. The model runs so slowly because of two main factors: the first reason is a complex multibody system dynamics and the second is a CPU intensive aerodynamic engine. As for the aerodynamic forces, choosing between a fixed or variable step solver does not affect the time needed to compute them because their update time is fixed. However, it is possible to reduce the CPU time relative to the multibody dynamics. This varies considerably with changes in geometry such as cables lengths which affect quadratically the components of the inertia tensors. Hence, in order to run the simulations in a shorter time, a continuous variable step[2] solver has been chosen so that the multibody dynamics accounts for less CPU usage.

The second choice to be done is between an explicit or an implicit solver. Explicit solvers require less computational efforts but are generally less accurate and might have stability problems, while implicit solvers are generally more accurate, with higher stability performance and computationally more expensive. For problems with extremely different time scales[3], implicit solvers are recommended, while for other problems explicit solvers can be used. For the kite simulator an explicit solver, ode45, is therefore used.

7.6 Tornado VLM parameters

7.6.1 VLM convergence analysis

The dimensions of the panels for the VLM aerodynamics are chosen by means of convergence analyses on lift and drag coefficients.

---

[1]CPU AMD Turion x64 1.5 GHz dual core.

[2]The maximum step size is set as the aerodynamic time step.

[3]Such problems are commonly defined 'stiff' problems (56).

Several VLM computations are performed with the same flight conditions while the number of panels is gradually increased both chordwise and spanwise. The analyses of lift and drag yield very similar results so only the lift coefficient graphs are presented.

As for the chordwise convergence fig. 7.7 shows the lift coefficient as function of the number of chordwise panels with 33 and 121 spanwise panels. It can be seen that the simulation results converge and that, whatever the number of spanwise panels, 4 chordwise panels are enough. As for the spanwise convergence fig. 7.8 shows the lift coefficient as function of the number of spanwise panels with 4 and 8 chordwise panels. It can be seen also here that the simulation results converge and that, whatever the number of chordwise panels, 60 spanwise panels is a suitable number.
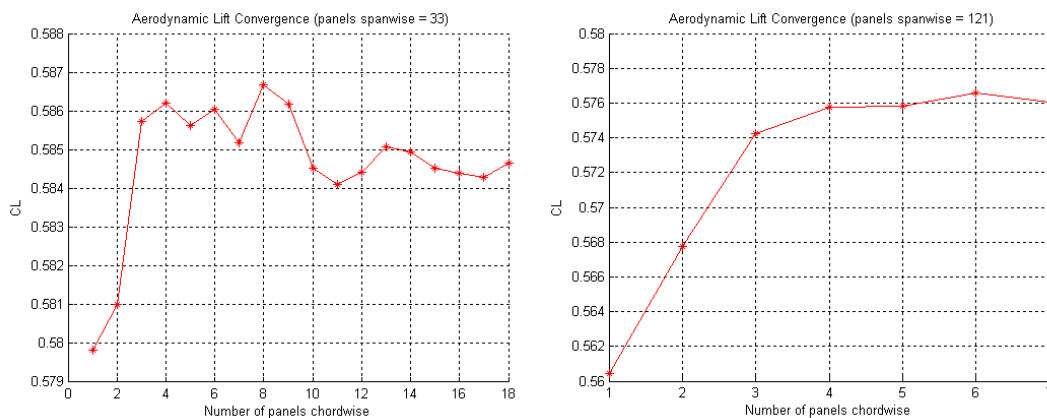
Figure 7.7: Convergence analysis - Aerodynamic lift coefficient as function of the number of panels chordwise.

Therefore the chosen vortex lattice is composed of 240 panels, 60 spanwise and 4 chordwise as shown in fig. 7.9.

7.6.2 Partitions detach code

Since the kite geometry is rigid, partition detach code is disabled in the analysis.

7.7 Wind profile

The wind profile with altitude is a key parameter which influences both cables drag and available wind power density. For example, with a constant wind profile, increasing
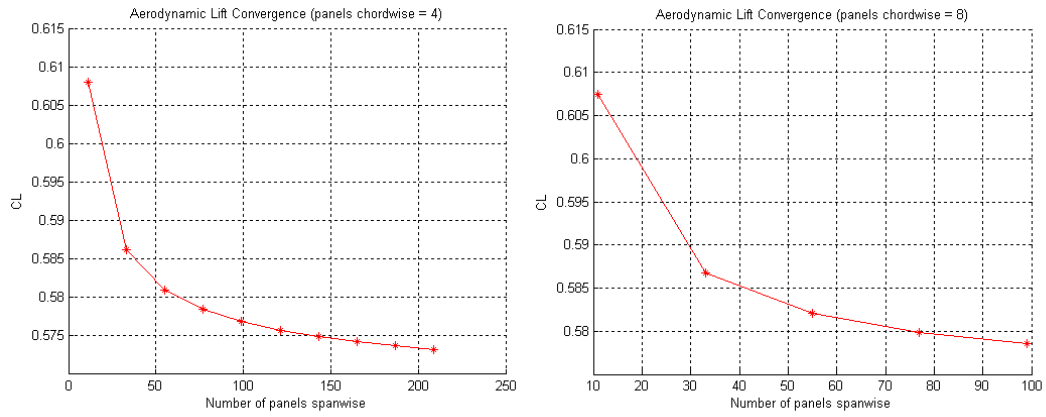
Figure 7.8: Convergence analysis - Aerodynamic lift coefficient as function of the number of panels spanwise.
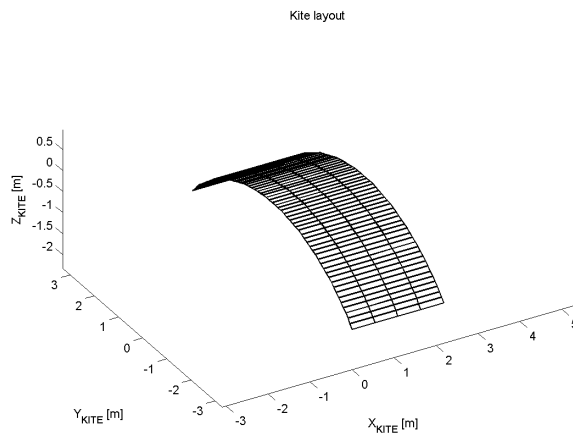
Figure 7.9: Chosen number of panels - Vortex lattice is based on 240 panels: 60 spanwise by 4 chordwise.

the tethers length[1] does not change the available power density while at the same time
reduces the aerodynamic efficiency of the system because of higher cables drag. By
contrast, with a profile that shows much higher wind speeds at higher altitudes, the
system would have a better performance increasing the tethers length and reaching
higher altitudes because the increase in cables drag would be less relevant than the
increase in wind power density.

Two different wind profiles, here called 'logarithmic wind' and 'tropospheric wind',
are studied. In both cases, the wind blows only towards the x direction (world coordi-
nate system).

7.7.1 Logarithmic wind

In this configuration the wind profile is logarithmic as shown in fig. 7.10, with 4 m/s
base speed.
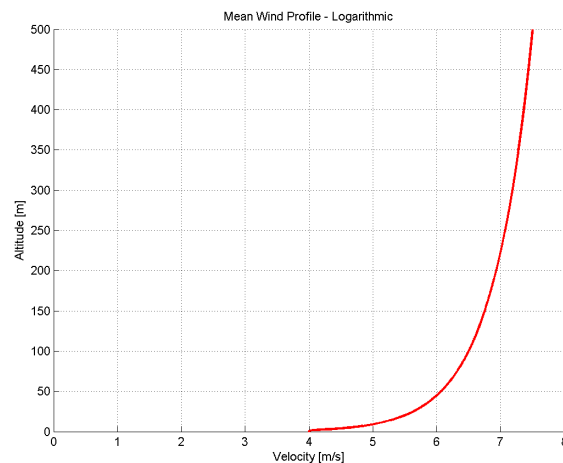
Figure 7.10: Wind average velocity at different altitudes - The figure shows the
logarithmic wind profile used in the VLM kite simulator. This atmospheric boundary layer
mean wind profile is in compliance with UK regulation ESDU 82026, terrain category = 0,
exposed to the open sea.

---

[1]A longer tether also results in a higher flight altitude if the elevation angle is greater than zero.

7.7.2 Tropospheric wind

In this other configuration the wind profile is tropospheric as shown in fig. 7.11 and it is based on the average European wind speed of 3 m/s at ground level. Higher altitudes than logarithmic wind are used.
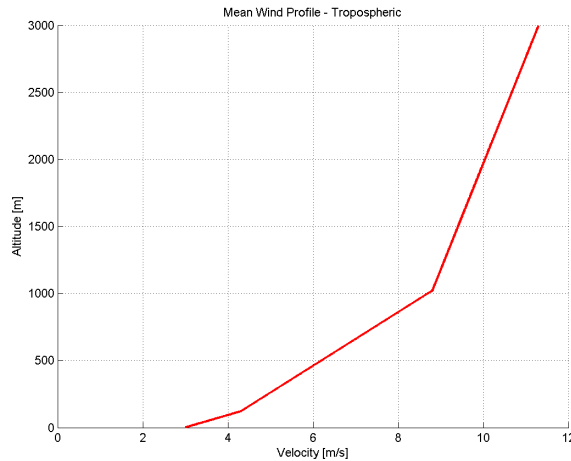
Figure 7.11: Wind average velocity at different altitudes - The figure shows the tropospheric wind profile used in the VLM kite simulator. Data from (23), originally from Delft University, Dr. Wubbo Ockels.

7.8 Power output estimation

7.8.1 Kite pulling force computation

When estimating the pulling force on the cables, the lift force itself is not completely accurate. Lift and drag forces are computed in the relative wind reference system while the tethers can be oriented in a different way.

The kite layout during horizontal flight is shown in fig. 7.12.

The relationships that follows are

$$\theta = \arctan \frac{V_{wind}}{V_{kite}} \tag{7.2}$$

$$T = L_{ift} \cos \theta + D_{rag} \sin \theta \tag{7.3}$$

101
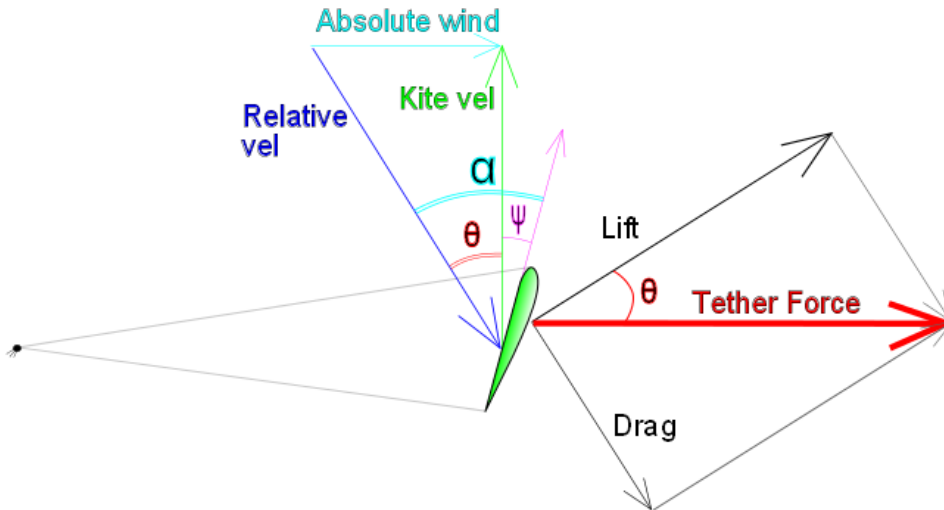
Figure 7.12: Tethers force - Top view. Due to the controller on the angle of attack, the kite reference system is not exactly perpendicular to the cables.

$$\alpha = \theta + \psi \tag{7.4}$$

Using the simulation wind absolute and relative velocity, it is possible to obtain the θ angle and to estimate the kite traction force on the cables T.

It is important to notice that the ψ value is always very low during the analysis and therefore the tether force estimated with this model is not significantly different than the total lift force[1].

7.8.2 Basic estimation of gravitational effects

The multibody environment does not take account of gravity during the simulations. However, gravity has an impact on power output because the total weight of the system reduces the traction force at the base station, therefore affecting the power output. As pointed out in (57), low mass or low elevation angles (altitude) result in a low impact of gravity in the power output, whereas an important reduction of performances would be caused by higher mass and higher elevation angles[2].

---

[1]The difference is usually below 1 %.
[2]See ref. (57) at equation (45). An application of this model can also be found on (58).

A simple sketch showing the model used for the gravity estimation is in fig. 7.13.
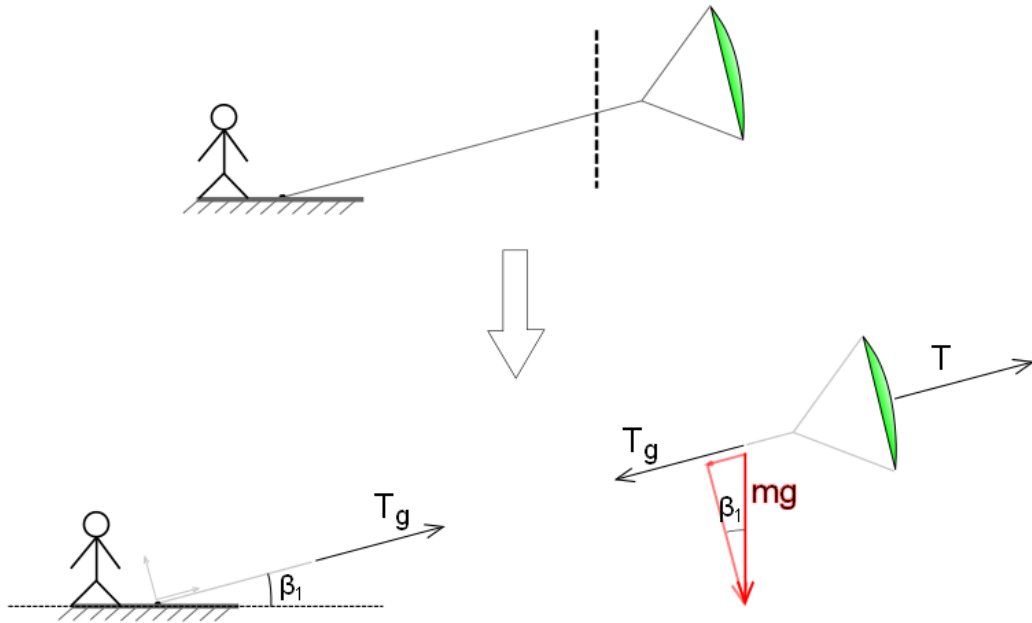
Figure 7.13: Gravity effect - The weight of the overall system has to be sustained by aerodynamic forces and reduces the traction force. Side view.

In order to consider the gravity effects, an elementary model to estimate the effective force T_g is

$$T_g = T - mg \sin \beta_1 \tag{7.5}$$

where m is the total mass of the kite plus two cables[1], β_1 is the elevation angle and T is the traction force already described in section 7.8.1. It is important to notice that this model is not a force equilibrium, but, instead, it is a very simple lumped model that allows to quickly estimate the gravity effect by subtracting a gravity force component from a traction force that is computed in an environment without gravity.

---

[1]Only two cables are considered in order to obtain results which are more compatible with the more common 2-cables layout such as that of Kitegen. This lumped approach is different from that of (57) because here the mass of the cables is entirely summed to the mass of the kite.

7.8.3 Power output model

The VLM kite simulator is capable of reeling out and reeling in the tethers during flight but, as described in section 6.6.1, the simulations do not reel out and reel in the tethers. The output power for a pumping yo-yo cycle in this configuration would therefore be zero and only the kite pulling force T can be estimated.

To obtain a reliable power output estimation the Loyd's model[1] is used.

Assuming that the kite is reeling out at 1/3 of the wind speed V_{wind}, the power output P_{opt} is

$$P_{opt} = T_{eff} * \frac{1}{3}V_{wind} \tag{7.6}$$

T_{eff} is the effective traction force of the kite considering that reeling out reduces the effective wind speed V_{effw} which becomes

$$V_{effw} = \frac{2}{3}V_{wind} \tag{7.7}$$

The VLM kite simulator provides the force T that the kite would create on the base station without reeling out according to equation 5.5.

$$T = \frac{1}{2}\rho V_{wind}^2 E^2 C_L A$$

According to this equation, the effective force is

$$T_{eff} = \frac{1}{2}\rho V_{effw}^2 E^2 C_L A$$

which, combined with eq. 7.7, yields

$$T_{eff} = \frac{1}{2}\rho\frac{4}{9}V_{wind}^2 E^2 C_L A \tag{7.8}$$

Therefore, using equations 7.8 and 7.6, the expression of eq. 5.6 is obtained

$$P_{opt} = \frac{1}{2}\rho V_{wind}^3 \frac{4}{27}E^2 C_L A$$

Substituting eq. 5.5 in eq. 5.6, the model that links the kite simulator force output T to the estimated optimal power output P_{opt} is eventually obtained.

$$P_{opt} = \frac{4}{27}V_{wind}T \tag{7.9}$$

---

[1]Described in section 5.1.2.

7.9 Model strengths and weaknesses

7.9.1 Strengths

The results obtained with this method are rigorous and comprehensive. The model takes account of the global aerodynamics of the system, from the ground station all the way up to the kite itself.

The 3D wind window is modelled together with wind profile and variable air density. The kite does change its speed when going in and out of the power zone.

Orders of magnitude of the results are reasonable and agree with what was expected.

7.9.2 Weaknesses

The model is not validated due to the unavailability of experimental equipments, especially aerodynamic cables.

The wind profiles represent an average constant wind and therefore important statistical parameters (see section 2.3) are not investigated in this analysis.

Rigid cables have inertia tensors with very different order of magnitude in their components. Longitudinal moment of inertia Izz_{Cable} becomes extremely smaller than radial moment of inertia Irr_{Cable} when the tethers length increases to several hundred meters. For this reason the simulation might need very small time steps which would result in a very large simulation time. Therefore, in order to have a reasonable simulation time[1], inertial properties of long cables are modified. Izz_{Cable} is assumed to be one tenth of Irr_{Cable} and Izz_{Cable} is limited when cables length is above $500\ m$.

The angle of attack α is controlled with a simple PD controller which keeps the kite in the linear aerodynamics range of validity (see section 6.3.3 and fig. 7.6) but has a steady state error that changes in each simulation. Therefore α is not precisely controlled and its effect cannot be completely removed from the final results which aim to simulate the performance increase due the aerodynamic cables only. However the α error has similar behaviours throughout the several batches of simulations and thus its effect may result in a reasonably constant, though not measurable, bias on each batch of simulations.

---

[1]50 *sec* of simulation time equal to about 8 *hours* of computations with a standard computer.

7.10 Results

7.10.1 Final plots

In this section four figures are described. Each of them has three curves. Each curve is the result of one batch of simulations as described in section 7.2. Each point of a curve is the result of one single simulation and represents the maximum power output[1] and the altitude at which that power output occurred during an horizontal flight[2].

Figs. 7.14, 7.15, 7.16 and 7.17 show the power output as function of altitude. The power output is estimated with equation 7.9 described in section 7.8.3.[3]

In figs. 7.14 and 7.15 the elevation angle is 30 *deg* and several aerodynamic cables percentages are used. In figs. 7.16 and 7.17 the cables are 50 % aerodynamic and 50 % round and the elevation angle is changed. The graphs show the results for tropospheric and logarithmic wind respectively.

Figure 7.14: Simulation results - Effects of different aerodynamic percentages in cables length. Tropospheric wind profile. 30 *deg* elevation angle.

---

[1]Estimated with equation 7.9.

[2]As shown in fig. 7.1.

[3]The effect of gravity is considered by using Tg (section 7.8.2) instead of T in equation 7.9.
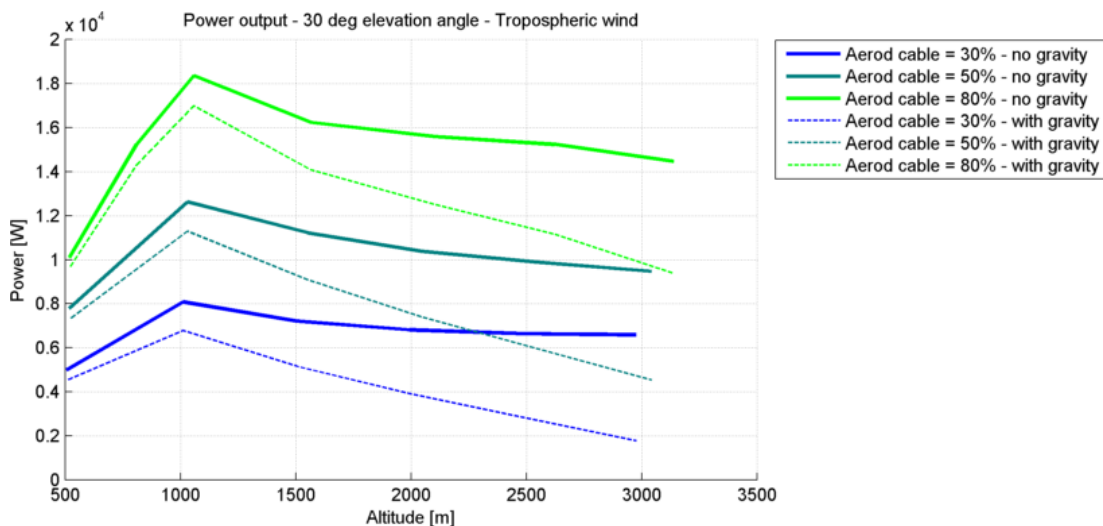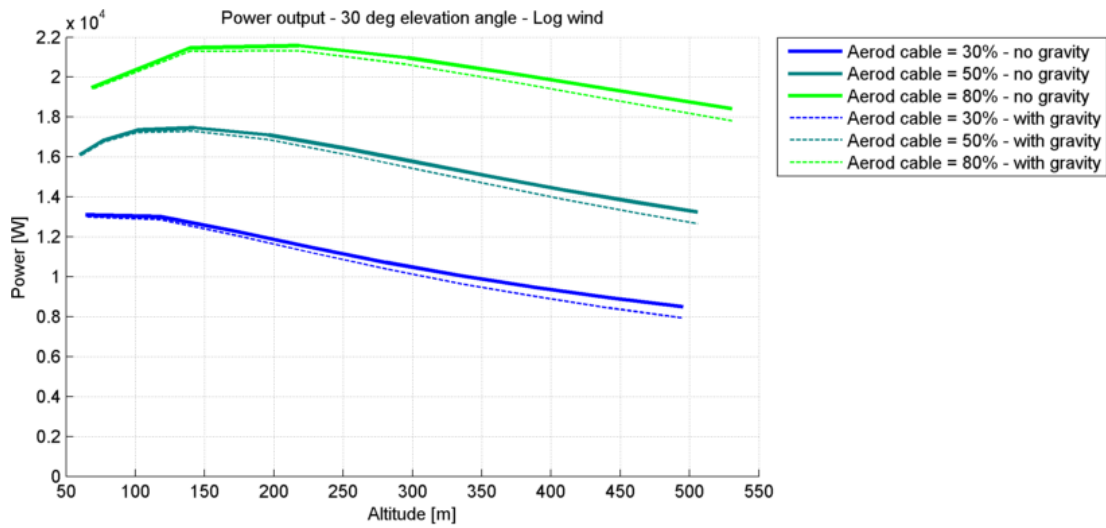
Figure 7.15: Simulation results - Effects of different aerodynamic percentages in cables length. Logarithmic wind profile. 30 *deg* elevation angle.
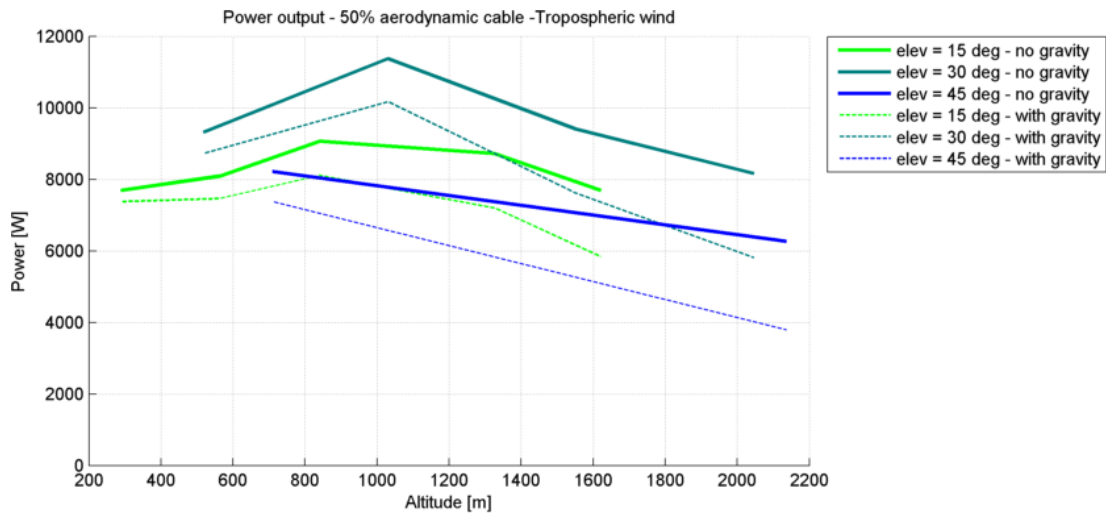

Figure 7.16: Simulation results - Effects of the elevation angle. Tropospheric wind profile. 50 % aerodynamic cable.
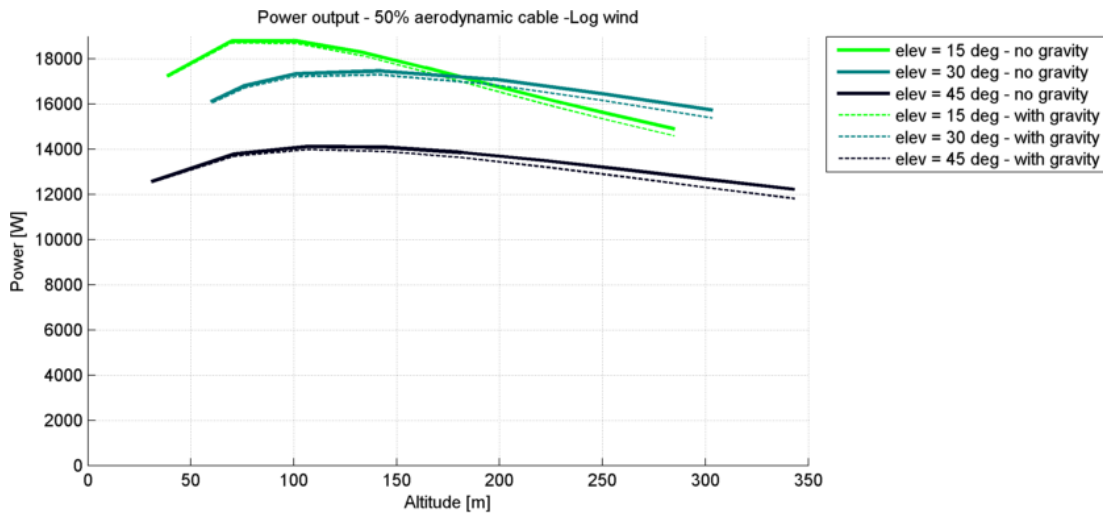
Figure 7.17: Simulation results - Effects of the elevation angle. Logarithmic wind
profile. 50 % aerodynamic cable.

7.10.2 Final remarks

As expected, the figures show that there is an optimal altitude at which the power
produced is maximum and the hypotheses on the wind profile greatly affect the final
results. This is because short cables result in better aerodynamics of the system but do
not allow to capture the higher wind power density of high altitude winds. By contrast,
long cables allow the kite to fly with stronger winds but increase the total drag of the
system.

Gravity effects are almost negligible with cable lengths up to 2000 m, but become
more significant when the tethers reach several km.

7.10.3 Effects of aerodynamic cables

The use of aerodynamic cables significantly improves the performance of the system.
When the percentage of airfoil section is increased, both the optimal altitude and the
power output increase. Changing the percentage of aerodynamic cables from 30 % to
80 % can approximately double the power output of the kite system.

For example, with reference to figs. 7.14 and 7.15, for a 16 m^2 kite in a tropospheric
wind with 3 m/s base velocity, using 30 % aerodynamic section would result in an

optimal altitude of about 1000 m and 7 kW of available power[1] whereas using 80 % of optimized cables increases the previous power output by 150 % resulting in 17 kW. Moreover, if the wind profile is logarithmic with 4 m/s base velocity, then using 30 % aerodynamic section yields an optimal altitude below 100 m and available power of 13 kW, while using 80 % aerodynamic cable results in an optimal altitude of about 200 m with a 65 % power increase, to 21 kW.

7.10.4   High altitude power zone

The wind profile has strong effects also on the power zone position, meaning the optimal elevation angle. For a uniform wind profile, the power zone is in the middle of the wind window at ground level[2], but changing the wind profile can shift this position upwards.

For example, with reference to figs. 7.16 and 7.17, using 50 % aerodynamic cable and considering only the values of 15, 30 and 45 deg of elevation angle, the best performance is achieved with 15 deg if the wind is logarithmic, while 30 deg is the optimal altitude if the wind is tropospheric.

---

[1]Notice that pumping cycle reel in phases as well as mechanical and electrical losses are not the subject of the present work and are therefore neglected.

[2]The description of the power zone is in section 3.4.1 and fig. 3.7

8

Conclusions

This thesis investigates the dynamics and aerodynamics of a kite-cables system in the field of high altitude wind energy, a young sector where the biggest steps towards industrial scale generators have been done in the last ten years.

A VLM simulator is developed to analyse the behaviour of different types of kites. It uses a multibody dynamics combined with a vortex lattice method aerodynamics. The simulator is a flexible tool that can investigate several variables of a kite design including geometry, structural model and aerodynamic properties. The simulator is then used to compare the performance of a kite-cables system that uses aerodynamically profiled cables instead of standard round ones. The results show a significant increase in power production.

Several future developments are possible. For example the structural model can be improved by removing geometrical discontinuities, cables sagging can be modelled using a more detailed tether model and unsteady aerodynamics can be implemented.

8. CONCLUSIONS

References

[1] GLOBAL WIND ENERGY COUNCIL. *Global Wind Statistics 2011.* http://www.gwec.net/fileadmin/images/News/Press/ GWEC_-_Global_Wind_Statistics_2011.pdf, 2011. 3

[2] WUBBO J. OCKELS. **Laddermill, a novel concept to exploit the energy in the airspace**. *Aircraft Design 4 (2001) 81-97.* 4

[3] CRISTINA L. ARCHER; KEN CALDEIRA. **Global Assessment of High-Altitude Wind Power**. *Energies, v 2, n 2, p 307-319*, June 2009. 6, 7

[4] W.; WOOLLEN J.; YANG S.; HNILO J.; FIORINO M.; POTTER G. KANAMITSU, M.; EBISUZAKI. **NCEP-DOE AMIP-II Reanalysis (R-2)**. *Bull. Am. Meteorol. Soc. 2002, 83, 1631-1643.* 6, 7

[5] ALBERT BETZ. *Windenergie und ihre Ausnutzung durch Windmhlen.* kobuch Verlag U. Versand, 1926. 5

[6] MASSIMO IPPOLITO. *Response to 'Jet stream wind power as a renewable energy resource: Little power, big impacts'.* http://www.kitegen.com/en/2012/03/22/the-max-planck-is-scared-to-fly/, 2012. 8

[7] F; KLEIDON A MILLER, L. M.; GANS. **Jet stream wind power as a renewable energy resource: Little power, big impacts**. *Earth System Dynamics, v 2, n 2, p 201-212*, 2011. 8

[8] EIA U.S. ENERGY INFORMATION ADMINISTRATION. *Electric Power Annual 2009.* http://www.eia.gov/electricity/annual/archive/ 03482009.pdf, April 2011. 9

[9] POLITECNICO DI MILANO. *Wind Energy Report 2012.* Collana Quaderni AIP, 2012. 9

[10] RAGUSA SALVATORE MARCO. *Valutazioni energetiche dell'eolico d'alta quota: Kitegen.* Politecnico di Torino - Tesi di laurea, 2007. 10, 11

[11] MILES L. LOYD. **Crosswind Kite Power**. *Journal of energy*, May-Jun 1980. 13, 41, 43

[12] SKYSAILS MARINE. *Skysails GmbH website.* http://www.skysails.info/english/media/photos-and-graphics/, 2012. 16, 30

[13] SKYSAILS. *Skysails GmbH website.* http://www.skysails.info/english/company/, 2012. 17

[14] GUINNESS WORLD RECORD. *Largest traction kite.* http://www.guinnessworldrecords.com/world-records/4000/largest-traction-kite, 2004. 15

[15] GUINNESS WORLD RECORD. *Largest kite ever flown.* http://www.guinnessworldrecords.com/world-records/1/largest-kite-flown, 2005. 15

[16] ROLAND SCHMEHL. *Large-scale power generation with kites.* http://www.lr.tudelft.nl/en/current/artikelen-homepage/large-scale-power-generation-with-kites/, 2012. 18

[17] MACKITE. *MACkite website.* http://www.mackiteboarding.com/kiteboarding-wind-window.htm, 2012. 19, 20

[18] CARLSON TW. *Spherical coordinate system.* http://commons.wikimedia.org/wiki/ File:Azimut_altitude.svg, 2012. 20

[19] JEROEN BREUKELS. *An Engineering Methodology for Kite Design.* Uitgeverij BOXPress, Oisterwijk, 2010. 21, 47, 48, 49, 57, 83, 87

[20] ROSS HUGHAN DAWSON. *Kite Turning.* University of Canterbury, Christchurch, New Zealand - Master's thesis, 2011. 21

[21] ROLAND SCHMEHL. *Kite power systems in automatic operation.* http://www.lr.tudelft.nl/nl/actueel/laatste-nieuws/artikel/detail/joint-demonstration-of-kite-power-systems-in-automatic-operation, May 2012. 25, 26

[22] KITEGEN. *EnergyKiteSystems website.* http://www.energykitesystems.net/KiteGen/index.html, 2010. 27

[23] MASSIMO CANALE; LORENZO FAGIANO; MARIO MILANESE. **Power Kites for Wind Energy Generation**. *IEEE Control Systems Magazine, v 27, n 6, p 25-38, 2007.* 27, 101

[24] KITEGEN. *Kitegen image repository website.* http://kitegen.com/press/repository.html retrieved on Aug-2012, 2007. 28

[25] MARCO GHIVARELLO. *Carbo-kite.* http://kitegen.com/2012/03/13/carbo-kite, March 2012. 29

[26] SKYSAILS MARINE. *Skysails GmbH website.* http://www.skysails.info/fileadmin/user_upload/ Presselounge/Dokumente/englisch/ EN_SkySails_Product_Brochure.pdf, 2012. 30

[27] WIND SYSTEMS MAGAZINE. *Wind Systems magazine.* http://windsystemsmag.com/article/detail/392/kiting-for-wind-power, July 2012. 31

[28] AMPYX POWER. *Ampyx Power website.* http://www.ampyxpower.com/PowerPlane.html, 2012. 32

[29] MAKANI POWER. *Makani Power website.* http://www.makanipower.com/home/, 2012. 33

[30] MAKANI POWER. *Makani Power website.* http://www.makanipower.com/why-airborne-wind/, 2012. 34

REFERENCES

[31] Association for the Study of Peak Oil. *EROEI*. http://www.aspoitalia.it, 2009. 35

[32] Fabrizio Bompani. *Bilancio energetico dell'impianto 'Kitegen Stem'*. Alma Mater Studiorum - Università di Bologna, Italy - Master's thesis, 2009. 35, 38

[33] Il Sole 24 Ore Nova 24. *Aquiloni energetici*. http://nova.ilsole24ore.com/nova24ora/2009/07/aquiloni-energetici.html, 2009. 35

[34] David J. Murphy; Charles A. S. Hall. **Year in review - EROI or energy return on (energy) invested**. *Annals of the New York Academy of Sciences*, 2010. 36

[35] Mrfebruary. *Ratio of Energy Returned on Energy Invested - USA*. http://en.wikipedia.org/wiki/File:EROI_Ratio_of_Energy_Returned_on_Energy_Invested_USA.svg, 2011. 36

[36] Kitegen. *Kitegen cables control discussion*. http://kitegen.com/2012/02/12/nasa-langley-research-center-e-kitegen/, 2012. 37

[37] Kitegen. *Kitegen website safety discussion*. http://kitegen.com/2012/03/02/rischi-e-sicurezza/, 2012. 39

[38] Makani Power. *Makani FAQ website*. http://www.makanipower.com/faq/, 2012. 39

[39] Richard Ruiterkamp Wubbo Ockels Paul Williams, Bas Lansdorp. **Modeling, Simulation, and Testing of Surf Kites for Power Generation**. *AIAA Modeling and Simulation Technologies Conference and Exhibit*, 2008. 45, 47

[40] R. Schmehl W.J. Ockels E.J. Terink, J. Breukels. **Flight dynamics and stability of a tethered inflatable kiteplane**. *Journal of Aircraft, v 48, n 2, p 503-513*, March-April 2011. 45

[41] Wubbo Ockels Paul Williams, Bas Lansdorp. **Modeling and Control of a Kite on a Variable Length Flexible Inelastic Tether**. *AIAA Modeling and Simulation Technologies Conference and Exhibit*, 2007. 48, 49

[42] Matlab documentation. *How Simscape Simulation Works*. http://www.mathworks.it/help/toolbox/physmod/simscape/ug/bql2kkl-2.html, 2012. 49, 50

[43] Steve Miller Matlab documentation. *Modeling Physical Systems as Physical Networks with the Simscape Language*. http://www.mathworks.com/tagteam/63431_Physical_Networks_In_Simscape_PDF.pdf, 2012. 49, 50

[44] Matlab documentation. *How Simscape Models Represent Physical Systems*. http://www.mathworks.it/help/toolbox/physmod/simscape/ug/bsl2lla.html, 2012. 49

[45] Tomas Melin. *A Vortex Lattice MATLAB Implementation for Linear Aerodynamic Wing Applications*. Royal Institute of Technology (KTH), Sweden - Master's thesis, 2000. 50, 51, 52, 79

[46] Tomas Melin. *Redhammer Consulting Website*. http://www.redhammer.se/tornado/index.html, 2010. 50

[47] DNV. *Recommended practice DNV-RP-C205 - Environmental conditions and environmental loads*. http://www.dnv.com/services/training/industries/energy/environmental_conditions_loads/index.asp, 2010. 59

[48] Massimo Canale; Lorenzo Fagiano; Mario Milanese. **A multibody dynamics approach to a cable simulation for kites**. *IEEE Control Systems Magazine, v 27, n 6, p 25-38*, 2007. 83

[49] C. H.; Chung S. C. Yen, J. Y. R.; Chen. **Coupling behavior of wire ropes subjected to tensile impulses**. *Journal of Engineering Mechanics, v 135, n 8, p 796-801*, 2009. 84

[50] W.J. Breukels, J.; Ockels. **Analysis of complex inflatable structures using a multi-body dynamics approach**. *Collection of Technical Papers - AIAA/ASME/ASCE/AHS/ASC Structures, Structural Dynamics and Materials Conference, 49th AIAA/ASME/ASCE/AHS/ASC Structures, Structural Dynamics, and Materials Conference*, 2008. 85

[51] Massimo Ippolito. *Aerodynamic cable patent*. US patent 2012/0036821, PCT/IT2010/000015, 2012. 91, 92

[52] FibreMax. *FibreMax Dyneema Cables Datasheet*. http://www.fibremax.nl/data/www.fibremax.nl/upload/files/Dyneema%20Cables.pdf, 2008. 92

[53] Steven Collicott E. L. Houghton, P. W. Carpenter. *Aerodynamics for Engineering Students*. Sixth edition, Elsevier, pag 509, 2012. 93

[54] Gian Mauro Maneia. *Aerodynamic study of airfoils and wings for power kites applications*. Politecnico di Torino, Italy - Master's thesis, 2007. 93, 94, 95

[55] Matlab documentation. *Choosing a Solver*. http://www.mathworks.it/help/toolbox/simulink/ug/f11-69449.html, 2012. 97

[56] Moler C. B. **Numerical Computing with MATLAB**. *Society for Industrial and Applied Mathematics, chapter 7*, 2004. 97

[57] P.; Silvennoinen R. Argatov, I.; Rautakorpi. **Estimation of the mechanical energy output of the kite wind generator**. *Renewable Energy, v 34, n 6, p 1525-1532*, June 2009. 102, 103

[58] R. Argatov, I.; Silvennoinen. **Asymptotic modeling of unconstrained control of a tethered power kite moving along a given closed-loop spherical trajectory**. *Journal of Engineering Mathematics, v 72, n 1, p 187-203*, February 2012. 102